A Fluorescence Study of the Interactions of Protein Synthesis Initiation Factors with Messenger RNA and Applications of Fluorescence Energy Transfer Techniques in Biopolymers

by

Chin-Chuan Wei

A dissertation submitted to the Graduate Faculty in Chemistry in partial fulfillment of the requirements for the degree of Doctor of Philosophy. The City University of New York

1998

Approval Page

This manuscript has been read and accepted for the Graduate Faculty in Chemistry in satisfaction of the dissertation requirement for the degree of Doctor of Philosophy.

12/15/97
Date

Chair of Examining Committee

12/23/97
Date

Executive Officer

Supervisory Committee

THE CITY UNIVERSITY OF NEW YORK

Abstract

A Fluorescence Study of the Interactions of Protein Synthesis Initiation Factors with Messenger RNA and Applications of Fluorescence Energy Transfer Techniques in Biopolymers

by

Chin-Chuan Wei

Advisor: Dixie J. Goss

Most eukaryotic mRNAs contain a 5' cap (m^7GpppX) and a 3' poly(A) tail to increase synergistically the translational efficiency. In this report the poly(A) binding protein (PABP) and cap-binding protein, eIF-4F, were found to interact. These data suggest that PABP may exert its effect on translational efficiency either by increasing the formation of initiation factor-mRNA complex or by enhancing ribosome recycling. In order to investigate the functional consequences of these interactions, the fluorescent cap analog, ant-m^7GTP, which is an environmentally sensitive fluorescent probe was used to investigate the cap-binding affinity. Our data show that the binding of eIF-(iso)4F or eIF-4F to cap analog enhanced their binding affinity towards PABP approximately 40-fold. Similarly, the eIF-4F/PABP or eIF-(iso)4F/PABP complexes show a 40-fold enhancement of cap analog binding compared to eIF-4F or eIF-(iso)4F alone. At least part of the enhancement of the translational initiation by PABP can be

accounted for by direct changes in cap binding affinity. The interactions of these components also suggest a mechanism whereby the poly(A) tail is brought into close proximity with m^7G cap. This effect was examined by fluorescence energy transfer and it was determined that the PABP/eIF-4F complex could bind both poly(A) and 5' cap simultaneously. Fluorescence resonance energy transfer techniques are also very powerful in studies of biopolymers. In this report, two models are constructed and good for studies of pseudoknotted RNA and RNA helicase activity.

Acknowledgments

I am grateful to my mentor Professor Dixie J. Goss for her generous support and pertinent guidance which made this research possible. and to my thesis committee - Professor Gary J. Quigley of Hunter College and Professor Thomas C. Strekas of Queens College for their enthusiastic assistant and insightful advice.

I would like to thank Professor Klaus Grohmann. Professor Pamela Mills. Professor Charles M. Drain and Ms. Edna Bornstein for their assistance in my Ph.D. study.

I am indebted to all the colleagues in this laboratory and school for their great help and opinion. They are - Luisa. Diana. Jiahau. Minxue. Chris. Vannesa. Marva. and Francia.

At last I would like to acknowledge my parents and my girlfriend. Ya-Ping Yang. for their constant encouragement.

TABLE OF CONTENTS

page

PART I: A Fluorescence Study of the Interactions of Protein Synthesis Initiation Factors with mRNA

LIST OF TABLES

page

LIST OF FIGURES

page

Abbreviations:

ant-m^{7}GTP	anthraniloyl 7-methyl-guanosine triphosphate
ATP	adenosine triphosphate
ATPγS	adenosine 5'-O-(3-thiotriphosphate)
εATP	1,N^6-ethenoadenosine 5'-triphosphate
BSA	bovine serum albumin
CD	circular dichroism
CPM	7-(diethylamino)-3-(4'-maleimidopheyl)-4-methylcoumarin
DTT	dithiothreitol
DMF	dimethylformamide
EDTA	(ethylenedinitrilo)tetraacetic acid
eIF	eukaryotic initation factor
FC	fluorescein 5-thiosemicarbazide
FRET	fluorescence energy transfer
HEPES	N-(2-hydroxyethyl)-1-piperazine-N'-(2-ethanesulfonic acid)
Gdn•HCl	guanidine hydrochloride
HPLC	high performance liquid chromatography
PEG	polyethylene glycol
PMSF	phenylmethylsulfonyl fluoride
poly(U)	poly(uridylic acid)
RNase	ribonuclease
SDS	sodium dodecyl sulfate
Tris	2-amino-2-(hydroxymethyl)propane-1,3-diol
VRC	vanadyl ribonucleoside complex

PART I: A fluorescence study of the interactions of protein synthesis initiation factors with mRNA

1. INTRODUCTION

Proteins are generated in a biosynthetic mechanism, translation, which necessitates the coordinate interplay of more than one hundred macromolecules. Transfer RNA (tRNA), messenger RNA (mRNA), and many proteins are required in addition to ribosomes to complete protein synthesis.

A protein is synthesized in the amino-to-carboxyl direction by the sequential addition of amino acids to the carboxyl end of a growing chain. The translation process can be divided into three stages: (i) *initiation:* this process results in the binding of the initiator tRNA to the start signal of mRNA, a template for protein synthesis. (ii) *elongation:* elongation starts with the binding of aminoacyl-tRNA to the other tRNA binding site on the ribosome, and a peptide bond then forms between the amino group of incoming aminoacyl-tRNA and the carboxyl group of methionine carried by the initiator tRNA; the mRNA complex moves to the next codon and elongation is continued, powered by the hydrolysis of GTP. (iii) *termination:* when ribosomal complexes reach a stop signal on the mRNA, read by a protein release factor, the protein synthesis stops and the completed chain is then released from the ribosome and mRNA. The released ribosome can then be utilized for the next cycle of protein synthesis.

Most eukaryotic mRNA has a very unique structure, which includes a 5' end cap structure, a 3' poly(A) tail, and varying secondary structure (Figure 1.1). The cap structure ($m^7G_{ppp}X$, where X is any nucleotide) is a 7-methyl guanosine conjugated with any other nucleotide by a triphosphodiester bond. On the 3' end, the length of poly(A) ranges from 25 to thousands of bases. mRNA also contains a hairpin structure, translational region (TR), and 5' & 3' untranslated regions (UTR). An mRNA starts to translate when the ribosome complex reaches the start codon of mRNA and stops translation when it reaches a stop codon. UTRs can not be translated to proteins, but enhance translational synthesis (review by Sonenberg, 1994).

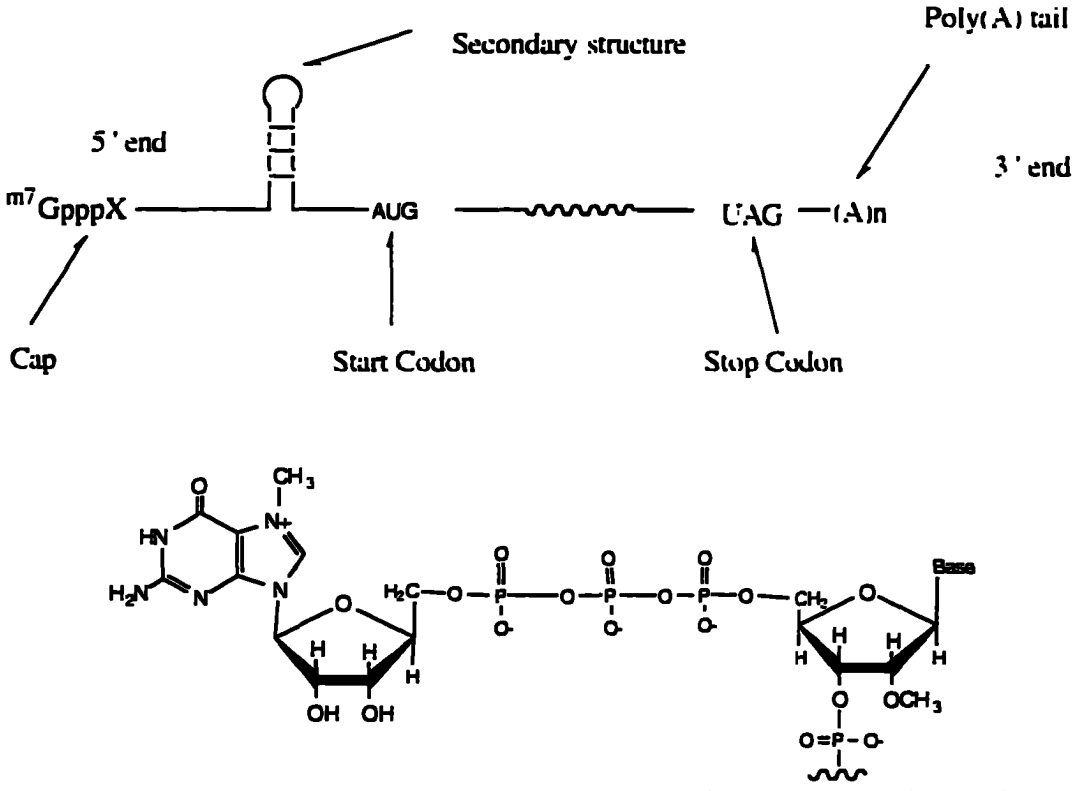

Figure 1.1 Schematic diagram of mRNA (top). Molecular structure of cap (bottom). The cap contains 7-methylguanylate attached by a triphosphate linkage to the sugar at the 5' end.

In our laboratory, our research interests focus on the initiation process of protein biosynthesis, particularly in the formation of mRNA with its associated proteins (i.e. complex III, see the following text). The possible mechanism for generation of an initiation complex is presented in Scheme I. The first step requires substantial amounts of free 40S ribosomes to be released from ribosomal complexes, and conjugate with eukaryotic initiation factor 3 (eIF-3) and eIF-4C to form complex I (Goumans et al., 1980). eIF-3 binds the AUG codon close to the 5' end of mRNA and eIF-4A, an ATP-driven protein, is responsible to search this site. In the absence of mRNA, a ternary complex containing eIF-2, GTP, and Met-tRNA forms and binds to the 40S subunit (complex II). The next step requires that the mRNA join these initiation complexes to form complex III. Finally, the 60S ribosome subunit associates with initiator tRNA, mRNA, and the 40S subunit to form an 80S initiation complex (complex IV).

For optimal attachment of mRNA to the 40S complex, three initiation factors are required as well as ATP. The eIF-4F, cap-binding protein, must recognize the m^7G structure of mRNA at the 5' end of eukaryotic mRNA. This is followed by the binding of eIF-4F to the cap structure. eIF-4B associated with eIF-4F and eIF-4A, performs an ATP-dependent unwinding of mRNA secondary structure, the so called helicase activity. With some or all of the initiation factors bound to mRNA, the mRNA/protein complex then binds to the 40S complex (complex II) to form complex III. The details of this mechanism still require further investigation.

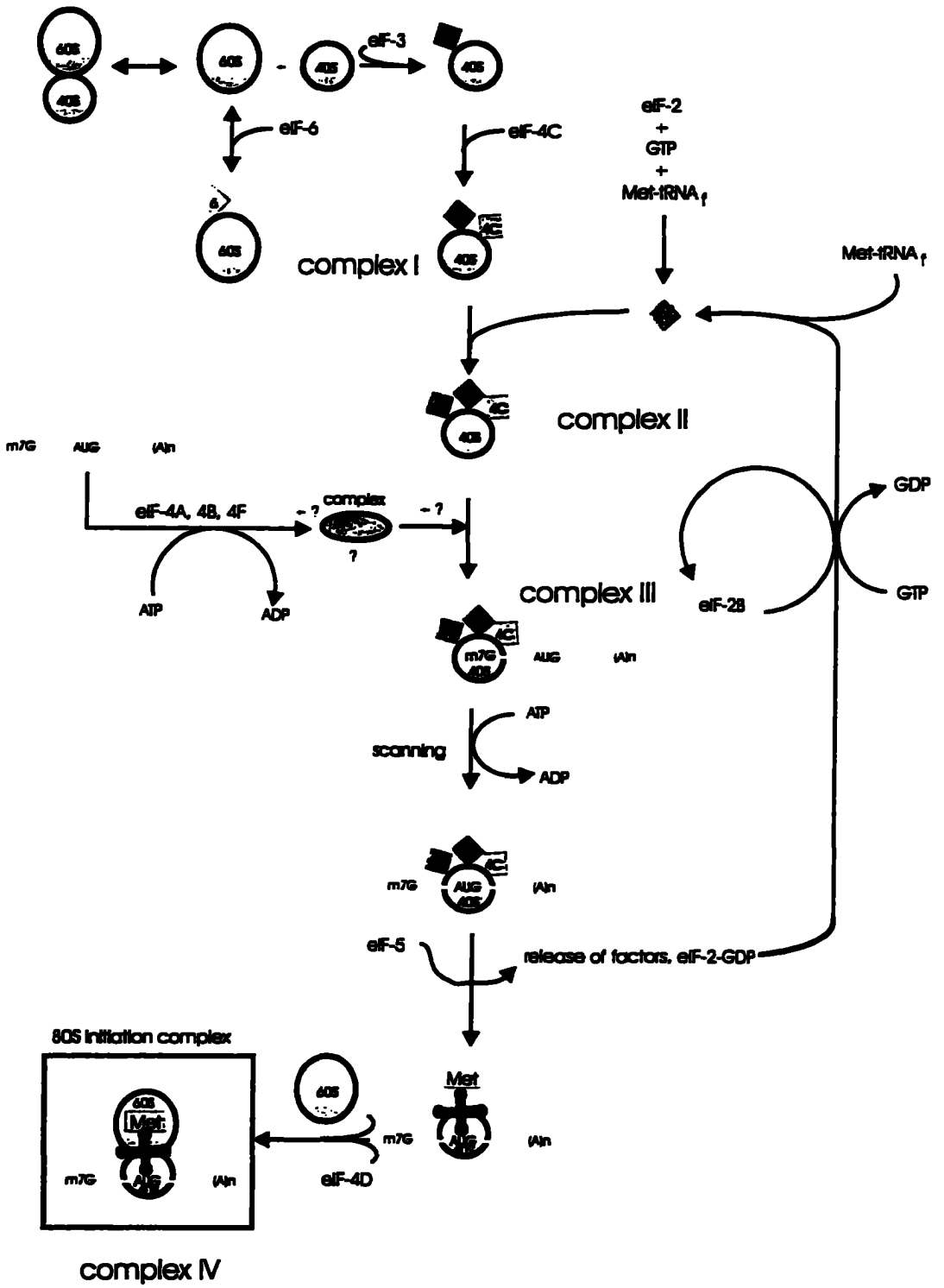

Scheme 1

In wheat germ, the cap-binding initiation factors are eIF-4F and its isoenzyme, eIF-(iso)4F. eIF-4F contains the essential 26 kDa cap binding protein, eIF-4E (p26), and another 220 kDa subunit, eIF-4G (p220) (Grifo et al., 1984). The eIF-4E binds directly to the cap structure and facilitates the formation of translational initiation complexes. Complexation of the cap structure and the cap-binding proteins is responsible for the recruiting the 40S ribosomal subunit to the mRNA via an interaction of eIF-4G subunit with the ribosome-bound eIF-3 (review by Hershey et al., 1996). Depending on its purification, eIF-4F may contain eIF-4A, a single 50 kDa polypeptide (Metz & Browning, 1993). Both eIF-4A and eIF-4E are also found as free polypeptides. While p220 and eIF-4E are in stable association, eIF-4A can be separated from the complex by phosphocellulose chromatography (Ray et al., 1985). Eukaryotic eIF-4A, an ATP-binding protein containing the conserved motif Asp-Glu-Ala-Asp ("DEAD" box) (Hodgman, 1988), allows the unwinding of double-stranded RNA in the presence of ATP (Linder et al., 1989) and another translational initiation factor eIF-4B, a 57 kDa polypeptide (Methot et al., 1996). Wheat eIF-4B is required for the binding of mRNA to 40S ribosomes and to stimulate approximately two fold ATP hydrolysis and ATP-dependent RNA helicase activity (Browning et al., 1987; 1989). Similarly, eIF-(iso)4F is a 110 kDa protein that contains the 82 kDa eIF-(iso)4G and 28 kDa eIF-(iso)4E (Lax et al., 1985, 1986a, 1986b).

The 5' cap structure and 3' poly(A) tail have been demonstrated to be important factors in promoting translational efficiency (review by Jackson & Standart, 1990).

Their roles in protein biosynthesis are well documented and are summarized in sections 1.1 and 1.2. However, recent evidence (Gallie, 1991; Iizuka et al., 1994; Tarun & Sachs, 1995) implies that these elements are codependent and must be in communication during translation, as is summarized in section 1.3. These findings prompted us to investigate how the 5' cap and 3' poly(A) tail interact during translation. The synergy between the 5' cap and poly(A) tail during translation suggests that these elements, in conjunction with their associated proteins, communicate during translation.

The most likely candidates for these interactions are poly(A)-binding protein (PABP) and cap-binding proteins. Cap-binding proteins recognize the cap structure while PABP interacts with the 3' poly(A). If these two proteins interact, the mRNA may form in a way in which the 5' and the 3' ends are in very close proximity. The translational efficiency may rely on this interaction, which provides an alternative view of initiation complex formation.

Although the sequence of amino acids in wheat germ PABP is not available at this time, PABP from yeast to human (Adam et al., 1986; Sachs et al., 1986; Grange et al., 1987; Zelus et al., 1989) has been shown to have highly conserved sequences and has four RNA-binding domains (RBDs). PABP has a strong affinity for poly(A) (Sachs et al., 1986). In addition, Yeast PABP is also known to stimulate the binding of the 40S ribosomal subunit to mRNA (Tarun & Sachs, 1995).

In this report, we obtained highly purified cap-binding proteins and PABP and assayed their interactions by direct fluorescence methods. To elucidate the possible complex which cap-binding proteins, mRNA, PABP, and poly(A) may form, the detailed binary interactions between individual species must be studied. From these data, it will be possible to extend our studies to ternary and multiple component systems to construct the assemblies of the initiation complex.

Even though PABP has been investigated since 1973 (Blobel, 1973), the spectroscopic studies of this protein and its interactions are not well defined. We have performed a spectrometric analysis of this protein with poly(A) and a fluorescent analog poly(εA). PABP not only has an affinity for poly(A), but also to poly(G) and poly(U), although with weaker affinity. In order to better understand these interactions and determine the cap affinity, we have investigated binary and ternary interactions among the various proteins, m^7G cap analog and poly(A) (or poly(εA)) using steady-state anisotropy and fluorescence titration methods. A ribo diol modified fluorescent cap analog, anthraniloyl-m^7GTP (ant-m^7GTP), has been advantageously employed to investigate this system (Ren & Goss, 1996). In this research, we have investigated the recognition of ant-m^7GTP and cap-binding proteins, eIF-4F and eIF-(iso)4F, by monitoring fluorescence anisotropy and fluorescence lifetimes.

Our results quantitate the interactions of cap associated proteins and PABP. These quantitative results have allowed us to determine the binding affinity of the cap-protein complex for PABP and the effects of PABP on the cap affinity of eIF-4F and

eIF-(iso)4F. PABP increased the cap affinity of both proteins approximately 40-fold. The fluorescence energy transfer measurements confirmed that a complex consisting of the cap analog, eIF-4F or eIF-(iso)4F, PABP, and poly(A) forms in solution. These data also suggest that an alternative initiation complex may form during the translation in which the 5' end and 3' termini interact via their associated proteins to synergistically promote translation. The synergistic effect of PABP on protein synthesis can be accounted for at least in part by a direct effect on cap affinity of the initiation factors.

1.1 cap structure of mRNA required to direct the translational machinery

Alkylated guanine nucleoside plays a special role in molecular biology. 7-methylguanosine, linked by a 5', 5'-triphosphate bridge to the other nucleotide, constitutes the 5'-cap (m^7GpppX) of eukaryotic mRNA. In early studies on vaccinia virus mRNA, removal of m7G from the mRNA by β-elimination resulted in significant loss of its ability to bind ribosomes (Muthukrishnan et al., 1976) and to stimulate protein biosynthesis (Muthukrishnan et al., 1978). The cap structure was shown to protect mRNAs against exonucleases (Furuichi et al., 1977) and to facilitate the initiation of translation (Shatkin, 1985). Therefore, the recognition of mRNA by components of the translation machinery is crucial in the control of protein synthesis. In the mRNA recognition step of protein synthesis initiation, the cap structure and

several cap-specific proteins participate in this process (Merrick, 1992; Sonenberg, 1994).

A number of initiation factors have been found to bind the cap structure directly or indirectly, including eIF-4E, eIF-4F, eIF-(iso)4F, eIF-4A, and eIF-4B (Lawson et al., 1989). Both eIF-4B and eIF-4A bind to the cap structure only in the presence of other initiation factors (Rozen et al., 1990). It is believed that they interact with cap via interaction with the cap-binding proteins. eIF-4F, eIF-4A, and eIF-4B have RNA helicase activity and are involved in the melting of RNA secondary structure in the leader region of mRNA (Rozen et al., 1990). Cap recognition and melting of RNA secondary structure are required for the subsequent binding of the 40S ribosomal subunit to most mRNAs (Rhoads, 1991).

1.2 The role of poly(A) tail

Since its discovery in 1973 (Blobel, 1973), the characterization of the poly(A) tail in eukaryotic mRNA has been well documented, but the detailed functioning of poly(A) has not been fully elucidated. Most newly synthesized mRNA is modified post-translationally by the addition of a poly(A) tail at the 3' terminus (reviewed by Brawerman, 1981). On transport into the cytoplasm, the poly(A) undergoes a shortening process but with a narrow size distribution (Brawerman, 1981). In general, the poly(A) tails are involved in mRNA processing and transport, mRNA stability, and protein synthesis (reviewed by Brawerman, 1981).

1.2.1 Poly(A) and poly(A)-binding protein in controlling mRNA stability

Most of the data regarding poly(A) and mRNA metabolism suggests that poly(A) is capable of protecting mRNA from rapid destruction (reviewed by Brawerman, 1981). Initial studies (Nudel et al., 1976) of rabbit globin mRNA, containing 32 or more adenylate residues, after injection into *Xenopus laevis oocytes*, provides evidence of functional stability equal to that of the native globin mRNA. On the other hand, the stability of the same mRNA containing only 16 adenylated residues was as low as poly(A)-free globin mRNA (Nudel et al., 1976). In this case, no mRNA degradation intermediate was detected, suggesting that once the poly(A) was removed, the mRNA was easily degraded. This is consistent with results of Brewer and Ross (1988), who claimed that removal of the poly(A) tail resulted in the degradation of c-*myc* mRNA *in vitro*.

A later study (Bergmann & Brawerman, 1977) showed that the role of poly(A) in controlling mRNA stability or translation cannot be considered in isolation of PABP, a 70 kDa protein common to most, if not all, eukaryotes. This observation can be explained by the fact that poly(A) is organized into a ribonucleoprotein by association of PABP, which is the most abundant messenger ribonucleoprotein (mRNP) in eukaryotes (Blobel, 1973). For example, Bernstein et al. (1989) showed that degradation of poly(A)$^-$ mRNA was not affected by PABP, but the degradation of poly(A)$^+$ mRNA was inhibited by addition of PABP. The sequence of PABP, from various organisms ranging from yeast to man, shows the conservation of four N-

terminal tandem RNA binding domains (RBDs) followed by a variable C-terminus (Adam et al., 1986; Sachs et al., 1986; Grange et al., 1987; Zelus et al., 1989). The RBD is composed of 80-90 amino acids and is present in one or more copies in proteins that bind pre-mRNA, mRNA, rRNA, and snRNA (Burd & Dreyfuss, 1994; Birney et al., 1993).

1.2.2 Poly(A) tail as a translational enhancer during translation

The sequence of poly(A) is considered a translational enhancer sequence, which stimulates translational initiation in much the same way that transcriptional enhancers are thought to stimulate the initiation of transcription (Ptashne, 1986, 1988). Translational enhancers are known to be orientation independent and several mRNAs containing 5' poly(A) sequences are found to be capable of binding PABP (Bertholet et al., 1987; Grange et al., 1987). This enhancer model predicts that the location of poly(A) on mRNA would be unimportant. This also raised the possibility that other sequences in the 3' untranslational region (UTR) have a translational regulatory role.

1.3 Functional codenpendence of 5' cap and 3' poly(A) tail

Although the cap structure and the poly(A) tail are on opposite ends of the mRNA molecule, evidence suggests that they interact to enhance translation and inhibit mRNA degradation.

Early evidence supporting 3' and 5' termini interaction during translation includes: (i) mRNA secondary structure map showing the 5' and 3' ends of mRNA to be in close proximity (Seidel & Somberg, 1978). (ii) electron micrography of the polysome with interacting 5' and 3' ends (Lockard et al., 1986). (iii) exogenous poly(A) stimulation of the translation of capped poly(A)$^-$ mRNA (Munroe & Jocobson, 1990). Sachs et al. (1987) proposed a co-recognition mechanism in which the cap, poly(A), and their associated proteins work to prevent the attempted translation of partially degraded mRNA.

Other supporting evidence for 5' and 3' termini interaction during translation includes: (i) in developing amphibian embryos, methylation of the cap of mRNA requires the presence of poly(A) tail (Kuge & Richter, 1995). (ii) mRNA with the cap and poly(A) tail stimulates translational initiation synergistically *in vitro* and *in vivo* (Gallie, 1991; Iizuka et al., 1994; Tarun & Sachs, 1995). (iii) In the presence of exogenous poly(A) bound PABP, the mRNA was prevented from decapping by decapping enzyme (Caponigro & Parker, 1995). (iv) degradation of mRNA requires poly(A) tail removal before the removal of the cap structure in yeast (review by Beelman & Parker, 1995).

The above evidence implies that the cap-associated factors, eIF-4F, eIF-(iso)4F, and eIF-4B, may play roles in mediating the interaction between the cap and poly(A). These initiation factors binding to poly(A) have functional consequences during translation *in vitro*. Addition of exogenous poly(A) to wheat germ lysate preferentially

repressed translation from uncapped mRNAs (1000 fold) compared to capped mRNA (4 fold) (Gallie & Tanguay. 1994). suggesting that the cap and the exogenous poly(A) were competing for the same activity that was required for translation.

2. EXPERIMENTAL PROCEDURE

2.1 Materials

m^7GTP was purchased from Sigma Chemical Co. (St. Louis. MO). Nuclease P_1. Poly(A). poly(G). poly(U). and poly(C) were purchased from Pharmacia Biotech (Piscataway. NJ). All of the homopolymers were exhaustively dialyzed against sterile water with several buffer changes at 4 °C. The synthesis of ant-m^7GTP was carried out as previously described (Ren & Goss. 1996). Protein concentrations were determined with Bio-Rad protein assay reagent (Bio-Rad Laboratory. Richmond. CA) as suggested by the manufacturer. Electrophoresis examination of proteins was performed in a polyacrylamide gel containing SDS (Laemmli. 1970). Nucleic acids and polypeptides were detected by silver staining (Merril et al.. 1981).

2.1.1 Preparation of the desired length of homopolymers

The preparation of $poly(A)_{30}$ was essentially as described by Chu et al. (1983) by heating of 10 mg poly(A) in the presence of 21 units of Nuclease P_1 at 37 °C. This was followed by phenol extraction. dialysis. and electrophoresis in a 15 % polyacrylamide gel containing 6.0 M urea and a running buffer containing 0.09 M

Tris-borate, 0.002 M EDTA. The gel was examined under UV light and the desired length of poly(A) was compared with oligonucleotide markers. The poly$(A)_{30}$ was cut from the gel and this gel slice was crushed and eluted with buffer containing 10 mM Tris, pH 8.0, 0.1 mM EDTA.

2.1.2 Preparation of 3' end fluorescein labeled poly$(A)_{30}$

The 3'-labeling of poly$(A)_{30}$ followed the procedure of Odom et al. (1980) with some modifications. All reactions were carried out in the dark. Oligonucleotides were oxidized at the 3' end by incubation with 0.09 M sodium periodate in 0.1 M sodium acetate, pH = 6.0, for 1 hr at 37 °C. The reaction was terminated by adding KCl to make a final concentration of 0.1 M. The KIO_4 precipitate was removed by centrifugation at 5,000 g for 10 min at 4 °C. The supernatant was dialyzed against 0.1 M sodium acetate, pH 6.0, at 4 °C. The sample was incubated with 1 mM fluorescein thiosemicarbazide at 37 °C for 2 hrs. At the end of the incubation, the sample was extracted with phenol followed by Sephadex G-25 purification. All samples were exhaustively dialyzed against several changes of the desired buffer at 4 °C.

2.1.3. Preparation of PABP from wheat germ extract

The preparation of PABP was essentially as described by Yang and Hunt (1992) and Le et al. (1997) with some modification. A 100 g sample of wheat germ was first frozen in liquid nitrogen and ground in a Waring blender in 45 sec intervals. The

powder was suspended in 300 mL buffer E (5 mM HEPES, pH = 6.9, 120 mM KOAc, 5 mM $Mg(OAc)_2$, 1 mM DTT, 5 mM PMSF, 100 µg/mL Soybean Trypsin Inhibitor, 10 mM benzamidine, 1.5 µg/mL Pepstatin, 1.5 µg/mL Chymostatin, 10 U/mL Aprotinin). All subsequent steps were carried out at 4 °C except where indicated.

The suspension was centrifuged for 30 min at 14,000 g. The fatty acid on top was removed. The supernatant was decanted and 1/10 volume of 0.1 M HEPES, pH = 7.5, was added and stirred another 10 min. The sample then was centrifuged again to remove some precipitate. To the supernatant, 14.4 g/100 mL of ammonium sulfate (25% saturation) was added, and the suspension was stirred for 45 min and centrifuged at 14,000 g for 20 min. The pellet was discarded, and 23.3 g/100 mL of ammonium sulfate (60%) was added to the supernatant. The resulting pellets were collected and dissolved in 50 mL buffer B (100 mM KOAc, 1 mM $CaCl_2$, 1 mM $Mg(OAc)_2$, 1 mM EDTA, 1 mM PMSF, 1 mM DTT, pH 7.5), and dialyzed against two four-liter changes of buffer B for 14 hr. The resulting preparation was clarified by centrifugation at 14,000 g for 1 hr, and followed by filtration in a 0.22 µm filter (Millipore, Bedford, MA). A 50 mL portion of sample was loaded into a 70 mL Affi-Gel Blue column (Bio-Rad Laboratory) at a flow rate of 50 mL/h. The column was washed with 1 liter of buffer B, 400 mL buffer B containing 4.0 M NaCl, and 200 mL buffer B. The desired protein portion was eluted with 2.0 M Gdn•HCl in buffer B. The peak fraction was collected and dialyzed against 3 4-liter changes of buffer C (50 mM KOAc, 1 mM $CaCl_2$, 1 mM $Mg(OAc)_2$, 1 mM EDTA, 1 mM PMSF, 1 mM DTT).

The resulting preparation was clarified by centrifugation at 14.000 g for 30 min and passed through a 0.22 μm filter. The filtered solution then was loaded into a Protein-Pak Q 15HR column (Waters, Inc., Milford, MA) at a flow rate of 1.5 mL/min. The flow-through was collected and the volume was decreased to around 10 mL by dialysis against 20 % PEG in buffer C.

The sample was dialyzed against buffer C followed by centrifugation at 14.000 g for 30 min. Poly(C) and Vanadyl Ribonucleoside Complex (VRC) (BRL, Bethesda, MD) were added to 0.5 mg/mL and 10 mM, respectively. This solution was passed twice through a 2 mL poly(A) Sepharose-4B column (Sigma, Inc.) at a flow rate of 50 mL/min. The flow-through was discarded. The column was then washed at a flow rate of 50 mL/h with the following: 5 mL buffer C with 5 mM VRC, 5 mL buffer C with 5 mM VRC and 1 mg/mL poly(C), 15 mL buffer C with 0.5 mg/mL poly(C), and 10 mL buffer C. PABP was eluted with buffer C containing 1.0 M urea and 2.0 M LiCl at a flow rate of 30 mL/h. Fractions (500 μL) were collected, dialyzed against buffer A (25 mM Tris, 100 mM KCl, 1 mM $Mg(OAc)_2$, 1 mM DDT, 1 mM PMSF, pH 7.6), and assayed in a 10% SDS-PAGE gel with silver staining. The fractions containing the desired protein then were combined and stored at -150 °C.

For preparation of poly(A) Sepharose-4B column, around 2 mL of solid gel was swollen in 1.0 M NaCl, pH 7.5, for 5 min. The material was packed in a column and washed with 0.1 M NaCl (25 mL/mL gel). The column was then washed with a 90% formamide buffer , pH 7.5, containing 0.01 M sodium phosphate and 0.01 M EDTA

(25 mL/mL gel. pH paper was used to detect the pH value). The column was next equilibrated with 10 bed volumes of the starting buffer. The column could be regenerated with 7M guanidine hydrochloride in a neutral buffer for protein contamination or formamide treatment for nucleic acid contamination.

The Affi-Gel Blue Column can be regenerated with treatment of 6.0 M Guanidine hydrochloride in a neutral buffer. Protein-Pak Q HR15 column must be washed exhaustively with a buffer containing 1.0 M NaCl.

2.1.4 Preparation of poly(εA)$_{30}$

The preparation was described as in Barrio et al. (1972) with some modifications. Poly(εA)$_{30}$ was prepared by incubating poly(A)$_{30}$ with 2.0 M chloroacetaldehyde, pH 6.0, at 50 °C in the dark. The degree of modification was monitored by UV and calculated as described in Ledneva et al. (1978). After completion of the reaction, the product was precipitated from the reaction mixture by ethanol. Concentrations were determined by spectrophotometry, using $\varepsilon_{(p)}(257) = 3.7 \times 10^3\ M^{-1}cm^{-1}$. This value was checked with poly(εA)$_{30}$ completely digested by micrococcal nuclease (Karpel et al., 1987). Approximately a 20 % hyperchromic change was observed and $A_{300}/A_{258} = 0.601$ was obtained.

2.2 Spectroscopy

2.2.1 UV measurements

Absorbance measurements were obtained using a Cary-3 double beam UV/VIS spectrophotometer.

2.2.2 Circular dichroism measurements

Circular dichroism (CD) spectra were obtained on a Jasco J-700 spectropolarimeter interfaced to a Digital computer. The cuvet-holding chamber was flushed with a constant stream of dry N_2 to avoid water condensation on the cuvet exterior. CD spectra for protein and nucleic acid measurements were measured from 300 nm to 190 nm in a 0.05 cm pathlength cuvet and 320 nm to 220 nm in a 0.1 cm pathlength cuvet, respectively. (+) 10-camphor-sulfonic acid at a concentration of 0.5 mg/mL was used as a calibration standard. The concentration was checked by UV spectroscopy using a molar extinction coefficient of 34.5 at 285 nm (Johnson, 1990).

2.2.3 Fluorescence spectroscopy

Fluorescence spectra were recorded on a Spex Fluorolog τ2 spectrofluorometer equipped with excitation and emission polarizers. All measurements were performed at 20 °C and corrected for wavelength dependence on exciting-light intensity through the use of a quantum counter, Rhodamine, (Lakowicz, 1983) in the reference channel.

All of the measurements were taken at least three times and the reported results were reproducible.

2.2.4 Studies of protein-nucleic acid interactions using intrinsic protein fluorescence

Two of the 20 amino acids, tryptophan and tyrosine, in a polypeptide have enough fluorescence to be utilized in spectroscopy. In these measurements, the emission spectra were measured upon excitation at 280 nm, where both of tryptophan and tyrosine residues are excited, and 295 nm were tryptophan residues were selectively excited. Due to the absorption overlap of nucleic acids and protein, the titration of protein with nucleic acids needed to be corrected for the inner filter effect according to the Beer-Lambert Law.

$$I_{corr} = I_{meas} \times 10^{Ac} \qquad \text{eq. 1}$$

where A is the absorbance at the excitation wavelength and c is the instrument constant which had to be determined experimentally. To determine the constant c, BSA and cytosine which do not have binding affinities were selected. This protein was titrated with nucleic acid, and the quenching curve was obtained to determine the inner-filter effect. Since there should be no interaction between them, the decrease in fluorescence intensity can be attributed to the inner filter effect (reabsorption). The fluorescence intensity of original signal was corrected for this effect. The constant, c, was determined from the known value of absorbance of titrant. We found that the

correction for the inner filter effect using this experimental method was more reliable than the theoretical equation correction (Lackowicz, 1983), which usually underestimated or overestimated the inner filter effect due to factors dependent on the fluorometer. Corrections for Raman scattering (as measured with buffer) were also made for the fluorescence intensity measurements.

When proteins interact with long lengths of nucleic acids.. the spectral changes observed in fluorescence shape and intensity are due not only to the fluorescence quenching, but also the change of fluorescence polarization anisotropy. No polarizer was required for this measurement because the anisotropy changes were small upon addition of nucleotides or RNA.

The light scattering intensity due to turbidity of the sample was estimated by extrapolation of the curve between 350 and 400 nm (Eriksson et al.. 1993). In this region no absorption was detected from the samples and the scattering was found to follow the following formula:

$$\log(\tau) = \log(a\lambda - b) \qquad \text{eq. 2}$$

where τ is turbity, λ is the wavelength, and a and b are constants. The calculated turbidity was subtracted from the absorption spectra prior to the inner filter correction because the light scattering reduces the fluorescence intensity considerably less than the absorption does.

For each data point, the fluorescence quenching ($Q = 100\ [F_0-F]/F_0$), where F is the measured fluorescence and F_0 is the fluorescence in the absence of nucleic acid.

was calculated and plotted against the concentration of nucleic acid. The binding constant then was fitted as elsewhere (Lakowicz, 1983).

2.2.5 Studies of protein-protein interactions

For measurements of protein-protein interactions, complex formation was studied by monitoring changes in the intrinsic protein fluorescence. In order to maximize the signal, the excitation wavelength was chosen to be 265 nm and emission signal was detected with a cut-on filter (50% transmission at 305 nm). Since no emission monochromator was used, the fluorescence intensity change due to fluorescence polarization did not need to be considered. The signal was corrected for light scattering by measuring the buffer under the same conditions. The excitation bandpass was chosen to eliminate photobleaching and the linearity of fluorescence intensity with protein concentration was determined. For each data point three samples were prepared. The fluorescence intensity of a solution containing 100 nM PABP was measured. A second sample with a specific amount of cap-binding protein was also measured and the corrected intensities of the two samples were summed together (F_S). A third sample containing the same amount of PABP and cap-binding protein mixed together, was incubated at 20 °C for 20 min, and the corrected fluorescence intensity for this complex was obtained (F_C). The difference in fluorescence intensity related to the complex was defined as $\Delta F = F_C - F_S$. The details of the fitting are described elsewhere (Firpo et al., 1996; Locke et al., 1992).

2.2.6 Measurement of protein-nucleic acid interactions with fluorescently labeled nucleic acids

For protein-nucleic acid interactions, the excitation wavelength for ant-m^{7}GTP was 332 nm and emission was monitored at 420 nm. The excitation wavelength for poly(εA) was 309 nm, and the fluorescence was monitored at 400 nm. The excitation slits were chosen to avoid photobleaching and the absorbance of the sample at the excitation wavelength was less than 0.02 to minimize the inner-filter effect. Emission spectra were corrected for wavelength-dependent lamp intensity and monochromator sensitivity.

Steady-state fluorescence anisotropy was measured using an L-format detection configuration. The excitation bandpass was 8.5 nm and the emission bandpass was 17.0 nm. All samples were incubated for at least 15 min at 20 °C before data were collected.

Phase-demodulation lifetime measurements were carried out using a 0.1 % (w/w) glycogen suspension with a reference lifetime of 0.0 nsec (scattering). The emission polarizer was placed at a magic angle (54.7° from vertical position) to correct for the different sensitivities of the polarized light on the photomultiplier tube and the monochromator.

2.2.7 Quantum yield measurement of fluorophores.

The measurement of relative quantum yield (Q) of fluorophore was calculated by comparison to a standard whose quantum yield is known (Brissette et al., 1989).

$$Q_x = \frac{IxQsAs}{IsAx} \qquad \text{eq. 3}$$

In the preceding formula x represents the unknown species, s represents the standard. I is the integrated fluorescence intensity, and A is the absorbance at the excitation wavelength. Disodium fluorescein in 0.01 N NaOH, Q = 0.92 (Weber & Teale, 1957), was used as a standard.

2.3 Data Analysis

2.3.1 Fluorescent nucleic acid analog-protein interactions

The equilibrium constant for the binding of ant-m^7GTP with eIFs

$$eIF + Cap^* \iff [Cap^*{\bullet}eIF]$$

is defined by eq. 4.

$$K_a = \frac{[Cap^*{\bullet}eIF]}{[Cap^*][eIF]} \qquad \text{eq. 4}$$

where [eIF], [Cap*], and [Cap*•eIF] are the equilibrium concentrations of the unbound protein, ant-m^7GTP, and ant-m^7GTP/protein complex, respectively.

The fluorescence anisotropy, r, is defined as (Lakowicz, 1983)

$$r = \frac{I_{VV} - GI_{VH}}{I_{VV} + 2GI_{VH}} \qquad \text{eq. 5}$$

where G is a factor that corrects for the difference in the measured intensities due to the difference in the sensitivity to the detector of vertically and horizontally polarized emitted light. G is defined as (Lakowicz, 1983).

$$G = \frac{I_{HV}}{I_{HH}}$$

where I_{HV} and I_{HH} are the fluorescence intensities measured with horizontal excitation polarization and with the emission polarizer aligned either vertically or horizontally, respectively.

In a mixture of eIF and ant-m^{7}GTP, the average anisotropy is related to the fraction of the total fluorophore which is bound (f_b) by

$$f_b = \frac{r - r_f}{(r_b - r)R + (r - r_f)} \qquad \text{eq. 6}$$

where $R = Q_b/Q_f$ is the ratio of quantum yield of the bound and the free ant-m^{7}GTP. r, r_f, and r_b are the anisotropy values of the mixture, the totally free ant-m^{7}GTP, and the totally bound ant-m^{7}GTP, respectively. It can be shown that the measured anisotropy is related to the total concentration of eIF by the following relationship:

$$r = \frac{ar_bR - ar_f + r_f}{1 + a(R-1)} \qquad \text{eq. 7}$$

$$\text{where a} = \frac{K[Cap^*]_T + K[eIF]_T + 1 - \sqrt{(K[Cap^*]_T + K[eIF]_T + 1)^2 - 4K^2[Cap^*]_T[eIF]_T}}{2K[Cap^*]_T}$$

$[Cap^*]_T$, $[eIF]_T$, and K were the total concentration of ant-m^7GTP, protein, and the equilibrium association constant, respectively.

2.3.2 Frequency phase and modulation lifetime measurements

Multifrequency phase and modulation data were analyzed by fitting to a sum of exponentials using the Globals Unlimited program (Urbana, IL). The fluorescence intensity decay was expressed as,

$$I(t) = \sum_i \alpha_i e^{-(t/\tau_i)} \qquad \text{eq. 8}$$

where α_i is the preexponential concentration factor and τ_i is the lifetime of the ith emitting component. The frequency response of the fluorophore is the Fourier transform of the intensity decay function, I(t), where G and S are the real and imaginary parts of the transform, respectively:

$$G = \int_0^\infty I(t)\cos(\omega t)dt \qquad \text{eq. 9}$$

$$S = \int_0^\infty I(t)\sin(\omega t)dt \qquad \text{eq. 10}$$

The phase angle, ϕ, and the modulation, M, measured at frequency ω are related to the sine and cosine Fourier transforms of the fluorescence decay function, S and G, as follows:

$$\tan \phi = S / G \qquad \text{eq. 11}$$

$$M = (S^2 + G^2) / I_{tot} \qquad \text{eq. 12}$$

$$I_{tot} = \int_0^\infty I_t dt \qquad \text{eq. 13}$$

where the sine and cosine transforms are related to the fluorescence lifetimes by

$$G = \sum_i \alpha_i \tau_i (1 + \omega^2 \tau_i^2)^{-1} \qquad \text{eq. 14}$$

$$S = \sum_i \alpha_i \tau_i (1 + \omega^2 \tau_i^2)^{-1} \qquad \text{eq. 15}$$

2.3.3 Fluorescence energy transfer measurements

In order to determine if energy transfer occurred between the cap binding analog and poly(A) when bound to the protein complex, 150 nM ant-m^7GTP, 50 nM eIF-4F, 50 nM PABP, and 50 nM 3'-fluorescein-poly$(A)_{30}$ were mixed together for complex formation with the absorbance at the excitation wavelength of less than 0.02. The fluorescence intensity ($F_{D,A}$) from 380 to 600 nm was recorded. Unlabled m^7GTP and poly$(A)_{30}$ were used as controls since they have almost identical binding affinity compared with ant-m^7GTP and 3'-fluorescein-poly$(A)_{30}$, respectively. The

fluorescence signal from the donor (F_D) in the absence of acceptor was determined using 150 nM ant-m^7GTP. 50 nM eIF-4F. 50 nM PABP. and 50 nM poly$(A)_{30}$. The fluorescence signal from acceptor (F_A) at this excitation wavelength was obtained using 150 nM m^7GTP. 50 nM eIF-4F. 50 nM PABP. and 50 nM 3'-fluorescein-poly$(A)_{30}$. Comparison of the spectra obtained from the mixture containing both donor and acceptor with the sum of the individual fluorescence intensities from the controls allowed us to detect any fluorescence energy transfer. The spectral overlap integral. J. of the emission spectra of the donor and the absorption spectra of the acceptor were calculated according to the relation:

$$J = \frac{\int F_D(\lambda)\varepsilon_A(\lambda)\lambda^2 d\lambda}{\int F_D(\lambda)\lambda^{-2} d\lambda}$$

where $F_D(\lambda)$ is the fluorescence spectrum of the donor and $\varepsilon_A(\lambda)$ is the molar absorptivity of the acceptor on a wavelength scale λ. The Förster distance. R_0. between the two dyes was not calculated because κ^2. a function of the relative orientation of the dyes. could not be measured directly and the orientation is unlikely to be random.

2.3.4 Stern-Volmer measurements

Quenching experiments in the presence of either acrylamide or sodium iodide were performed by sequential addition of aliquots form 3-6 M stock solution. The inner filter effect of acrylamide was very low at 300 nm and corrected according to Calhoun

et al (1983). In the case of iodide, 0.1 mM sodium thiosulfate was added as a reference (Mendoza et al., 1992) in order to prevent I_3^- formation. The fluorescence quenching curve in the presence of acrylamide or iodide was analyzed according to the Stern-Volmer equation.

$$F_o/F = 1 + K_{sv}[Q] \qquad \text{eq. 16}$$

where F_o and F are the fluorescence intensity, respectively, in the absence or the presence of quencher. K_{sv} is the collisional Stern-Volmer constant and [Q] is the concentration of quencher.

3. RESULT AND DISCUSSION

3.1 Characterization of PABP

Poly(A)-binding protein from different species have the following in common: (i) a tandem repeat N-terminal domain of 80-90 residues; (ii) degree of sequence conservation of the N-terminal domain; (iii) C-terminal domain that could be removed without effecting the poly(A) binding activity. In order to study the properties of PABP from wheat germ, we carried out the purification following the procedure described in the Experimental Procedure section. The first attempt to purify this protein using only Soybean Trypsin Inhibitor (STI) was not successful since the final sample contained some short polypeptides which were PABP fragments. These

fragments were most likely the proteins after proteolysis. PABP has been demonstrated to be a non heat-shock protein (Lefrere & Duncan. 1994). but more sensitive to protease. The combination of protease-inhibitors. STI. benzamine. Pepstatin. Chymostatin. and Aprotinin were found to be an effective set of inhibitors. Changing the inhibitors enhanced the purity of the final product (data not shown).

The results of the protein purification are shown in Lane 1 and 3 in Figure 3.1.1. The final product obtained from the poly(A)-Sepharose 4B column was analyzed in PAGE gel containing SDS. The molecular weight of PABP in wheat germ was determined to be 70 kDa compared with protein markers (Figure 3.1.2). Since only one band is visible in the gel. we conclude that the PABP purified from this protocol should not be contaminated with any nucleic acid since nucleic acids are more sensitive than protein to silver staining. From this protocol. the properties of wheat germ PABP can be summarized as follows: (i) PABP is very easy to denature and renature since these protocols utilized its properties. (ii) wheat germ PABP is a basic protein since it is not bound to a strong anion exchange column. This is similar to human PABP (hPABP) (Görlach et al.. 1994).

Protein was easily lost in the purification process due to repeated denaturation and renaturation of the protein. The product yield was therefore low with only about 200 µg of PABP obtained per preparation. The intrinsic fluorescence of this protein showed that PABP contains more tyrosine than tryptophan since the maximum emission wavelength is around 300 nm (data not shown).

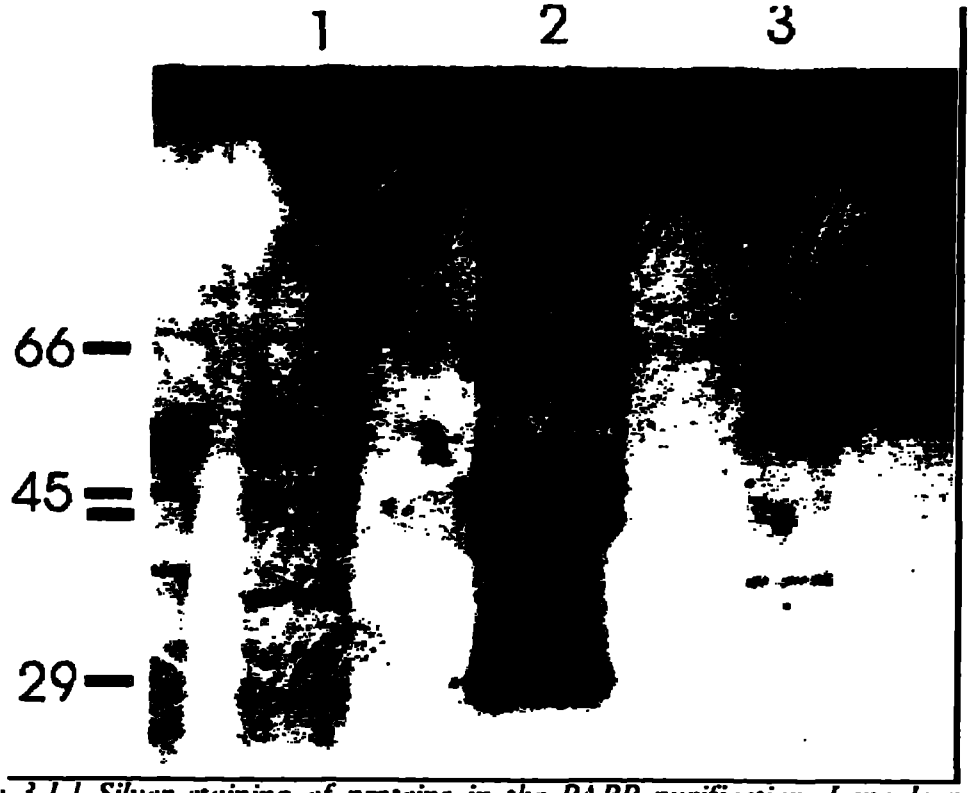

Figure 3.1.1 Silver staining of proteins in the PABP purification. Lane 1: proteins after Affi-Gel blue chromatography. Lane 2: protein makers. Lane 3: protein after Mono Q FPLC chromatography.

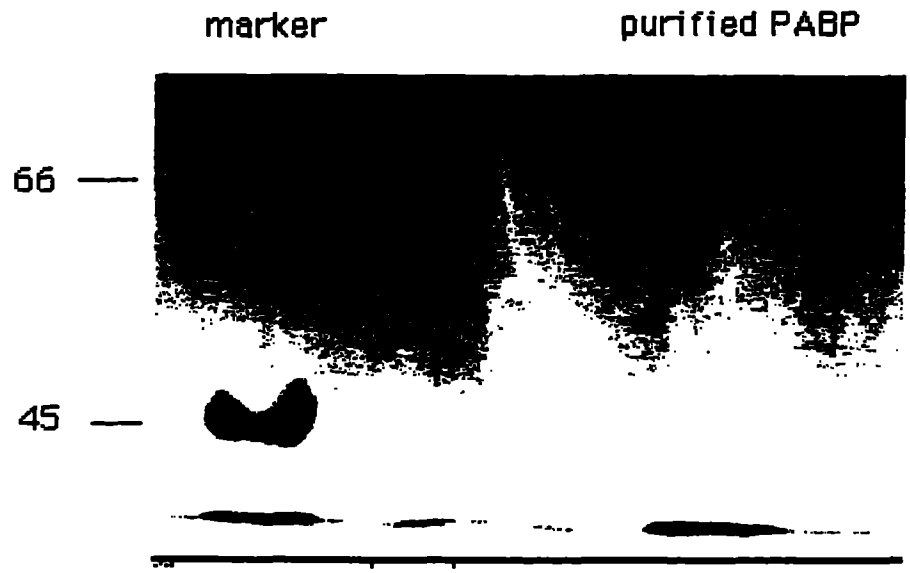

Figure 3.1.2 Silver staining of the PABP after the poly(A) Sepharose-4B column. The dark background of the PABP lane is due to incomplete removal of the denaturant and salts.

3.2 Preparation of the fluorescent poly(A) analog, poly(εA)

Most eukaryotic mRNAs contain a poly(A) tail, ranging from 25 to thousands of bases. In order to determine the packing density of PABP, the fluorescence analog, poly(εA) was prepared as the procedure described in Barrio et al. (1972). Under these conditions when poly(A) is treated with 2 M choloacetaldehyde at pH 4.5, 37 °C, the final product contained only partially modified adenine (data not shown). This is attributed to the fact that poly(A) forms a double helix structure and the base-pairing inside the alpha helix form in the acidic condition prevents chloroacetaldehyde from

approaching the nucleotide. Upon increasing the pH value to 6.0 and the temperature to 55 °C, the secondary structure of poly(A) in solution is almost destroyed, and all A bases became equally accessible to chloroacetaldehyde. The molar extinction coefficient and the degree of modification for poly(A) was calculated as described in Ledneva et al. (1978). The degree of modification for this reaction is approximately 100%. The corrected fluorescence excitation and emission spectra (Figure 3.2.1) of poly(εA) are essentially superimposible and comparable to a spectrum of the monomer εA•HCl. The excitation maximum is 300 nm, and the emission maximum is around 400 nm in a neutral solution. The excitation wavelength at 309 nm is useful for studies of protein-nucleic acid interactions since it does not overlap with the absorption spectra of the protein or nucleic acid, and reasonable fluorescence intensity was obtained. According to absorption and emission measurements, the fluorescence quantum yields (Q_0) of a single fluorescent base in poly(εA) (poly(εA)$_p$) is greatly reduced relative to εATP ($Q_0 = 0.59$). The quantum yield of poly(εA)$_p$ was calculated to be 0.05.

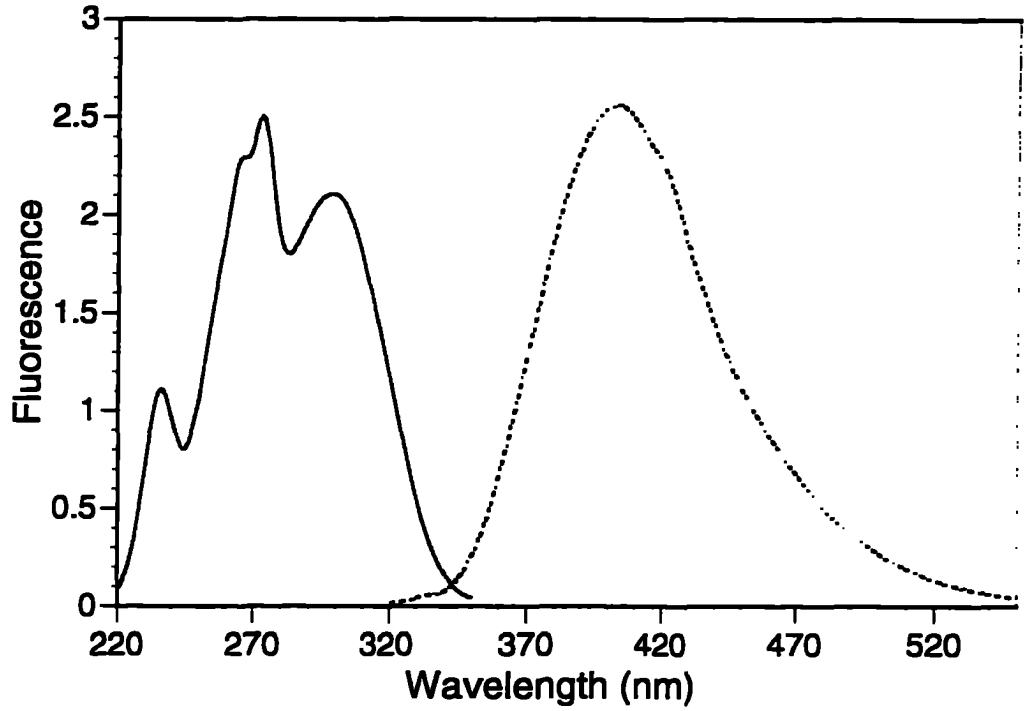

Figure 3.2.1 Corrected excitation and emission spectra of poly(εA) in a neutral buffer. The excitation spectra (solid line) was monitored at 400 nm and the emission spectra (dash line) was excited at 309 nm.

In order to examine the properties of this poly(A) analog, a fluorescence melting curve was carried out (Figure 3.2.2). The fluorescence melting measurement has an advantage over the UV melting measurements since the fluorescence measurement is more sensitive and can detect a subtle conformational change. The normalized fluorescence intensity was monitored as a function of temperature. Since poly(εA) contains secondary structure, the fluorescence intensity depends on the quenching due to the temperature and also the secondary structure change. Therefore, a control should be included to correct for the temperature effect. The εA monomer was used as

a control and the signal decreased as the temperature increased. After the correction, the fluorescence intensity of poly(εA) could be easily interpreted as a conformational change upon increasing temperature. There are three melting transitions observed in this melting curve, which occur at approximately 17, 25, and 35 °C. The melting curve of poly(εA) is almost identical to that of poly(A) (Inners & Felsenfeld, 1970), which demonstrates that poly(εA) should have very similar properties to poly(A). Poly(εA) is a very potent candidate for a fluorescence poly(A) analog.

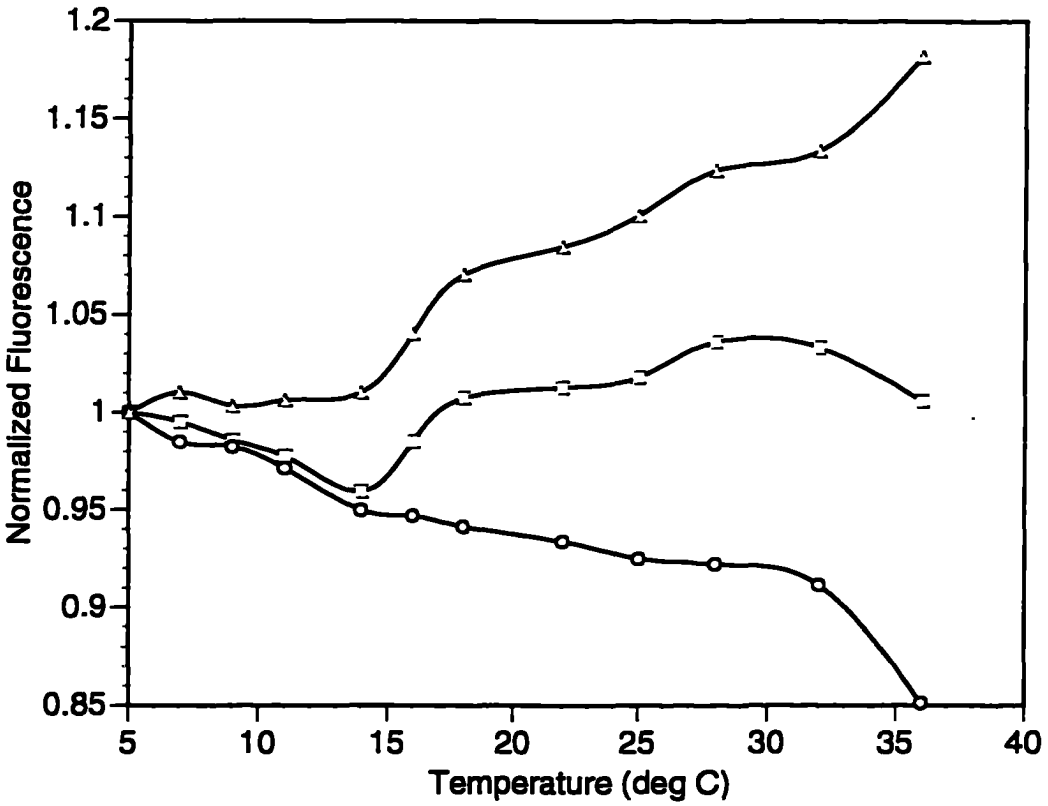

Figure 3.2.2 Fluorescence melting curve of poly(εA). Circles were the fluorescence intensity of εA monomer, as a function of temperature, squares were the melting curve of poly(εA), and triangles were the data after correction.

3.3 Determination of poly(A) binding size of PABP

Messenger RNA contains a poly(A) tail ranging from 25 bases to a thousand bases (review by Brawerman. 1981). PABP was found to bind the poly(A) very tightly (Sachs & Kornberg. 1985). Poly(εA) could be advantageously used to determine the binding size of PABP. Fig. 3.3.1 shows the titration of poly(εA) with PABP at very low ionic strength. which assured the maximum binding affinity. Poly(εA) bound with PABP has enhanced fluorescence intensity due to base unstacking of the poly(εA). This phenomena was demonstrated in the CD spectra (see the following text). The packing density was obtained from the stoichiometry of poly(εA) saturated with protein. Saturation occurred at a ratio of approximately 23 residues per molecule of PABP protein. This data was consistent with other reports (Sachs & Kornberg. 1985) and also indicated the shortest poly(A) tail of mRNA could have at least one PABP bound to it.

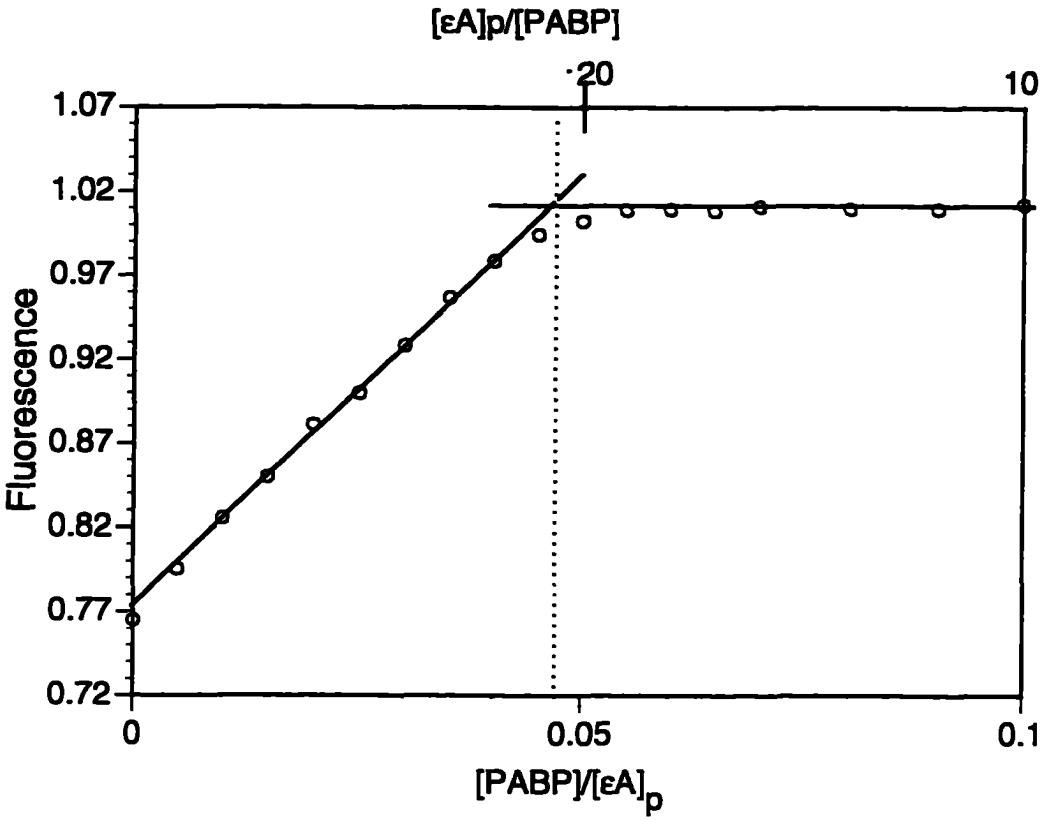

Figure 3.3.1 Determination of PABP binding size by using the fluorescent poly(A) analog, poly(εA). The excitation wavelength was 332 nm and the emission was monitored at 420 nm. The single residue concentration of nucleic acid ($[\varepsilon A]_p$) was used for this calculation.

3.4 Binding affinities of poly(A)$_{30}$ and poly(εA)$_{30}$ to PABP

From the melting curve and packing density measurements of poly(εA), it seems that poly(εA) has properties similar to poly(A). The binding measurements for poly(A) and poly(εA) to PABP from direct fluorescence titrations are summarized in Table. 1. In neutral buffer, PABP bound poly(εA)$_{30}$ with an affinity about 100-fold lower than that of poly(A)$_{30}$. The binding isotherms were fitted using a stoichiometric

1:1 ratio of oligonucleotide and protein. PABP contains four tandem repeat RNA-binding domains (RBDs), but it only bound one molecule of poly(A)$_{30}$ in this solution. When the concentration of NaCl is more than 1.0 M, the binding affinities for both poly(εA)$_{30}$ and poly(A)$_{30}$ decreased and the binding site size decreases to approximately 13 bases (Figure 3.4.1). These results are consistent with other literature (Kühn & Pieler, 1996), which states that PABP selects for oligo(A) with a minimum RNA chain length of 12 nucleotides.

Interaction	K_a (K_d)
poly(εA)$_{30}$ + PABP	$1.2 \pm 0.1 \times 10^6$ M^{-1} (0.83 ± 0.07 μM)
Poly(A)$_{30}$ + PABP	$8.7 \pm 0.3 \times 10^7$ M^{-1} (11.4 ± 0.4 nM)

Table 1 Fluorescence measurements on binding poly(εA)$_{30}$ and poly(A)$_{30}$ to PABP.

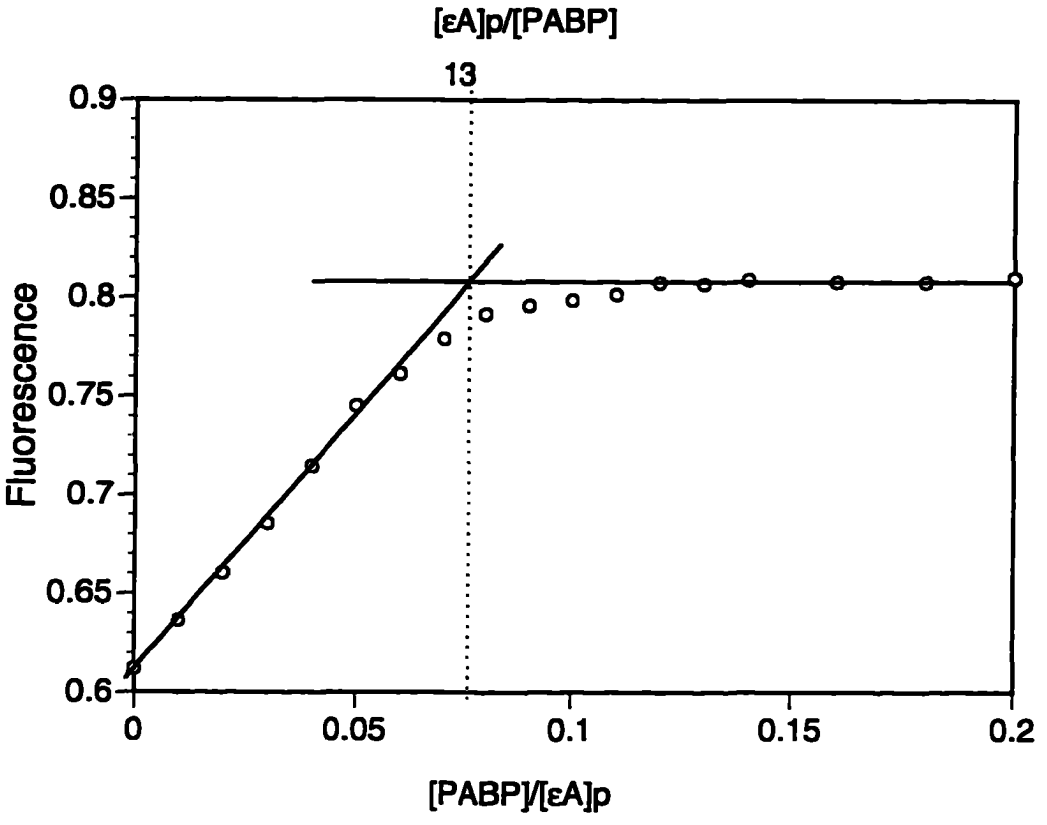

Figure 3.4.1 Determination of PABP binding size by using the fluorescent poly(A) analog, poly(εA), in a neutral solution containing 1.0 M NaCl. The excited wavelength was 332 nm and the emission was monitored at 420 nm.

CD techniques allowed us to detect the formation of a complex of PABP with poly(A). The poly(A) was used because the CD bands occur in a 250 nm - 300 nm region free from protein contribution. In a mixture of poly(A) with different amounts of PABP, there is a decrease in the CD absorption at 250 nm - 300 nm (Figure 3.4.2).

This phenomena indicates that addition of protein destroys the secondary structure of poly(A) by unstacking its bases.

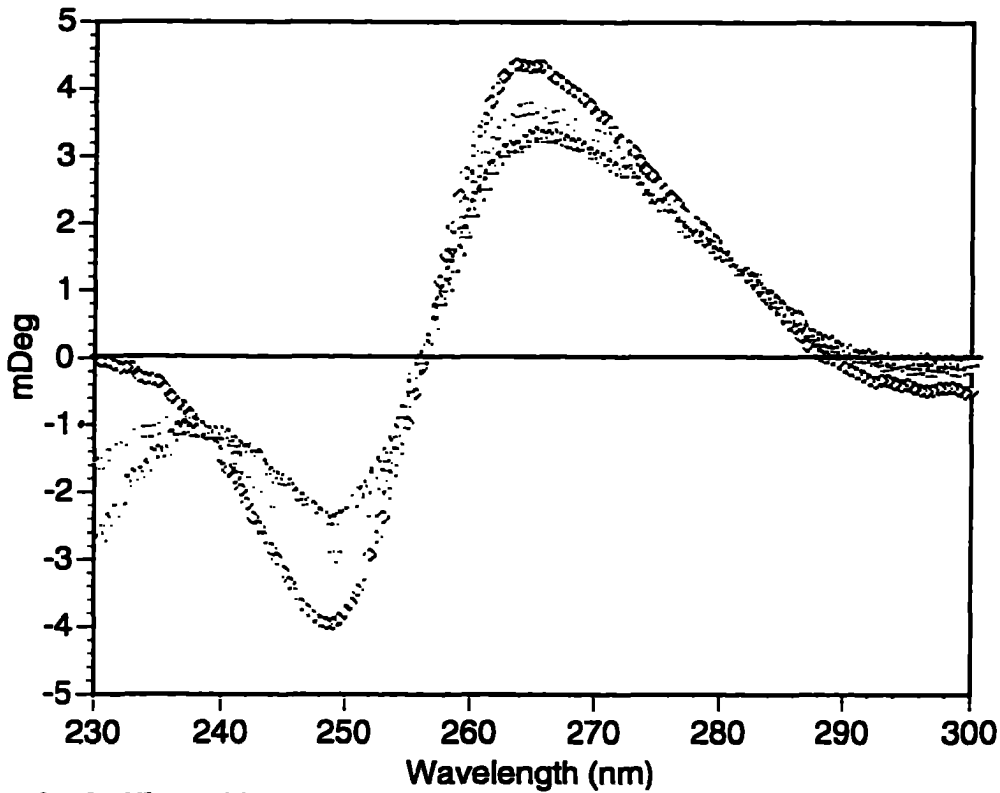

Figure 3.4.2 Effect of PABP on the CD spectrum of poly(A). The ratios of PABP to nucleotide are 0 (squares), 0.02 (circles), and 0.1 (triangles). The temperature was 20 °C.

The Stern-Volmer plot of poly(εA) and the poly(εA)/PABP complex are shown in Figure 3.4.3. The fluorescence quenching in the poly(εA)/PABP complex was less

than that shown by poly(εA) alone, indicating that εA bases were buried inside the PABP making the bases less accessible. It is interesting that poly(εA) contains many fluorescent motifs, but showed a linear relationship in a Stern-Volmer plot, suggesting that the polymer formed a conformation that was homogenous as far as quenching was concerned.

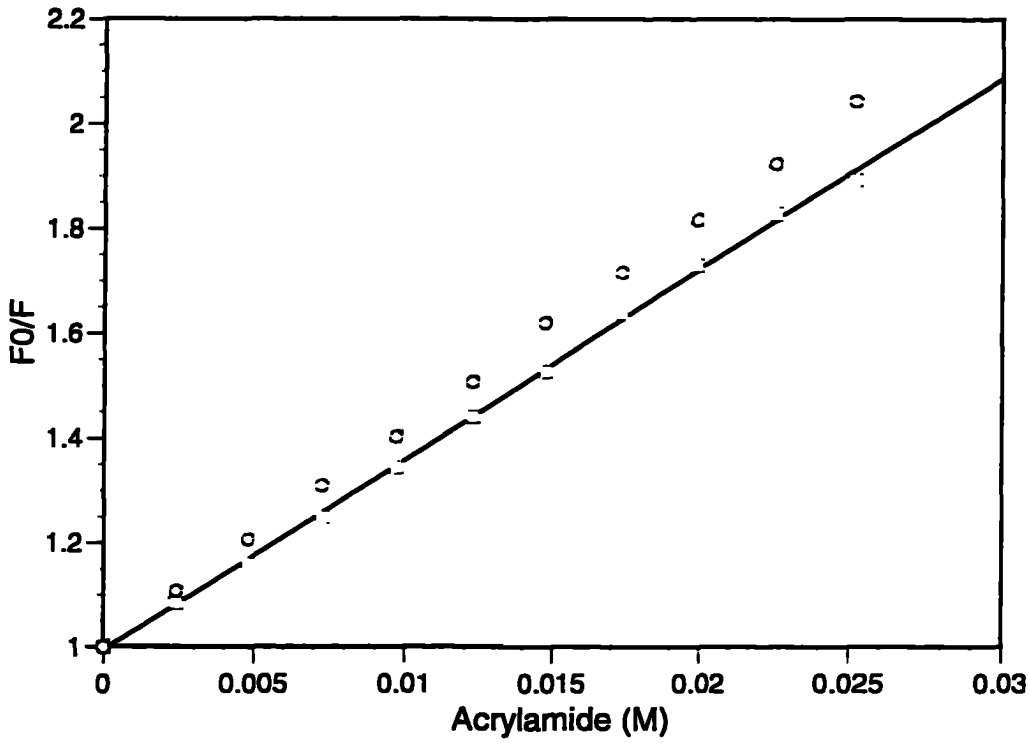

Figure 3.4.3 Stern-Volmer Plot for poly(εA) alone (circles) and poly(εA)/PABP complex (squares). The data showed that fluorescence quenching of poly(εA) complex was less than poly(εA) alone, indicating that fluorescence motifs were buried inside the PABP, so that they were less solvent accessible.

3.5 Interaction of PABP with other homopolymers

Poly(A)-binding protein was originally named from its binding to poly(A). As a matter of fact, this protein not only binds to poly(A), but also to other homopolymers. The competitive titration of poly(A), poly(G), poly(U), and poly(C) for PABP in poly(εA)/PABP complexation is shown in Figure 3.5.1. As would be expected, poly(A) competes for PABP very efficiently. The fluorescence intensity decreased sharply due to the release of poly(εA) from the complex. Poly(U) and poly(G) also showed a binding affinity for PABP, but not as strong as poly(A). In contrast, poly(C) was not capable of competing with poly(εA). The PABP interaction with poly(A) is at least 100-fold greater than that for most other polynucleotides, such as poly(G) and poly(U). This observation that PABP does not bind poly(C), has prompted us to investigate which parts of polynucleotides are involved in this interaction. Even though there is a lack of direct evidence, a search through the literature has led to the conclusion that the possible interaction sites in the homopolymer may be their ribose-phosphate group. In other words, the orientation of bases in the polymer plays a very important role in these interactions. A synthetic unicapeptide (GKSKGFGFV) which was found in all the sequenced eukaryotic PABP was determined to have a β-sheet conformation (Rubin & Halim, 1993) and believed to be the binding site for poly(A). Solution spectroscopic data (Evans & Sarma, 1976; Prescott et al., 1974; Brahms et al., 1966) suggests that poly(A) at neutral pH forms a righted-hand single helix, with nucleotides in 3'-*endo* conformation, classifying this helix as a member of the A

family helices. Bases are *anti* oriented and stacked parallel to each other. Poly(U) does not have a unique conformation in physiological conditions. At low temperatures the structure is best defined as a hairpin loop formed by folding of the poly(U) molecule back on itself, resulting in a double-helix, anti-oriented arrangement with asymmetric double helices (Young & Kallenbach, 1978; Rabczenko & Shugar, 1971). Poly(G) can form a quadruple complex and can also exist as ordered single, double, and hexamer helical structure (Sarkar & Yang, 1965; Thiele & Guschlbauer, 1973). It is clear that poly(A), poly(G), and poly(U) have structures where the bases of homopolymer are located inside the helix core. All of the ribose-phosphate groups were solvated by the surrounding solution. In contrast, poly(C) has a very different structure from the polymers mentioned above, as proposed by NMR studies in the neutral solution (Broido & Kearns, 1982). Poly(C) belongs to the A family with left-handed helix structures which are similar to the poly(dT) structure. In such a conformation, the ribose-phosphate backbone is buried inside and bases are on the periphery. This geometry is different from that derived on the basis of the fiber diffraction of poly(C). The cytosine base prevents its ribo-phosphorous group form interacting with PABP. This may explain why poly(C) has no binding affinity to PABP. The larger core sizes of poly(U) and poly(G), partially due to multimer formation, makes it difficult for these homopolymers to approach the binding site of PABP. Any modification of poly(A), for instance poly(εA), changes its conformation but the macro structure still remains a similar helical structure. This decreases its

PABP binding activity. The proposed models for these homopolymers are summarized in Figure 3.5.2.

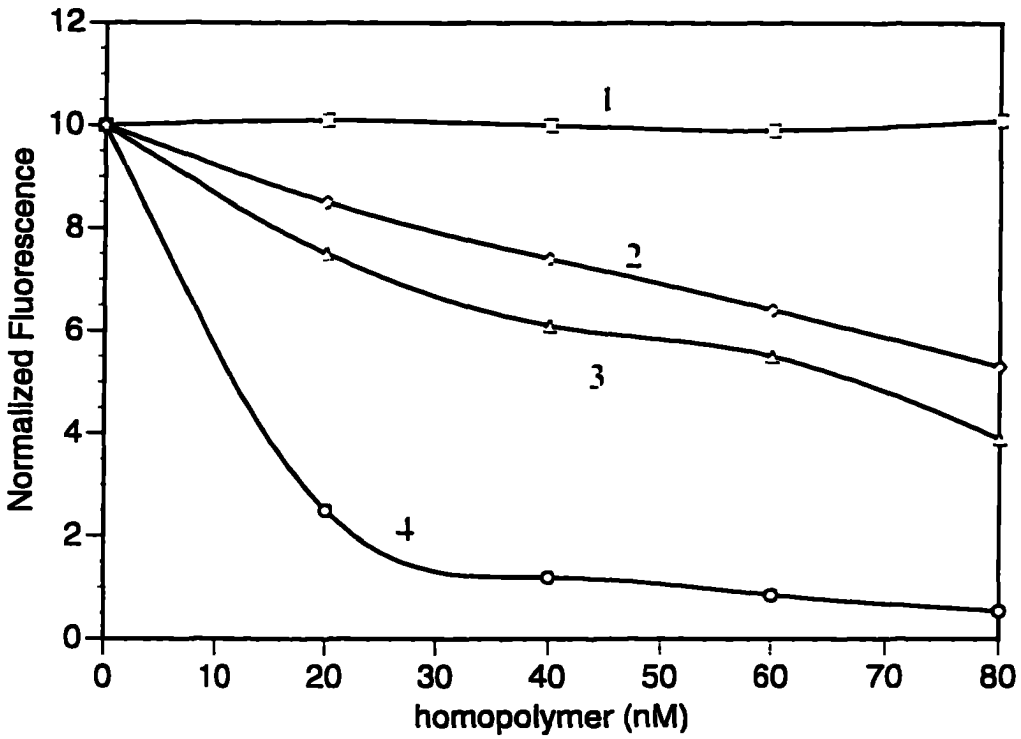

Figure 3.5.1 Competitive curves of poly(εA) to PABP with poly(A) (line 4), poly(U) (line 3), poly(G) (line 2), and poly(C) (line 1). Emission was measured at 420 nm with excited at 332 nm. The concentration of poly(εA)30 and PABP were 2.0 μM. The average lengths of the homopolymers used were approximately 200 bases.

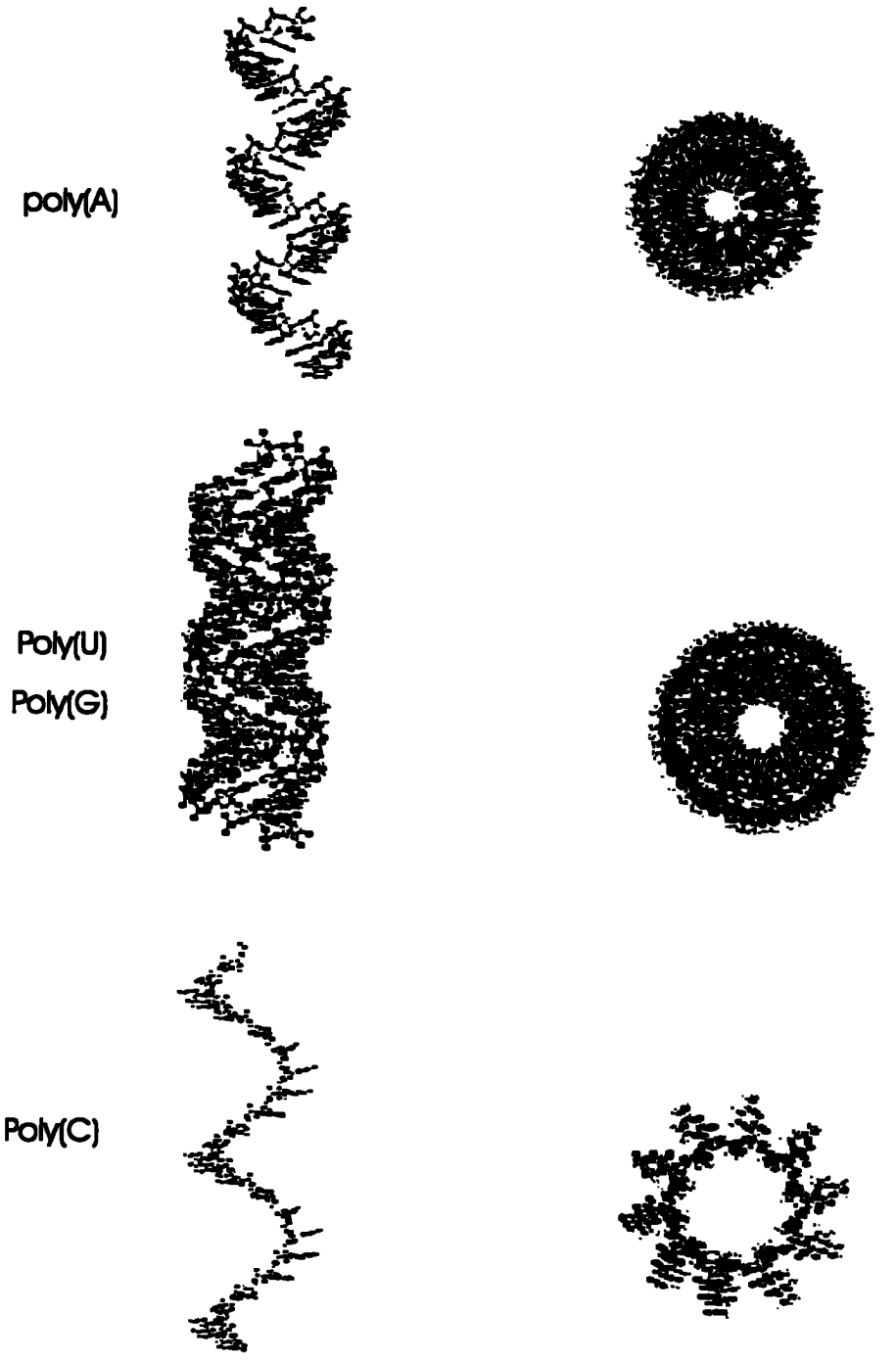

Figure 3.5.2 Proposed structure of poly(A), poly(G), poly(U), and poly(C)

3.6 Protein-protein interactions of PABP and cap-associated proteins, eIF-4B, eIF-(iso)4F, and eIF-4F

Cap-associated proteins, eIF-4F, eIF-(iso)4F, and eIF-4B, were first demonstrated to have binding affinity for PABP by far Western Blotting and fluorescence spectroscopy (Le, et al. 1997). The direct fluorescence titration showed that they interacted and enhanced the fluorescence intensity (Figure 3.6.1). In a titration where protein concentrations were in the μM range, their K_ds were found to less than 40 nM for eIF-4F and eIF-(iso)4F. For eIF-4B, the K_d was approximately 15 nM (data not shown). In order to determine the high binding affinities, more dilute protein solutions were used. Instead of using an emission monochromator, a cut-on filter (50% transmission at 305 nm) was used to give a higher signal. The fluorescence intensity of the protein-protein complex is greater than the sum of individual fluorescence intensities indicating that one or both of these proteins undergo a conformational change upon complex formation (Figure 3.6.2). The K_d values of the three cap-associated proteins, eIF-4B, eIF-4F, and eIF-(iso)4F, interacting with PABP are shown in Table 2. These data showed that the cap-associated proteins have binding affinities of 4-9 nM. The eIF-4B had the strongest binding affinity toward PABP. In contrast, eIF-4A did not bind to the cap region and showed no interaction with PABP. These data showed a significant standard deviation due to the low fluorescence intensity associated with the concentration of protein needed to obtain these equilibrium constants. The possibility of trace amounts of poly(A) contamination can be ruled out

based on the fact that cap-associated proteins bound to PABP stoichiometrically in a 1:1 ratio and the fact that SDS-PAGE gels of purified PABP when silver stained showed no oligonucleotides present. As a further control, a solution containing T2 RNase was incubated with PABP, and then the solution was titrated with the above initiation factors. The binding constants did not show any significant change. These data demonstrated that PABP does not require poly(A) to bind cap-associated proteins in contrast to the data for the yeast protein (Tarun & Sachs, 1996). The authors claimed eIF-4G from yeast *saccaromyces cerevisiae* species did not have the ability to bind PABP in the absence of the poly(A).

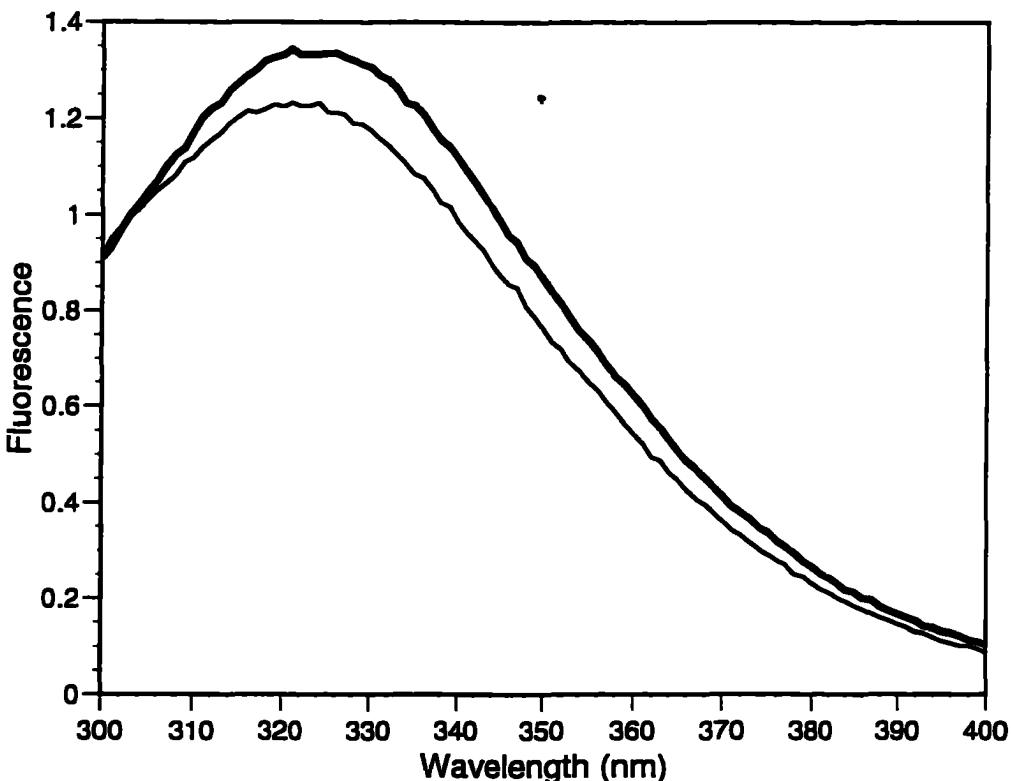

Figure 3.6.1 A fluorescence spectra of a solution of PABP/eIF-(iso)4F complex (thick line) is compared with the sum of their individual fluorescence spectra (thin line). The fluorescence enhancement indicates these proteins interact.

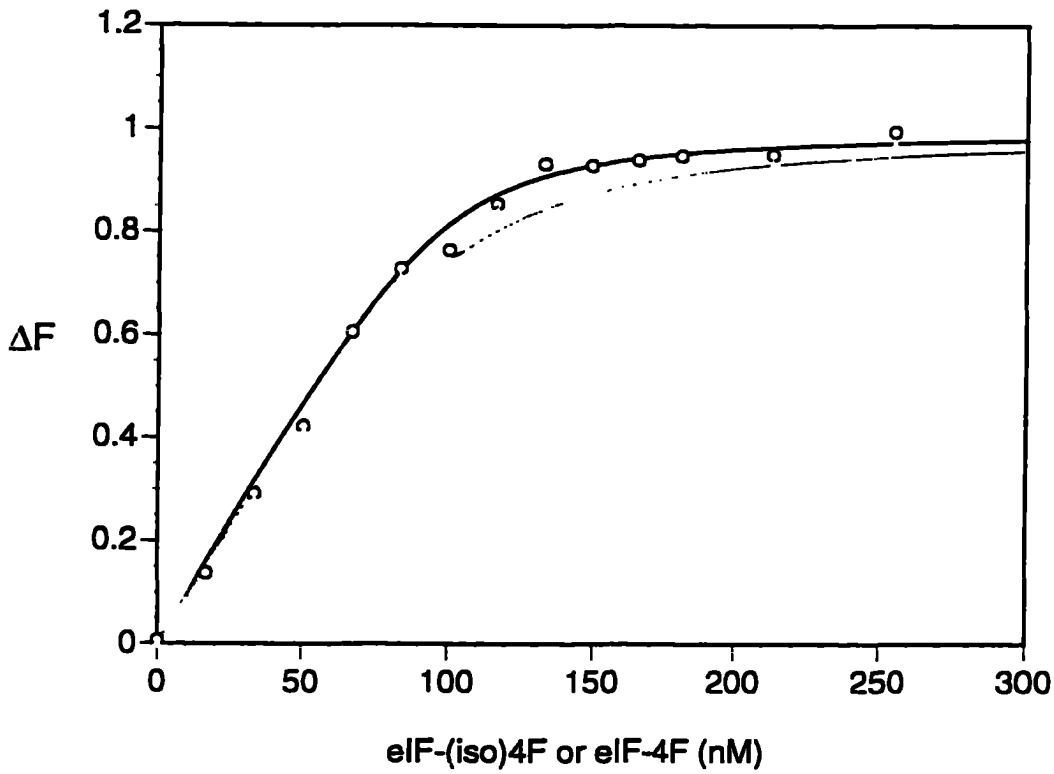

Figure 3.6.2 A solution of 100 nM purified PABP was titrated with eIF-(iso)4F (circles) and eIF-4F (triangles). The excitation was 265 nm and emission was monitored with a 305 nm cut-on filter. The solid lines represent the best fitting curves as described in Experimental Procedure and the K_ds were determined to be 4.3 ± 1.9 nM and 9.1 ±4.1 nM for eIF-(iso)4F/PABP and eIF-4F/PABP.

Interaction	K_d
eIF-4B + PABP	2.5 ± 1.1 nM
eIF-4F + PABP	9.1 ± 4.1 nM
eIF-(iso)4F + PABP	4.3 ± 1.9 nM
eIF-4A + PABP	ND*

Table 2 Summary for the dissociation constants for the various initiation factors to PABP.
** ND: not detected.*

3.7 Interaction of ant-m^{7}GTP and m^{7}GTP with cap-binding proteins

It has been shown (Sonenberg & Shatkin. 1978. Sonenberg et al.. 1981; Tahara et al.. 1981; Grifo et al.. 1983) that only the 7-methylguanosine. ribose. and phosphoryl moiety are necessary for cap-binding protein recognition. It has been demonstrated that the binding properties of m^{7}GDP and m^{7}GTP are very similar to dinucleotide caps (m^{7}GpppX) (Goss et al.. 1987) and have been used as a cap analog (Carberry et al.. 1989; Goss et al.. 1990). A derivative of m^{7}GTP should therefore serve as a suitable substrate for cap-binding proteins.

A suitable fluorescence label on m^{7}GTP provides a better application in cap-binding studies since it will eliminate the inner-filter correction in a direct fluorescence titration of the intrinsic protein fluorescence. The synthesis strategy (Ren

& Goss, 1996) was chosen to put a fluorescent probe, an anthraniloyl group, on the ribose of m^7GTP following a similar procedure described elsewhere (Hiratsuka, 1983). When GDP was treated with isatoic anhydride in alkaline solution, almost 100% 3' modified GDP was obtained. In contrast, treatment of m^7GTP with the same procedure produced approximately 20 % of anthraniloyl labeled products. The final products contained two isomers, 2' and 3' modified m^7GTP in a 1:3 ratio (Ren & Goss, 1996). This demonstrated that a small methyl group attached to guanine induced a polarity change of the whole motif which affects the activity and selectivity of this reaction. Figure 3.7.1 shows the synthesis scheme.

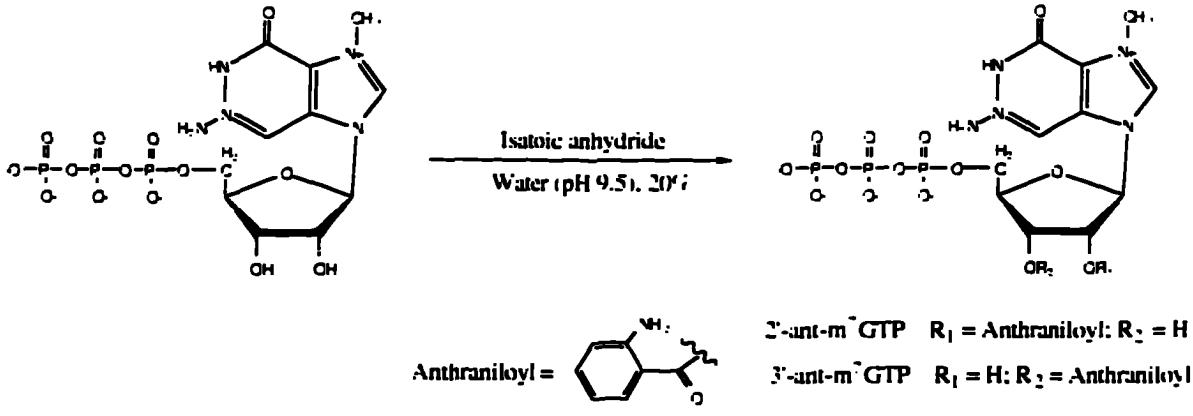

Figure 3.7.1 Synthesis scheme for 2'-ant-m^7GTP and 3'-ant-m^7GTP

The 2' and 3'- ant-m^7GTP could be easily separated by simple gel filtration. Ren and Goss (1996) found that they did not show any significant binding difference to cap-binding proteins and that the separation of these isomers is not necessary for cap-binding measurements. The corrected fluorescence spectra showed an excitation maximum at 332 nm and emission maximum at 420 nm (Figure 3.7.2). The fluorescent quantum yield was determined to be 0.15 in aqueous solution and several fold larger in organic solutions. AM1 semi-empirical calculation by HyperChem program (Hypercube, Inc., Ontario, Canada) of 3'-ant-m^7GTP is shown in Figure 3.7.3 indicating that the guanine, triphosphate diester, and ribose-labeled anthraniloyl group were located away from one another without distortion of structure.

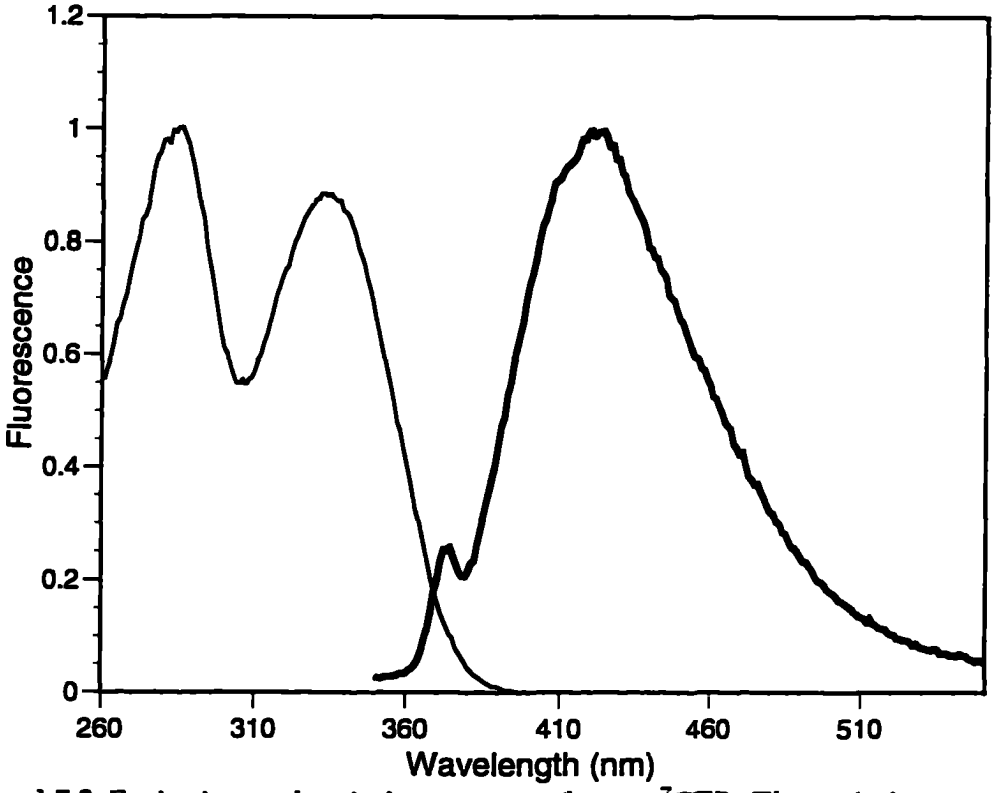

Figure 3.7.2 Excitation and emission spectra of ant-m^{7}GTP. The emission spectrum (thick line) was excited at 332 nm, and the excitation spectrum (thin line) was monitored at 420 nm.

Figure 3.7.3 AM1 semi-empirical calculation of 3'-ant-m^{7}GTP.

The anisotropy ranged from 0.03 for unbound fluorophore to 0.12 for ant-m^{7}GTP/eIF-(iso)4F (Figure 3.7.4). The ant-m^{7}GTP/eIF-4F complex had an anisotropy value of 0.16. By fitting the data according to eq. 7. the K_ds were calculated to be 8.93 ± 1.04 μM for ant-m^{7}GTP/eIF-(iso)4F and 4.69 ± 0.07 μM for ant-m^{7}GTP/eIF-4F (Figure 3.7.4). To determine whether this modification affected the cap binding, the binding affinities for these cap-binding proteins with unmodified cap analog, m^{7}GTP, were determined by direct fluorescence titration using intrinsic fluorescence of protein with inner-filter correction. The data are summarized in Table

3. The binding affinity for the modified and unmodified cap analogs were almost identical.

The characteristic anisotropy of the ant-m^{7}GTP/eIF-4F complex was higher than that of the ant-m^{7}GTP/eIF-(iso)4F complex because the eIF-4F has almost twice the molecular weight of eIF-(iso)4F (246 kDa as compared to 114 kDa) while the fluorescence lifetimes of the complexes were similar. The observed steady-state anisotropy depends on the correlation time (t_c) of fluorophore and its lifetime (Lakowicz. 1983). Free ant-m^{7}GTP has a fluorescence excited state lifetime of 2.0 nsec (Figure 3.7.5). Lifetime measurements on the ant-m^{7}GTP/eIF-(iso)4F showed a longer lifetime of 6.8 nsec attributable to the protein complex. The ant-m^{7}GTP/eIF-4F complex has a shorter lifetime of 5.0 nsec. The fluorescence enhancement and longer lifetime of the protein bound form of ant-m^{7}GTP may be due to the formation of hydrogen bond(s) which stabilize its charge transfer excited state or the cap binding pocket may be a more hydrophobic region (Birmachu & Reed. 1988). The recent X-ray crystal structure of murine eIF-4E (Marcotrigiano et al. 1997) indicates that the 7-methyl G recognition is mediated by the guanosine base interaction between two conserved tryptophans. plus formation of three hydrogen bonds and a van der Waals interaction between its N-7 methyl group and a third conserved tryptophan. The ribose of cap is located in a hydrophobic region which may allow the non-protonated chromophore of the ant-m^{7}GTP to enter the binding pocket. Stabilization of the polar excited state would result in a longer lifetime. These data showed no significant

binding affinity change consistent with the observation that most nucleotide-binding proteins are sensitive to structural variations in the purine ring, but modifications of the ribose moiety have little effect on binding affinity (Darzynkiewicz et al., 1987, 1988, 1989).

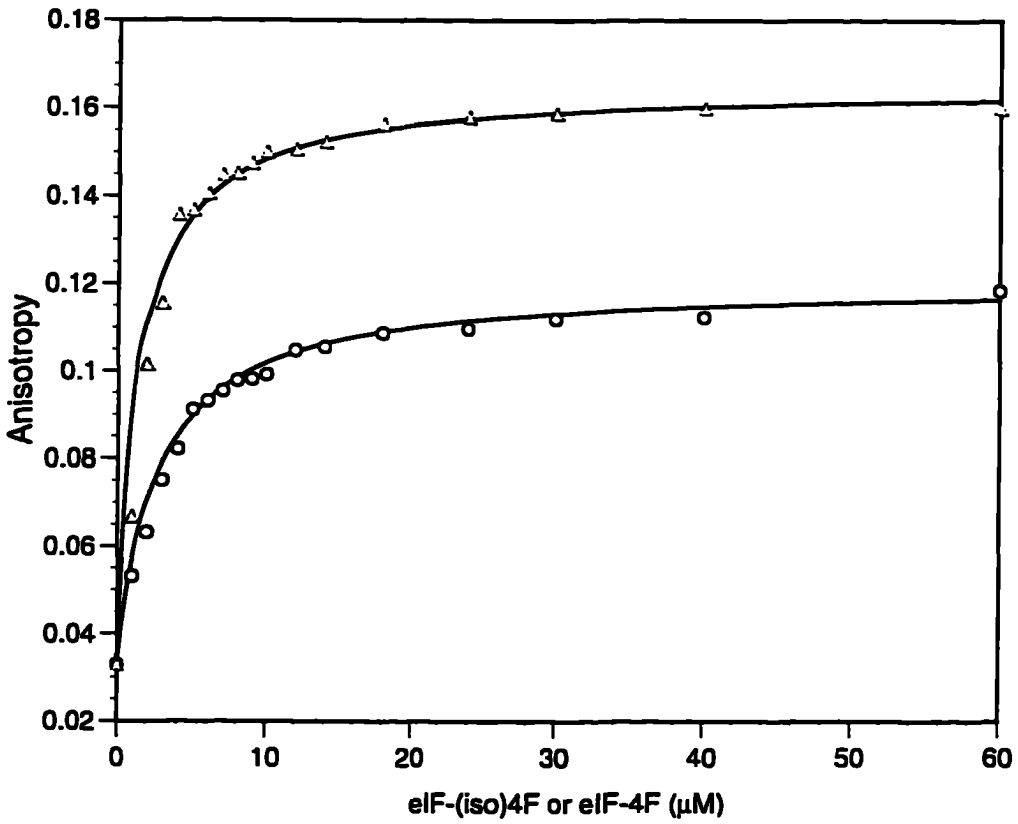

Figure 3.7.4 Steady state anisotropy measurement of eIF-(iso)4F (circles) and eIF-4F (triangles) with ant-m^{7}GTP interaction. Excitation wavelength was 332 nm, and emission was monitored at 420 nm.

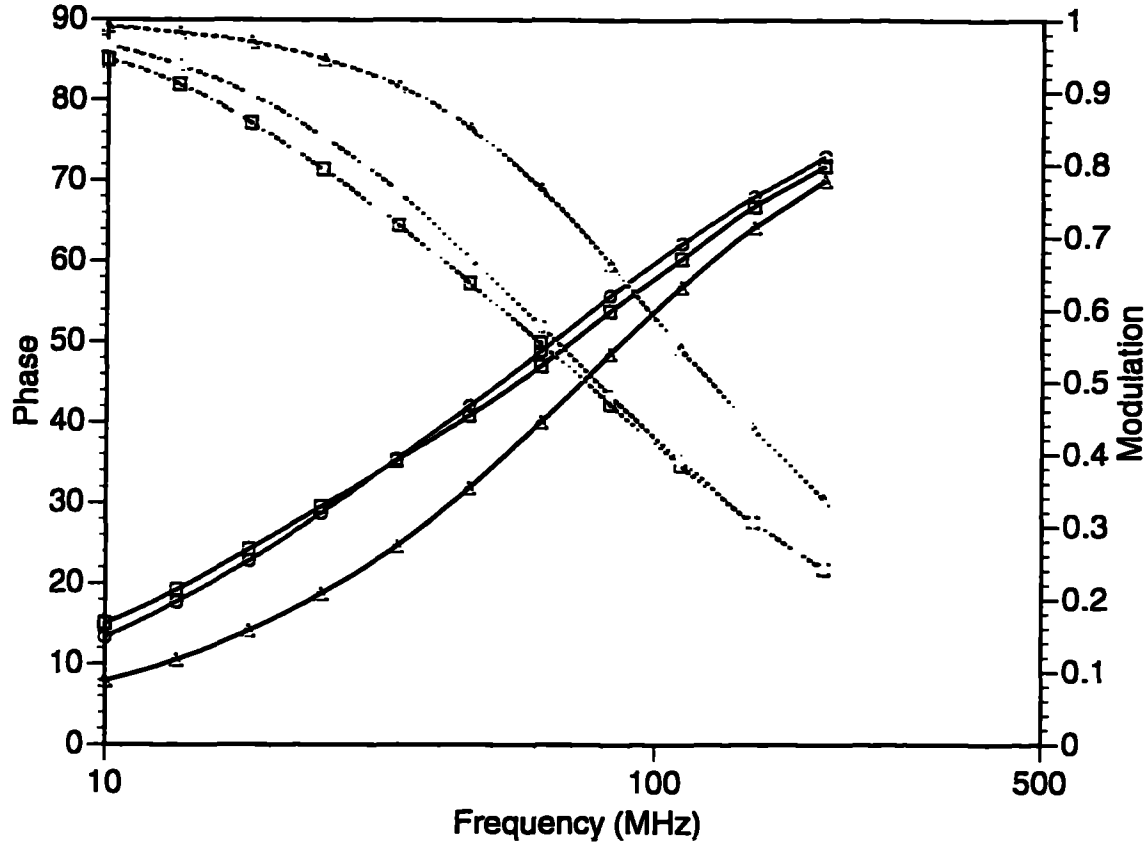

Figure 3.7.5 Phase and modulation values as a function of frequency for ant-m^{7}GTP bound to eIF-(iso)4F. 1. ant-m^{7}GTP alone (triangles). The solid line was fitted as a one-exponential decay with a lifetime of 2.0 nsec. 2. ant-m^{7}GTP and eIF-(iso)4F (squares). The solid line corresponds to a two-exponential component fit of the data with lifetimes τ_1 = 1.98 ns and τ_2 = 6.93 ns having a fractional amplitude f_1 = 0.513 and f_2 = 0.487. 3. ant-m^{7}GTP and eIF-4F (circles). The solid line represents τ_1 = 2.01 nsec and τ_2 = 5.04 nsec having a fraction amplitude f_1 = 0.404 and f_2 = 0.596.

Complex	K_a (M^{-1})
eIF-4F/ant-m^7GTP	(2.12 ± 0.15) x 10^5
eIF-(iso)4F/ant-m^7GTP	(1.12 ± 0.13) x 10^5
eIF-4F/m^7GTP	(2.2 ± 0.2) x 10^5
eIF-4F/m^7GTP	(1.0 ± 0.2) x 10^5
eIF-4F/$m^7G_{ppp}G$[b]	(2.1 ± 0.1) x 10^5

Table 3 Summary of the association binding constants (K_as) for various protein/cap analog interactions.[a]

[a] *All solution prepared in pH 7.6 buffer.*

[b] *Goss et al. (1990) Biochim. Biophys. Acta 1050, 163-166.*

3.8 Studies of Ternary system - ant-m^7GTP, PABP, eIF-4F, and eIF-(iso)4F

For ternary ant-m^7GTP/eIF-(iso)4F/PABP and ant-m^7GTP/eIF-4F/PABP studies, steady-state fluorescence spectra were examined. Figure 3.8.1 showed the emission spectra of different ant-m^7GTP complexes excited at 332 nm. The ant-m^7GTP, when excited at 332 nm, shows a maximum fluorescence intensity at 420 nm. Upon addition of PABP, no fluorescence intensity change was observed, indicating that no interaction between this cap analog and PABP occurred. This result was confirmed using anisotropy and lifetime measurements (data not shown) which also do not show any change upon addition of PABP. Fluorescence intensity was enhanced and the

emission wavelength maximum shifted when eIF-(iso)4F was added to the cap analog. Under conditions where concentrations of eIF-(iso)4F and PABP are larger than the concentration of cap analog. no significant fluorescence intensity difference between cap analog/eIF complex and cap analog/eIFs/PABP complex was observed. The lifetime analysis on this ternary system could be fitted to a two-exponential decay with the same results as the ant-m^7GTP/eIF-(iso)4F system (one short lifetime for ant-m^7GTP and one longer lifetime for the protein complex). This suggested that the microenvironment of the cap analog was similar in the cap analog/eIF and the cap analog/eIF/PABP complexes.

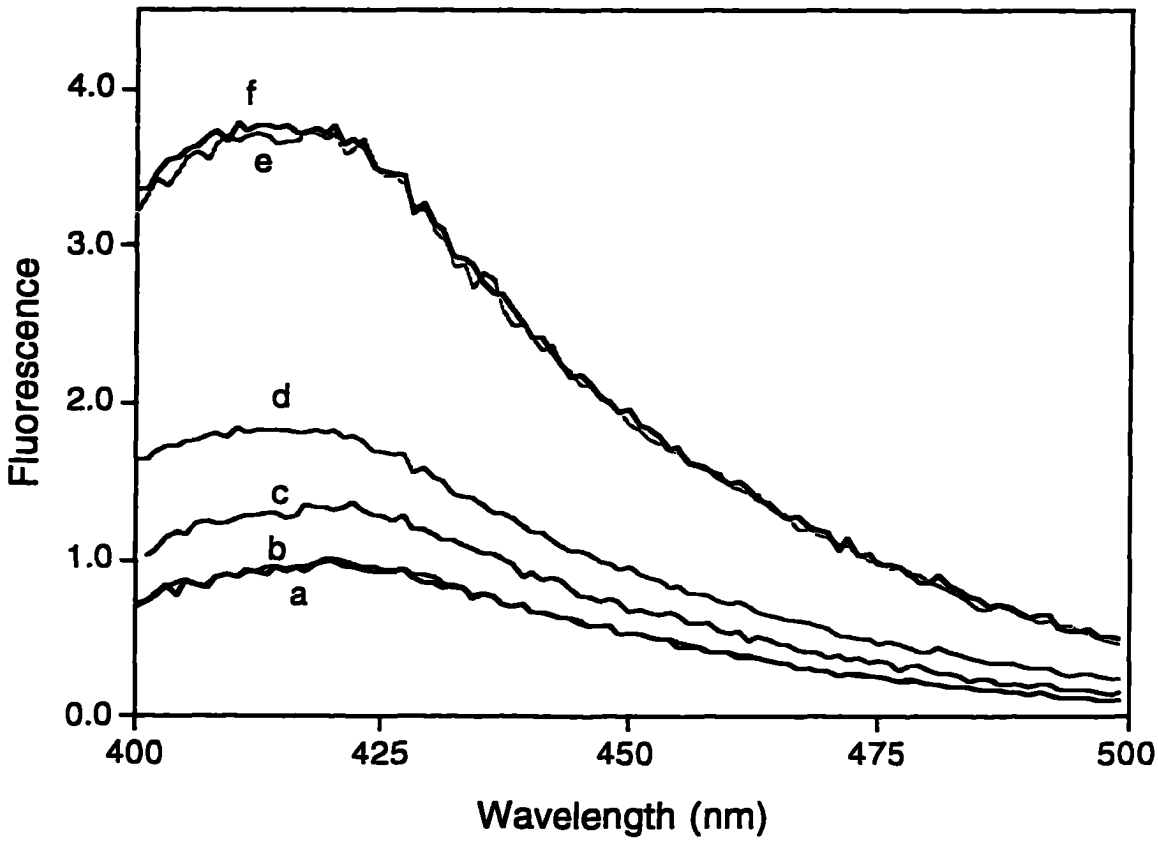

Figure 3.8.1 Corrected fluorescence emission spectra of 25 nM ant-m^7GTP (a) ant-m^7GTP alone (b) + 0.4 μM PABP (c) + 0.02 μM eIF-(iso)4F (d) + 0.02 μM eIF-(iso)4F + 0.01 μM PABP (e) + 1.5 μM eIF-(iso)4F (f) + 1.5 μM eIF-(iso)4F + 25 μM PABP. All samples were excited at 332 nm.

A typical binding isotherm can be developed as described elsewhere (Heyduk & Lee, 1990). For a simple binary reaction,

$$\text{Cap}^* + \text{eIF} \Longleftrightarrow \text{Cap}^*\cdot\text{eIF}$$

$$F = \frac{KF_1[eIF] + F_o}{1 + K[eIF]} \qquad \text{eq. 17}$$

$$[eIF] = \frac{-(1 + K[Cap^*]_T - K[eIF]_T) + \sqrt{(1 + K[Cap^*]_T - K[eIF]_T)^2 + 4K[eIF]_T}}{2K}$$

Eq. 17 can be solved for association constant (K) and where cap*, eIF, and cap*•eIF are free fluorescent ant-m^{7}GTP, cap-binding protein, and ant-m^{7}GTP/eIF complex, respectively. $[Cap^*]_T$ and $[eIF]_T$ are the total concentrations of ant-m^{7}GTP and protein, respectively. F is the measured value of the fluorescence intensity at any point in the titration. F_0 and F_1 are the fluorescence intensities at the start and at the end of the titration, respectively. Thus, K can be obtained by fitting the experimental data using nonlinear regression analysis. In principle, any one point will give a K value if the initial and final points are known, there is therefore, considerable redundancy in the data fitting.

For the ternary system, the fluorescence data were treated analogously. Binding of eIFs to PABP in the presence of cap analog can be described as shown in Scheme 2.

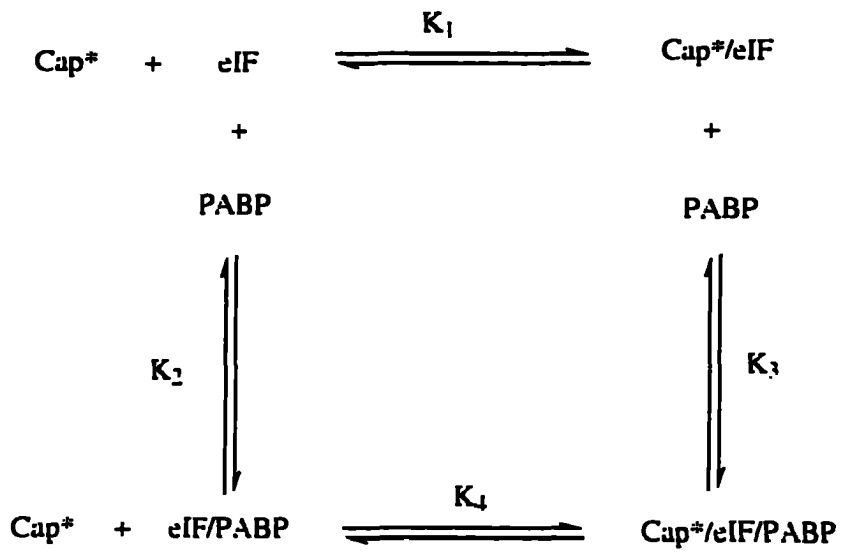

Scheme 2

From our previous data, PABP does not bind to the cap analog under these conditions. K_1 and K_2 are dissociation constants for ant-m^7GTP/eIF and eIF/PABP, respectively. K_3 and K_4 are dissociation constants for cap analog/eIFs to PABP and eIFs/PABP to cap analog, respectively. Thermodynamically, $K_1K_3 = K_2K_4$. In accordance with Scheme 2, the apparent association constant (K_{app}) is derived as follows.

$$K_{app} = \frac{([Cap^* \bullet eIF]) + (F_2 / F_3)[Cap^* \bullet eIF \bullet PABP]}{[Cap^*]([eIF] + [eIF \bullet PABP])}$$

$$= \frac{\dfrac{([Cap^* \bullet eIF]) + (F_2 / F_3)[Cap^* \bullet eIF \bullet PABP]}{[Cap^*][eIF]}}{\dfrac{[Cap^*]([eIF] + [eIF \bullet PABP])}{[Cap^*][eIF]}}$$

$$= \frac{(1/K_1)+(F_2/F_3)(1/K_1)(1/K_3)[PABP]}{1+(1/K_2)[PABP]} \qquad \text{eq. 18}$$

where [PABP] was the concentration of free PABP and F_2 and F_3 are fluorescence intensities (integrated from 400 to 500 nm) of ant-m^{7}GTP/eIF and ant-m^{7}GTP/eIF/PABP complexes, respectively. Under conditions where [PABP] >> [Cap*] and [PABP] >> [eIFs], [PABP] = $[PABP]_T$, where $[PABP]_T$ was the total concentration of PABP. This equation has only one variable, K_3 or K_4. A titration curve where 25 nM ant-m^{7}GTP and 20 μM PABP was titrated with eIF-(iso)4F is shown in Figure 3.8.2. The solid line represents the best fit of the data for eq 17. The K_{app} value obtained was (5.02 ± 0.12) x 10^6 M^{-1} and (8.13 ± 0.24) x 10^6 M^{-1} for ternary cap ant-m^{7}GTP/eIF-(iso)4F/PABP and ant-m^{7}GTP/eIF4F/PABP system, respectively. Theoretically, from eq. 18, K_{app} is a function of [PABP]. By changing the concentration of PABP, we could solve for all of the K_d values in Scheme 2 by nonlinear regression analysis without individual binding measurements. However, limitations on the amount of protein needed made this impractical. The values of the K_3 and K_4 were fitted as nM and μM for ant-m^{7}GTP/eIF to PABP and eIF/PABP to ant-m^{7}GTP, respectively. Increasing the concentration of PABP two fold did not alter Kapp significantly (Figure 3.8.2). This result was reasonable considering the K_1 and K_2 values obtained from separate titrations since any concentration of PABP used in the μM range will be canceled out in eq. 18. The exact values of K_d for eIF-(iso)4F

and eIF-4F are summarized in Table 4. The presence of cap analog enhances the binding of eIF to PABP approximately 40 fold. The binding affinities of the eIF/PABP complexes to cap analog were enhanced approximately 40-fold compared to the affinity of cap-binding proteins alone. The two cap-binding proteins . eIF-4F and eIF-(iso)4F behaved very similarly. In both cases, the presence of PABP enhanced cap binding affinity and the presence of the cap enhanced protein complex formation. Figure 3.8.3 is the titration curves for eIF-(iso)4F to ant-m^7GTP alone and ant-m^7GTP/PABP complex, which shows clearly that PABP enhances the cap binding affinity of cap-binding protein.

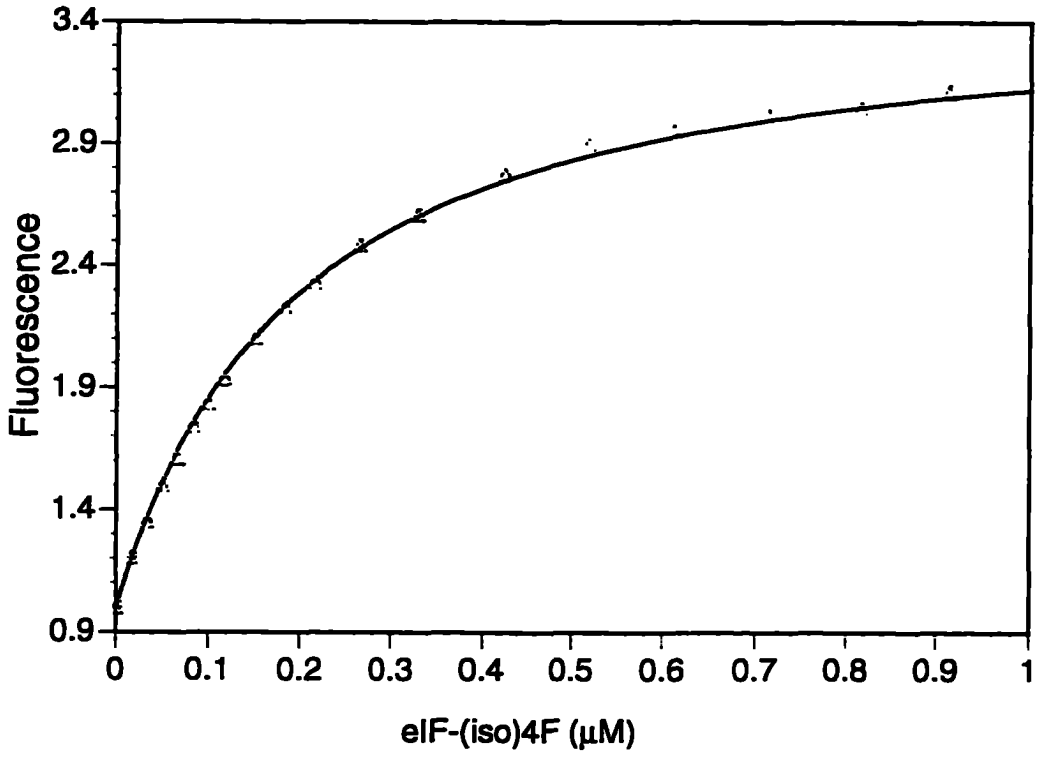

Figure 3.8.2. Binding of eIF-(iso)4F to PABP/ant-m^{7}GTP. (a) Concentrations of ant-m^{7}GTP and PABP were 25 nM and 20 μM (circles), respectively. The solid line represents the best fit to eq. 17. (b) Concentrations of ant-m^{7}GTP and PABP were 25 nM and 40 μM (triangles), respectively. Excitation was at 332 nm and fluorescence emission was integrated from 400 nm to 500 nm.

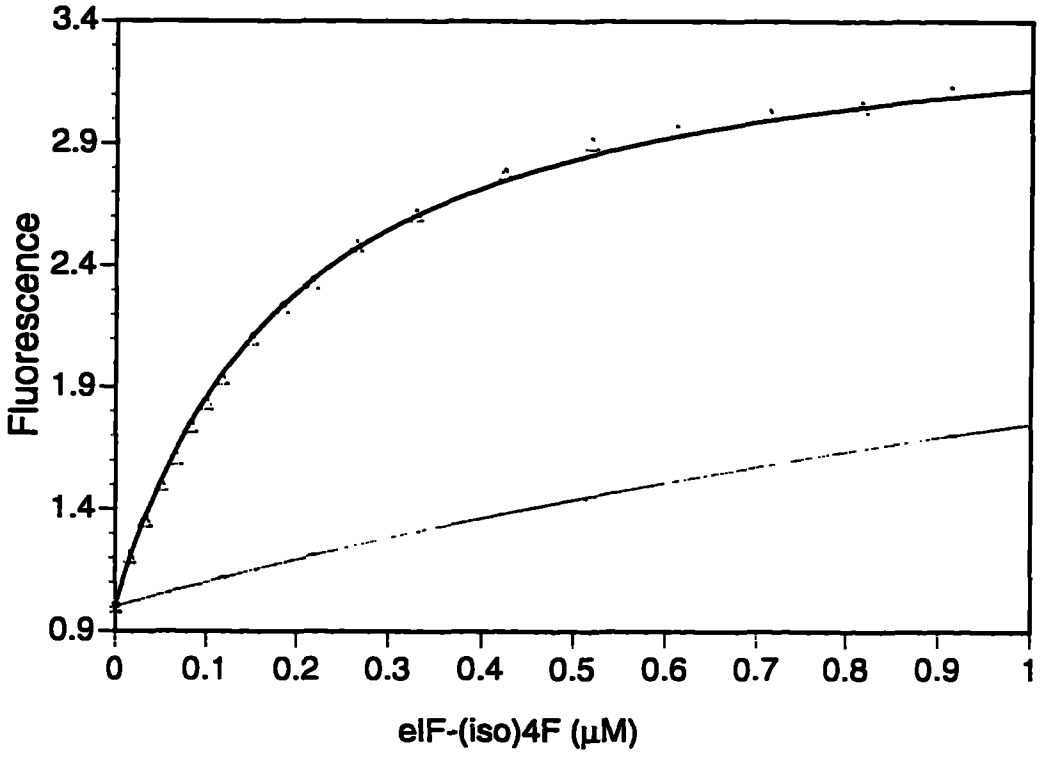

Figure 3.8.3 Comparison of binding for ant-m^{7}GTP/PABP (triangles) and ant-m7GTP (circles) to eIF-(iso)4F. The concentrations of ant-m^{7}GTP and PABP were 25 nM and 25 μM, respectively. The steeper binding curve for titration of ant-m^{7}GTP/PABP with eIF-(iso)4F than that of ant-m^{7}GTP alone demonstrates that the PABP enhances the cap binding affinity of cap binding protein.

Interactions	ant-m^{7}GTP/eIF-(iso)4F/PABP	ant-m^{7}GTP/eIF-4F/PABP
K_1[a]	8.93 ± 1.04 μ M	4.69 ± 0.33 μ M
K_2	4.3 ± 1.9 nM	9.1 ± 4.1 nM
K_3	0.099 ± 0.045 nM	0.23 ± 0.11 nM
K_4	0.21 ± 0.09 μ M	0.12 ± 0.06 μ M

Table 4 Summary of dissociation binding constants for the cap/eIF/PABP ternary complex

3.9 Fluorescence energy transfer measurement in ant-m^{7}GTP/eIF-4F/PABP/3'-fluorescein-poly(A)$_{30}$

It has been previously reported (Gallie & Tanguay, 1994) that eIF-(iso)4F, eIF-4F, and eIF-4B bind to the mRNA poly(A) tail. The size of the binding sites of eIF-4F and eIF-4B were estimated to be 25 bases in a buffer containing 150 mM KCl (Goss et al., 1987). These results suggested that eIF-4F and eIF-(iso)4F bind to the poly(A) at a different site from the 5' cap binding site. Direct fluorescence quenching titration of eIF-4F and poly(A)$_{30}$ indicated that they have a binding affinity, K_d = 400 nM (Figure 3.9.1). From the packing density measurement, PABP was also found to bind 25 A residues per molecule (Sachs et al., 1987). In order to determine whether the cap and poly(A) tail were bound to separate sites on this protein complex, energy transfer experiments were performed. The fluorescence probe, fluorescein, was attached to the 3' end of poly(A)$_{30}$. The spectral overlap between fluorescence emission of ant-m^{7}GTP and absorbance of fluorescein labeled poly(A) allowed fluorescence energy transfer to be monitored (Figure 3.9.2). Titration of 3'-fluorescein-poly(A)$_{30}$ with eIF-4F and PABP showed no significant fluorescence intensity changes, but an anisotropy change was observed indicating formation of a nucleic acid-protein complex. As a control, m^{7}GTP and unlabeled poly(A)$_{30}$ were used. Figure 3.9.3 shows the spectrum obtained from the complex, ant-m^{7}GTP/eIF-4F/PABP/3'-fluorescein-poly(A)$_{30}$ and the spectrum from the sum of the spectra for m^{7}GTP/eIF-4F/PABP/3'-fluorescein-poly(A)$_{30}$ and ant-m^{7}GTP/eIF-4F/PABP/poly(A)$_{30}$. The fluorescence quenching at

420 nm and enhancement at 510 nm demonstrated that eIF-4F/PABP bound both fluorescent cap analog and fluorescent poly(A) simultaneously. These data suggested that a complex associated with the cap, poly(A), PABP, and cap-binding protein was formed.

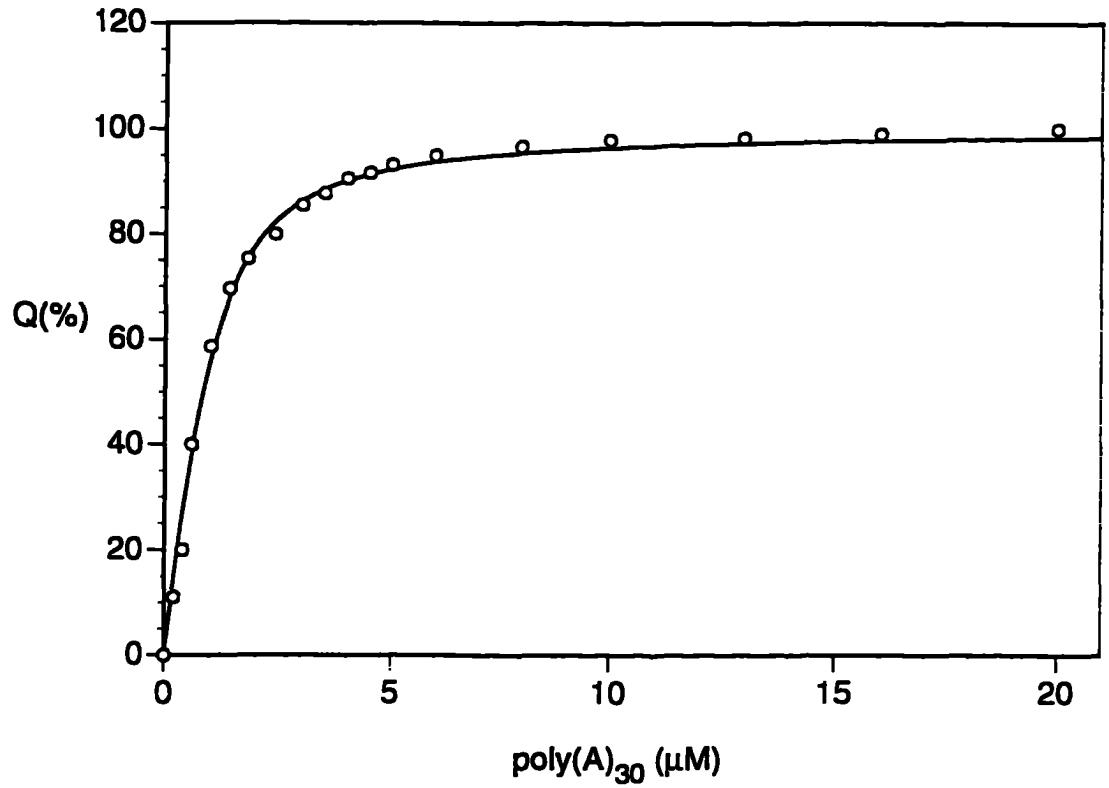

Figure 3.9.1 A graph of percentage of fluorescence quenching (Q%) against concentration of poly(A)30. The eIF-4F was excited at 295 nm and the emission was monitored at 336 nm. The concentration of protein was 1.0 μM. The solid line represents the best fit to these data and Kd was calculated to be 400 nM.

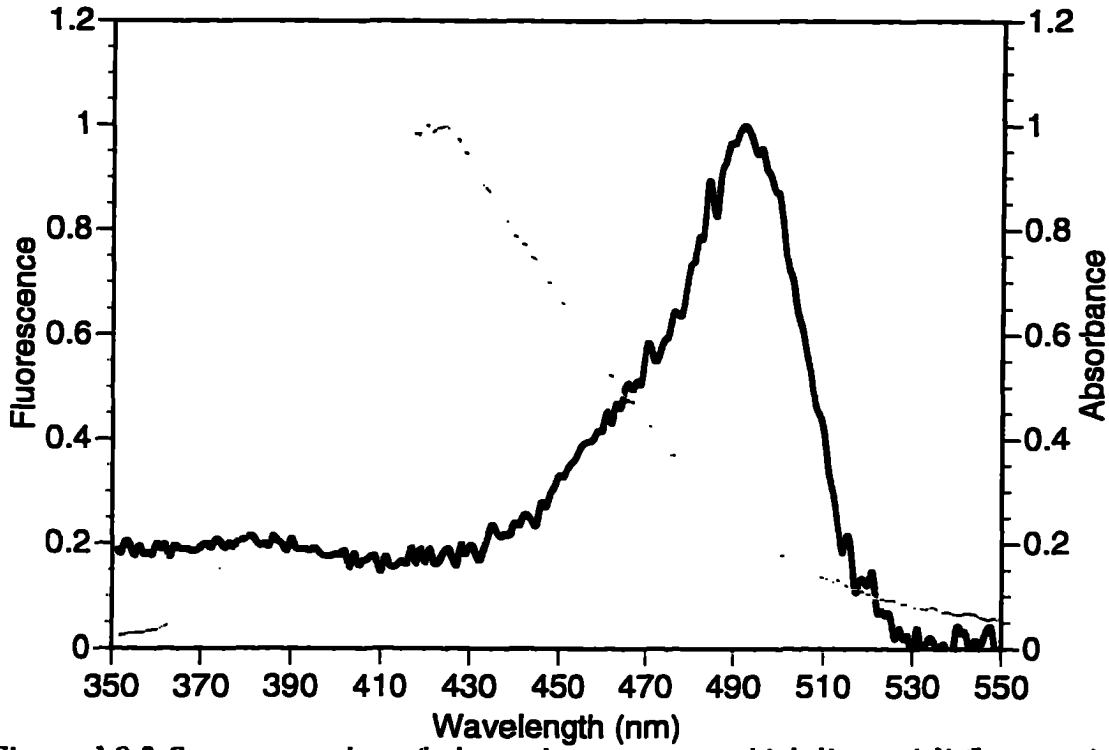

Figure 3.9.2 Spectra overlap of absorption spectrum (thick line) of 3'-fluorescein-poly(A)$_{30}$ and emission spectrum (thin line) of ant-m^{7}GTP in the buffer A. For presentation, absorbance and fluorescence were normalized to have the same maximum value.

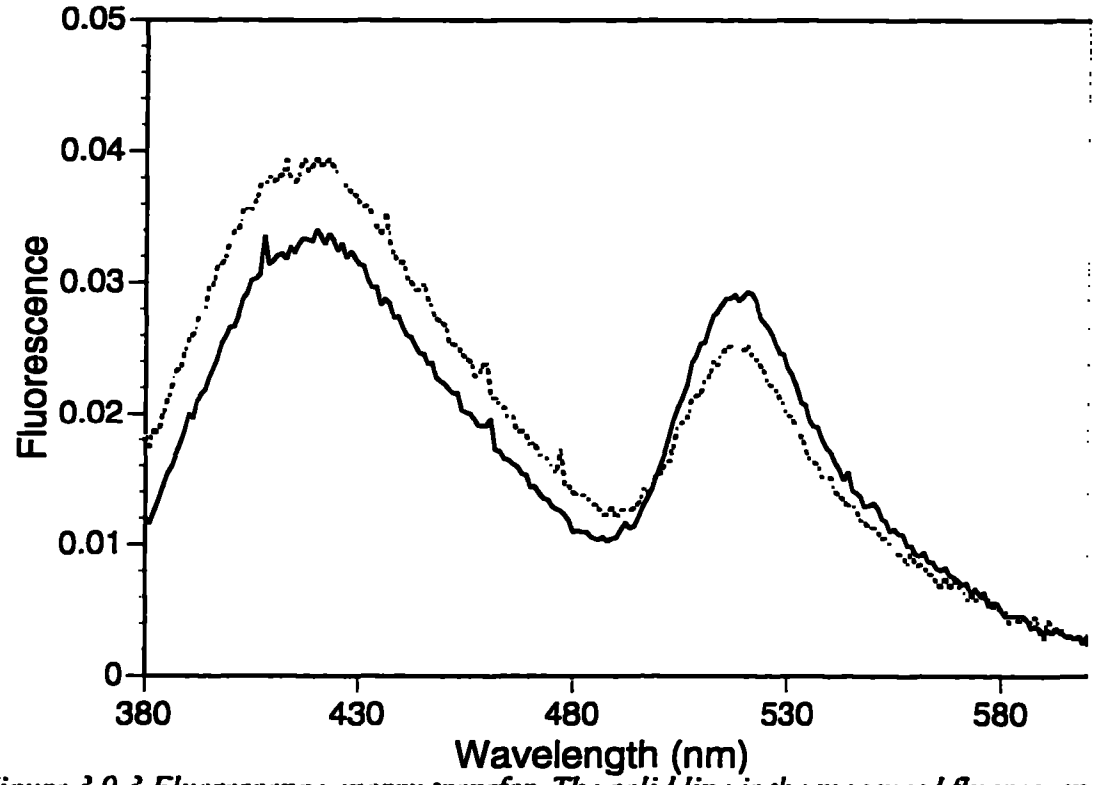

Figure 3.9.3 Fluorescence energy transfer. The solid line is the measured fluorescence intensity of ant-m^7GTP/eIF-4F/PABP/3'-fluorescein-poly(A)$_{30}$. The broken line is the sum of the fluorescence spectra for m^7GTP/eIF-4F/PABP/3'-fluorescein-poly(A)$_{30}$ and ant-m^7GTP/eIF-4F/PABP/poly(A)$_{30}$. The increase in acceptor fluorescence at 510 nm and corresponding decrease in fluorescence at 420 nm indicates energy transfer between the cap and poly(A) tail. The concentration used for ant-m^7GTP (m^7GTP), eIF-4F, PABP, and 3'-fluorescein-poly(A)$_{30}$ (poly(A)$_{30}$) were 150 nM, 50 nM, 50 nM, and 50 nM, respectively.

4. SUMMARY

PABP was demonstrated to bind poly(A), poly(G), and poly(U), but not poly(C). The binding site for PABP of these homopolymers may be their ribose-phosphate backbones. A poly(A) tail with 23 bases is required to bind to one PABP molecule under physiological conditions. The interactions are also salt dependent. The competition studies of poly(εA)/PABP complex with different homopolymers demonstrated that poly(A) has higher affinity toward PABP. Poly(U) and poly(G) had a binding affinity a hundred fold less than that of poly(A). In contrast, poly(C) did not compete for poly(εA) to PABP. CD measurements suggest that secondary structure of poly(A) was altered when poly(A) bound to PABP.

Direct fluorescence titration studies of protein-protein interactions of cap-binding initiation factors and PABP indicate that they have very strong binding affinities. PABP recognized the eIF-4F subunit, eIF-4G, probably via its C-terminal peptide. eIF-(iso)4F also has a very similar binding affinity as eIF-4F. Another cap associated protein, eIF-4B, had the strongest interaction.

Fluorescence cap analog, ant-m^7GTP, is a potential analog for cap studies since the modification on ribose did not effect its recognition of cap-binding proteins. The lifetime measurement of the fluorescent probe bound to the cap-binding site indicates that the microenvironment is nonpolar.

Studies of ternary complex of ant-m^7GTP, PABP, and cap-binding proteins indicate that the cap-binding protein binds simultaneously to the cap and PABP. Even

though the cap binds to eIF-4F or eIF-(iso)4F with a K_a of about 10^5 M^{-1}, in the presence of PABP, cap binding is enhanced 40-fold. Similarly, cap bound cap-binding protein will enhance the binding affinity to PABP. Since cap analogs have been demonstrated by CD analysis to induce a conformational change of eIF-(iso)4F (Wang et al., 1996), this may explain the higher affinity of cap/eIF for PABP due to cooperative binding. The data presented here support a model where eIF-4F, PABP, and the cap are involved in the formation of an RNA complex which is summarized in Figure 4.1. The model is based on the fact that the microenvironment of the cap must be similar in the ant-m7GTP/eIF-(iso)4F and ant-m^{7}GTP/eIF-(iso)4F/PABP complexes since no significant change in the fluorescence intensity or lifetime measurements was observed. The binding of the cap to eIF-(iso)4F results in a conformational change in eIF-(iso)4F, which subsequently enhances the binding to PABP. The eIF-(iso)4F bound to PABP may induce a conformation change in order to bring the nonpolar domains together and enhance cap binding.

The fact that PABP enhances the affinity of eIF-4F or eIF-(iso)4F for the cap analog is an interesting observation in light of fact that the PABP interacts with the 4G subunit (Le et al. 1997; Tarun & Sachs, 1996) and not directly with the cap binding subunit, 4E. These results suggest that a conformational change is propagated through the 4G (p220) subunit to the cap binding subunit, 4E (p26).

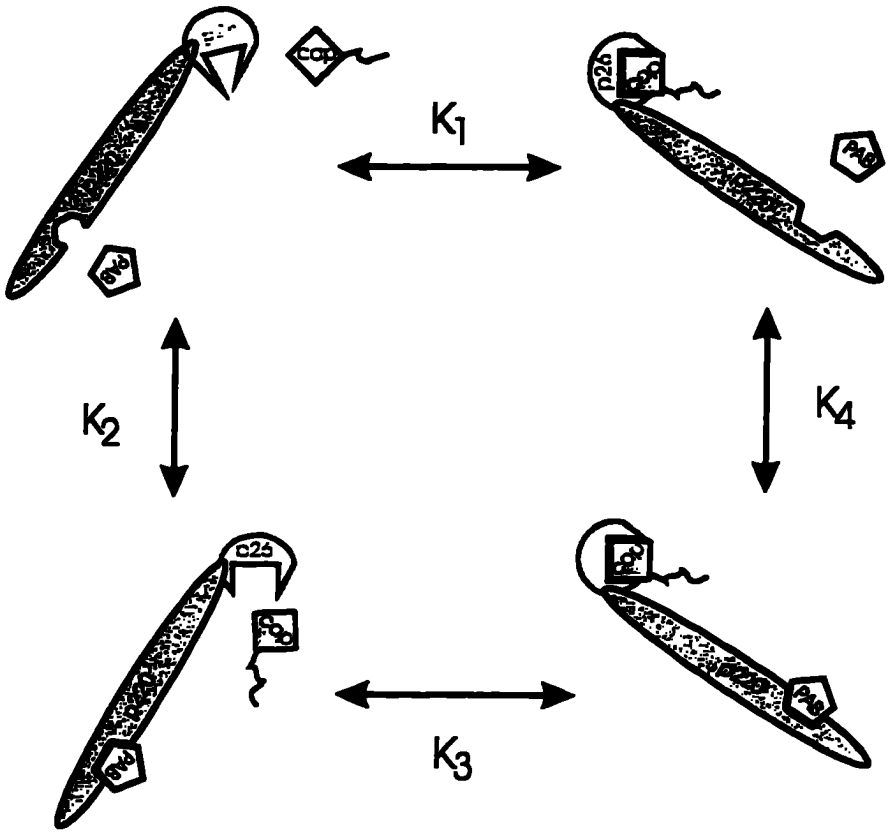

Figure 4.1 Schematic diagram for ant-m^{7}GTP/EIF/PABP ternary complex

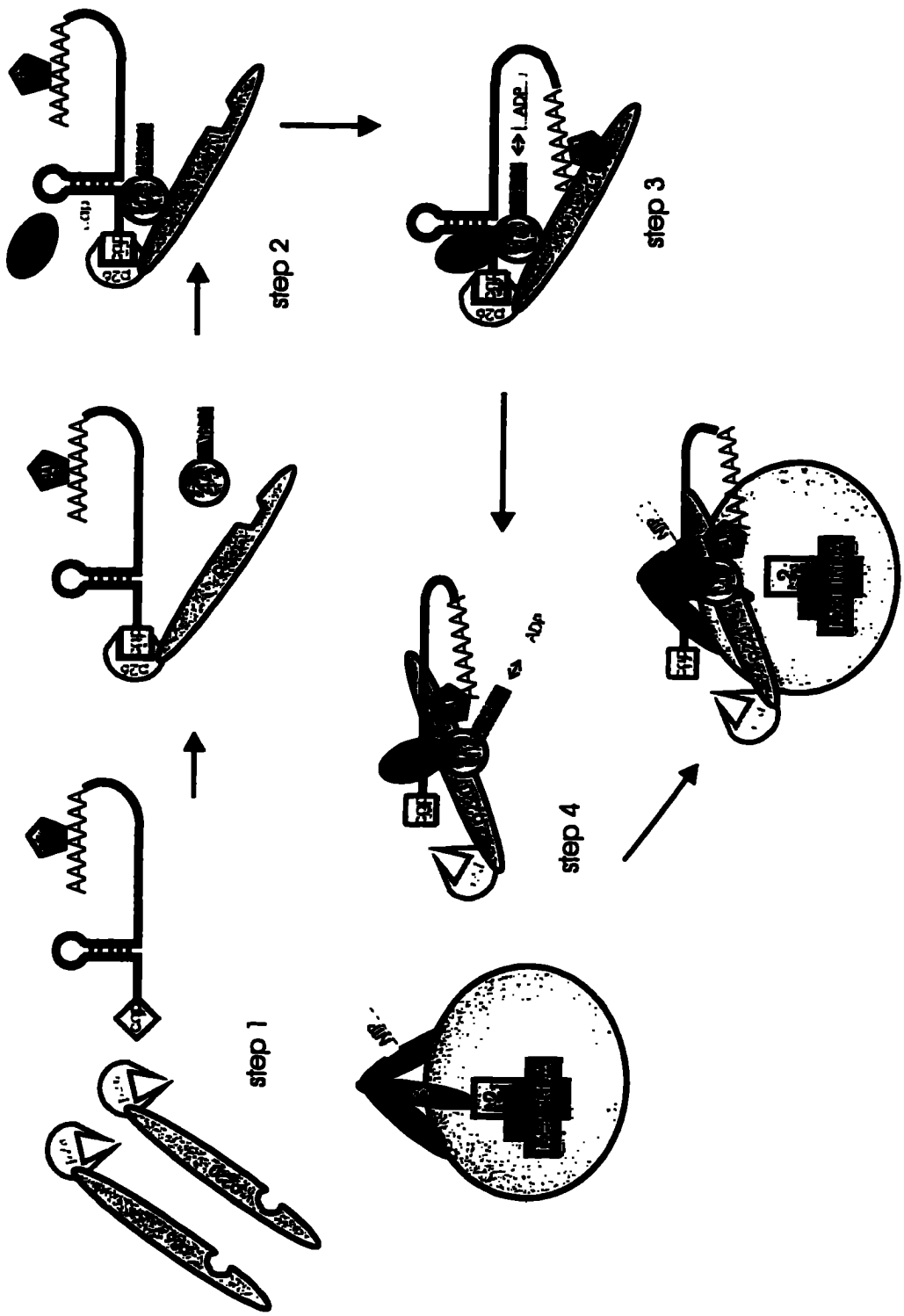

Figure 4.2 Proposed mechanism for the formation of 80S initiation complex

The results from these studies suggest that an alternative mechanism regarding the initiation complex formation may occur during translation. The proposed mechanism is presented in Figure 4.2. Initially, the 5' cap structure of mRNA is recognized by a cap-binding protein (step 1), i.e. eIF-4E subunit of eIF-4F or eIF-(iso)4E subunit of eIF-(iso)4F. The secondary structure of mRNA, such as hairpin structure, is unwound by association with helicase proteins (eIF-4A, eIF-4B, and eIF-4F). This allows the mRNA to become accessible to other proteins. ATP hydrolysis is required in this step (step 2). In the meantime, poly(A) tail bound PABP may interact with a subunit of cap-binding protein, eIF-4G, to form a loop-like mRNA structure (step 3). Although our results indicated that cap-binding protein is capable of binding with the cap and the poly(A) tail, it still remains unclear whether eIF-4F will bind to poly(A) in the presence of PABP. This complex is formed and stabilized while more proteins are involved due to their cooperative binding phenomena. The cap structure is subsequently released and the whole complex is prepared for another ribosome-contained initiation complex (step 4).

The question arises if this initiation complex forms during translation, what benefit would an interaction between the cap-associated initiation factors and PABP confer. The possibilities are (i) the interaction between the termini may stabilize the association of translational machinery with mRNA. This is reflected in this report and evidence from other groups (Le et al., 1997). While introducing more cap-binding protein and PABP into the mRNA, cooperative binding was observed. Recent

evidence was shown that in the presence of poly(A) bound PABP, decapping on mRNA was retarded (Caponigro & Parker, 1995), which could explained why in our model PABP indirectly interacts with 5' cap. As a consequence, decapping enzyme may be unable to contact the cap structure. (ii) mRNA containing a cap and a poly(A) tail could effectively complete the translational machinery. Degraded mRNA either without a cap or poly(A) tail therefore could not be recruited for translation. Although this model did suggest the co-dependent communication of the 5' and 3' end, the reason that loop-form of mRNA competes more efficiently with ribosome complex remains further investigated. (iii) The mutual stabilization may also serve as a means to ensure the ribosomes stay committed to a particular message during multiple rounds of translation. (iv) Finally, translation efficiency may be simply described as enhanced binding affinities to cap structure or enhanced recycling of ribosomes during translation.

PART II: Applications of fluorescence energy transfer technique in biopolymers

5. INTRODUCTION

The pseudoknot RNA structure and helicase activity of some eukaryotic initiation factors have caught us much attention because of their biological importance in RNA enzyme activity and protein biosynthesis (see the following text). In this report, we would like to construct the models which can be utilized in the studies of these mechanisms by using fluorescence resonance energy transfer (FRET) technique. Some important reviews regarding this unique RNA structure and helicase activity of some proteins are summarized in section 5.1 and 5.2. The principle of FRET in this application is presented in section 5.3.

5.1 Pseudoknot structure of RNA

A detail knowledge of RNA spatial folding is required to understand the function of RNA. In recent years, a pseudoknot structures of RNA was proposed. A pseudoknot structure is defined as a structural element of RNA formed upon standard base pairing of nucleotides of a loop region with residues outside that loop (Figure 5.1.1). As a consequence, a pseudoknot is always defined by two stems (Pleij et al., 1985). Some alternative ways to present the pseudoknot structures are summarized in Figure 5.1.2. If L2 is absent, stem S1 and S2 become adjacent and can be stacked coaxially to form a quasicontinuous double strand helix as is the case in the tRNA-like

structure of turnip yellow mosaic virus (TYMV) (Pleij et al., 1985). The first example was based on experiments by Rietveld and coworkers (1982) who proposed a pseudoknot structure to explain the tRNA-like properties of the 3' end of TYMV based on chemical modification, enzymatic digestion, and sequence comparisons.

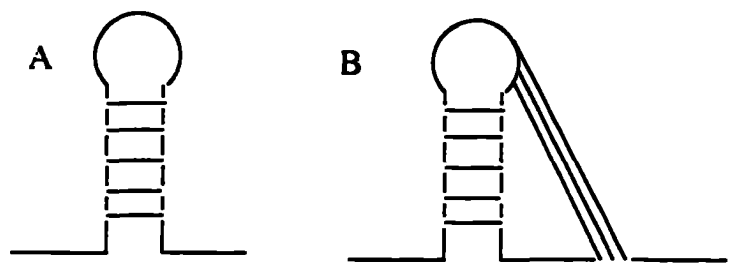

Figure 5.1.1 Base pairing formation in RNA. (A) hairpin structure (B) pseudoknot structure.

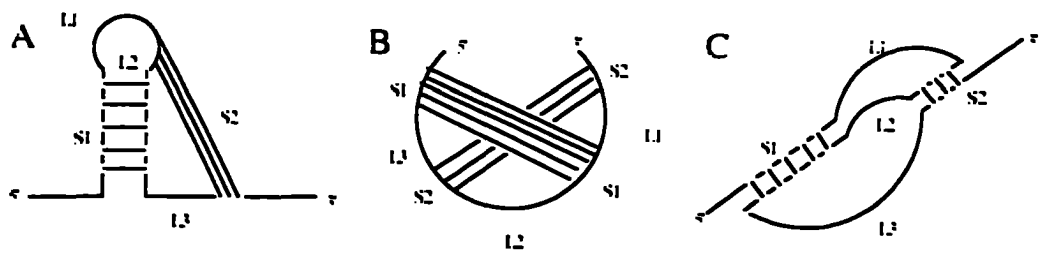

Figure 5.1.2 Three alternative ways to represent the pseudoknot structure. Stem regions (S1, S2), and loops (L1, L2, L3) are numbered from the 5' end.

This unique structure has been found in virtually every class of RNA. Most described pseudoknots were found either in small subunit ribosomal RNAs or autoregulated mRNA. Pseudoknot structures have been considered to have special functional roles that can not be fulfilled by standard hairpin structures. Pseudoknots in mRNAs have been shown to be an essential part of the regulatory mechanism for translational efficiency, frameshifting, and readthrough (Chamorro et al., 1992). In ribosomal RNA (rRNA), the pseudoknot structure is required for the RNA enzyme activity (Jeng et al., 1996). In general, the function of pseudoknot structures can be summarized as the following:

(i) *stabilization of tertiary structure*: Darr et al. (1992) suggested the loss of pseudoknot in RNase P RNAs leaded to a more flexible structure. Because of this, it is understandable that most large RNA motifs contain pseudoknot structures at a critical point or near the binding sites. A pseudoknot also forms a part of the structure of 16S ribosomal RNA (Moazed & Noller, 1987).

(ii) *recognition and regulation :* The pseudoknots were first recognized by a tRNA processing enzyme (Rietveld et al., 1982; Van Belkum et al., 1985). The mRNA pseudoknot was also recognized by S4 ribosomal protein and has an overall stability of -7.7 kcal, which is comparable to a moderate-size hairpin (Spedding et al., 1993). Recent evidence is that the pseudoknot is required for efficient translational initiation and regulation of the *Escherichia coli* rpsO gene coding for ribosomal protein S15 (Ehresmann et al., 1995). These results showed the binding of ribosomal protein and

its mRNA is stabilized by a pseudoknot structure that exists in an equilibrium with two stem-loop structures.

(iii) *enzymatic activity and ribosomal frameshifting:* Jeng et al. (1996) suggested that the pseudoknot structure of ribozymes of hepatitis delta virus (HDV) were active *in vivo* and required for hepatitis delta virus RNA regulation. The mutant ribosomes lacking formation of a pseudoknot structure, lost the ribozyme activity, and yielded no replication. The pseudoknot structure was also required for efficient ribosomal frameshifting in a retroviral mRNA (Chamorro et al., 1992).

5.2 Helicase activity of eukaryotic initiation factors

Binding of the 40S ribosomal subunit to mRNA is the rate limiting step in eukaryotic translation initiation (Jagus et al., 1981). The concerted action of three translational initiation factors eIF-4A, 4F, 4B, and the hydrolysis of ATP is required for ribosome binding (Trachsel et al., 1977) and for maximal protein synthesis in a fractionated translation system (Grifo et al., 1983). These factors bind the 5' end of mRNAs and melt the 5' proximal secondary structure in an ATP-dependent manner to facilitate 40S ribosomal subunit attachment (Sonenberg, 1988; Merrick, 1992; Rhoads, 1991). Wheat Germ eIF-4F and eIF-4B are described in Part I of this thesis. eIF-4A is a 50 kDa polypeptide which could be part of eIF-4F and also exist in a free form (Conroy et al. 1990) that exhibits RNA-dependent ATPase and bi-directional RNA helicase activity (Grifo et al., 1984).

5.3 Application and principle of fluorescence resonance energy transfer techniques in biopolymers

Spectroscopy methods in solution provide a compromise between simplicity of application and the amount of information predicted in determination of biopolymer structure. Although X-ray and nuclear magnetic resonance (NMR) are shown to be very successful techniques in determination of biopolymer structure. difficulties for X-ray and NMR limit their wide application. For rapid distance measurements of selective sites in biopolymers. FRET provides a powerful and simple technique.

In 1948. Förster had derived an equation that was capable of determining the distance between donor (D) and acceptor (A) chromophores from the nonradiative dipole-dipole interaction between two motifs that occurred (Förster. 1948). The scheme for this interaction is presented in Figure 5.3.1.

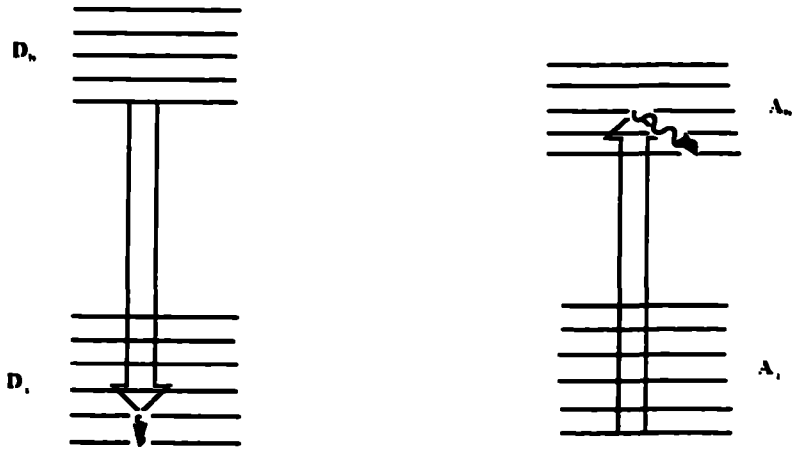

Figure 5.3.1 Donor deexcitation and acceptor excitation couple in a resonant interaction that leads to energy transfer.

In this case, only single ground states (D_a, A_a) and first single excited states (D_b, A_b) of each chromophore are considered. This dipole-dipole interaction shifts the relative population of excited donor and acceptor. The donor becomes quenched and the acceptor becomes excited. As the acceptor is also fluorescent, this will result in enhancement of acceptor fluorescence intensity. Consider the transition of both donor and acceptor only at the same frequency, ν, the rate of energy transfer (k_T) should be proportional to

$$k_T(\nu) \propto |\langle \Psi_{Da}\Psi_{Ab}|V|\Psi_{Db}\Psi_{Aa}\rangle|^2 \qquad \text{eq. 19}$$

where Ψ_{Da} stands for the ground state (a) wavefunction of donor (D) and V is dipole-dipole coupling operator and expressed as

$$V = (\mu_D \cdot \mu_A)/ R^3 - 3 (\mu_D \cdot R)(R \cdot \mu_A)/R^5 \qquad \text{eq. 20}$$

Where **R** is the distance operator between the donor and acceptor. and μ_D . μ_A are dipole moment operators. By introducing another parameter. κ. in the eq. 20. eq. 19 could be rewritten as

$$k_t(\nu) \propto |(\kappa/R^3)\langle \Psi_{Da} \Psi_{Ab} | \mu_D | \mu_A | \Psi_{Db} \Psi_{Aa} \rangle|^2 \qquad \text{eq. 21}$$

$$k_t(\nu) \propto (\kappa^2/R^6)|\langle \Psi_{Da} | \mu_D | \Psi_{Db} \rangle|^2 |\langle \Psi_{Ab} | \mu_A | \Psi_{Aa} \rangle|^2 \qquad \text{eq. 22}$$

Eq. 22 is obtained since μ_D depends upon the electronic coordinates of donor and μ_A depends on the electronic coordinates of the acceptor. The second term in eq. 22 could be easily converted to eq. 23 since it is just the absorption strength of the acceptor which is

$$\langle |\Psi_{Ab} | \mu_A | \Psi_{Aa} \rangle|^2 \propto \varepsilon_A \nu^{-1} \qquad \text{eq. 23}$$

where ε_A is the absorbance coefficient of acceptor. Similarly. μ_D could be related to the Einstein equation :

$$\langle \Psi_{Da} | \mu_D | \Psi_{Db} \rangle^2 = \nu^{-3} \tau_R^{-1} = \nu^{-3} \phi_D / \tau_D \qquad \text{eq. 24}$$

substituting eq. 23 and eq. 24 to eq. 22. eq. 25 was obtained

$$k_T(\nu) \propto (\kappa^2/R^6)(\phi_D/\tau_D)\varepsilon_A \nu^{-4} \qquad \text{eq. 25}$$

Expanding this case to the general case in which acceptor absorption and donor emission occurs over a broad band. and the total rate of energy transfer can be computed by integrating the whole spectra. If $f_D(\nu)$ is the fraction of fluorescence intensity:

$$k_t(\nu) \propto (\kappa^2/R^6)(\phi_D/\tau_D) \int \varepsilon_A(\nu) f_D(\nu) \nu^{-4} d\nu = (\kappa^2/R^6)(\phi_D/\tau_D) J \qquad \text{eq. 26}$$

where $J = \int \varepsilon_A(\nu) f_D(\nu) \nu^{-4} d\nu = \int \varepsilon_A(\lambda) f_D(\lambda) \lambda^2 d\lambda \cdot \int f_D(\lambda) \lambda^{-2} d\lambda$. The Förster distance ($R_0$) is then defined as the distance when 50 % energy transfer occurs and is given by

$$R_0 = 8.97 \times 10^{-5} (J k^2 n^{-4} \phi_D)^{(1/6)} \text{ Å} \qquad \text{eq. 26}$$

and the energy transfer efficiency (E) then was related to R_0 and R as

$$R = R_0[(1-E)/E]^{1/6} \qquad \text{eq. 27}$$

FRET technique was not applied to biological systems until Stryer and Haugland (1967) demonstrated that Förster resonance energy transfer could be used as a basis for distance measurements using a series of end-labeled oligopeptides. Since this pioneering work, FRET has been used in a number of studies involving proteins and nucleic acids. For example, Beardsley and Cantor (1970) described the 3'-terminal labeling of tRNAs to probe tRNA-ribosome complex structure. FRET also was applied in DNA studies (Ozaki & McLaughlin, 1992). However, the limitation in studies with nucleic acids or protein/nucleic acid complexes is typically the difficulty in generating a series of donor acceptor pairs.

FRET was also utilized to reveal the "X" geometry in the four-way DNA junction (Murchie et al., 1989). The application of fluorescence energy transfer techniques to ribozyme was performed by Tuschl et al. (1994). These authors attached different donor and acceptor pairs in the hammerhead ribozyme and their corresponding distances were measured by fluorescence energy transfer. With the assistance of computer simulation, a three-dimensional model for the ribozyme was constructed leading to the determination of the spatial arrangement of the three Watson-Crick helices of this molecule in solution.

These successful experiments prompted us to utilize FRET to examine the RNA pseudoknot structure and the study of helicase activity of initiation factors. In this report, we chose a 19-mer oligoribonucleotide (PK1) for our model since its structure was demonstrated to be a pseudoknot structure based on the map of enzymatic digestion (Puglisi et al., 1988). For the helicase studies, specific length of homopolymer poly(U) and poly(A) were used for double strand RNA to mimic the hairpin structure in RNA. Our results showed FRET techniques are a powerful technique in studies of these two systems.

6. EXPERIMENTAL PROCEDURE

6.1 Materials

T4 polynucleotide Kinase and T4 RNA ligase were purchased from Pharmacia Biotech (Piscataway, NJ). Adenosine-5', 3' monophosphate was purchased from Sigma Chemical Inc. (St. Louis, MO), and 7-(diethylamino)-3-(4'-maleimidopheyl)-4-methylcoumarin (CPM) and fluorescein 5-thiosemicarbazide (FC) were purchased from Molecular Probes (Eugene, OR). The preparation and purification of the desired length of poly(A) and poly(U) were described in Part I.

6.1.1 Preparation of oligoribonucleotides

Oligoribonucleotides were synthesized chemically on a solid support using phosphoramidite procedures in an Applied Biosystems DNA synthesizer (Foster. CA). The sequence of all the oligoribonucleotides used in this research were 5'-GGCUU-3' . 5'-CGGCGCCUAGCCG-3'. and 5'-GGCUUACGGCGCCUAGCCG-3'. The synthetic RNA was deprotected according to the procedure provided by the manufacturer and further purified and desalted with a C-18 Sep-Pak cartridge (Water. Inc.). The sample was purified by RP-HPLC and analyzed on a 6 M urea-20 % polyacrylamide gel with half the strength of TBE (0.1 M Tris-HCl. pH 8.6. 0.084 M boric acid. 1 mM EDTA) buffer.

6.1.2 3' end labeling on RNA

The 3' end labeling method was followed as described in Odam et al. (1980) with some modification. RNA was first oxidized at 37 °C for 1 hour in the dark in a 0.1 M solution of sodium acetate. pH = 5.0. containing 0.09 M sodium periodate. After the incubation. the reaction was stopped by adding stock 1.0 M KCl to make the final concentration 0.1 M. The mixture was mixed in a Vortex mixer and centrifuged at 5000 g for 10 min. The pellet was discarded and the supernatant then was dialyzed against the same buffer at 0 °C in the dark overnight with several changes of buffer. Oxidized RNA was incubated with 0.01 M fluorescein semithiocarbazide (FC) at 37 °C for 2 hours in the dark. After the incubation. the solution was extracted with phenol

3 times and CH_3Cl one time. The sample then was dialyzed against three changes of the desired buffer. The yield from the labeling procedure was calculated to be around 100 % based on UV spectra where the absorbance coefficient of fluorescein at 487 nm was 72 x 10^3 cm^{-1} M^{-1}.

6.1.3 5' end labeling of RNA

Two methods for labeling the 5' end of oligoribonucleotides are described in these experiments. Samples were labeled on the 5' end of synthetic RNAs with a thio-reactive probe, CPM. The first method required 5' terminal phosphorylated RNA. Since the synthetic oligoribonucleotides do not bear the phosphoryl group at the 5' end, purified oligoribonucleotide was phosphorylated in 100 µL of reaction mixture containing 5 mM ATP, 100 units of T4 Polynuleotide Kinase (T4PNK), 80 units of RNase inhibitor, 70 mM Tris-HCl (pH 7.6), 10 mM $MgCl_2$, and 5 mM DTT. The mixture was incubated at 37 °C for 3 hr (Czworkowski et al., 1991). The solution was brought to 200 µL and the mixture was extracted with 1:1 phenol-chloroform solution followed by extraction with pure chloroform. The sample was desalted in a C-18 Sep-Pak cartridge. Cystamine was added to the 5' end of RNA as described by Chu and Orgel (1992), and the product was purified as described by Teare and Wollenzien (1989). Phosphorylated RNA was mixed in water containing 0.1 M 1-methylimidazol (pH 7.0) and 0.1 M carbodiimide. The use of carbodiimide from a freshly opened vial significantly improved the yield of cystamine derivative. After a 3.0 hour incubation at

50 °C. the reaction was introduced into a 25 cm Sephadex G-25 column equilibrated with H_2O. The first peak which contained oligoribonucleotide was collected and dried via speed vacuum. The pellet then was suspended in 0.5 M cystamine in water (pH 7.0) and the mixture was incubated for 30 min. at 50 °C. The excess cystamine then was removed using Sephadex G-10 and the cystamine derivative of RNA was then collected and dialyzed against water. The sample was dried via speed vacuum and dissolved in 400 µL TE buffer. To reduce the disulfate bond. 40 µL of 1.0 M DTT solution was added. After one hour incubation at room temperature. the mixture was applied to a Sep-Pak C18 column followed by washing with 10 mL water and 10 % ethanol. RNA was eluted with 2 mL of 50 % ethanol into a tube containing 40 µL of 1.0 M DTT. To covalently attach CPM to the RNA derivative. 200 µg/mL solution of CPM in methanol was added immediately. and the mixture was incubated for 2 hr at room temperature in the dark. The reaction was quenched by addition of 100 µL of 0.1 M DTT. Unreacted probe was removed from the mixture by dilution of the sample to 15 mL with TE buffer (10 mM Tris-HCl. pH 8.0. 1 mM EDTA) and loading into a Sep-Pak C18 column. The column was washed with 10 mL methanol and RNA was eluted with 2 mL of 50 % methanol and subsequently dialyzed against several changes of the desired buffer in the dark. The final product was determined to contain 0.5-1.0 mol of probe per mole of RNA based on UV spectra using $\varepsilon(CPM) = 4.6 \times 10^4\ M^{-1}cm^{-1}$.

In the second method, synthetic RNA was thiophosphorylated at its 5' end as in the procedure described above except ATP-γS was substituted for ATP. The thiophosphorylated RNA was dissolved in 80 μL of 50 mM Bicine-KOH (pH 8.4). Then 100 μL of DMF was added followed by 20 μL of 20 mM 7-diethylamino-3-(4'-maleimidylphenyl)-4-methylcoumarin (CPM) dissolved in DMF. The reaction mixture was shaken at room temperature for 4 hrs. after which the mixture was brought to 1.0 mL with water, extracted and purified as described above.

6.1.4 Ligation of two oligoribonucleotides

The ligation reaction was followed as described by Ohtsuka et al. (1978). The reaction between the oligoribonucleotide donor and the acceptor were performed in 200 mL polyethylene microcentrifuge tubes containing 50 mM HEPES (pH 8.3), 20 mM $MgCl_2$, 3.3 mM DTT, 10 μg/mL BSA, 8.3 % (v/v) glycerol, 0.1 mM acceptor RNA, 0.3 mM donor RNA, and RNA ligase at 300 units/mL. Each reaction was incubated at 37 °C for 1 hr. The mixture was extracted with phenol and $CHCl_3$ to remove the proteins. After dialysis against sterile water, the mixture was separated on a G-10 Sephadex column equilibrated with sterile water.

6.2 Spectroscopy

Absorption spectra were carried out in a Cary-3 double beam UV/VIS spectrometer equipped with temperature control. The data was recorded on a IBM 386

personal computer. Fluorescence spectra were obtained in a SPEX τ_2 Fluorometer equipped with an excitation and emission polarizer. Lifetime measurements were used with either the T (no emission monochromator) or S channel (with monochromator). When the S channel was used, the emission polarizer was placed in a magic angle to correct the difference in sensitivity of the photomultiple tube and monochromator. The lifetime of the probe was compared to a reference with a known lifetime, for example, fluorescein in 0.05 N NaOH or 0.1 % glycogen in water.

6.2.1 UV melting curve measurements

Absorbance measurements in the UV region were made on a Cary-3 spectrophotometer. The melting curve was measured at 260 nm or 280 nm with spectrophotometer connected to a thermoprogrammer. The heating rate was 1 °C per min. Water condensation on the cuvet exterior at low temperatures was avoided by flushing it with a constant stream of dry N_2. The concentration of oligonucleotides was adjusted to have an optical density of approximately 0.7 at 260 nm in 25 mM phosphate buffer (pH 7.6).

6.2.2 Fluorescence energy transfer measurement

The procedure and data analysis for the fluorescence energy transfer measurements were similar to those described before. The efficiency of energy transfer from the donor quenching is defined as:

$$E = 1 - F_{DA}/F_D = 1 - \tau_{DA}/\tau_D \qquad \text{eq. 28}$$

where F_{DA} and τ_{DA} are the fluorescence intensity and lifetime of RNA with donor and acceptor, respectively. F_D and τ_D are fluorescence intensity and lifetime of RNA with donor only, respectively. Care must be taken in measuring steady state fluorescence intensity in FRET, especially in a case where labeling may not be homogenous.

For the steady-state measurement in FRET, a calculation is required to correct the distance determination when using RNA that was not 100% labeled because it did not undergo the fluorescence energy transfer. In this report, the labeled products were not separated and, therefore, unlabeled and labeled PK1s were existed in the mixture after the labeling reaction. The value of F_{DA} and F_A in eq. 28 were determined from the measured fluorescence of labeled PK1 as follows: Three samples containing donor-labeled PK1, acceptor-labeled PK1, and donor-acceptor-labeled PK1 in the same concentrations were required to determine the energy transfer. For the donor-labeled PK1, the fraction of labeling was determined to be X_D % by UV spectrometry and the fluorescence intensity was recorded (F'_D). Similarly, the fraction of labeling for the acceptor-labeled PK1 was determined to be X_A % and the fluorescence intensity was measured (F'_A). The fluorescence intensities for 100% labeling were therefore calculated to be F'_D/X_D and F'_A/X_A, respectively. F_D was calculated as

$$F_D = F'_D/X_D + F'_A/X_A \qquad \text{eq. 29}$$

The percentages of donor- and acceptor-labeling in the donor-acceptor-labeled PK1 sample were also determined to be X'_D and X'_A %. The fluorescence intensity of this sample was recorded (F'_{DA}). From the statistical view, only ($X'_DX'_A$) % of total sample have donor and acceptor labeled simultaneously, which is capable of doing energy transfer. The fractions of sample containing only donor-labeled PK1 and only acceptor-labeled PK1 were calculated to be [X'_D - ($X'_DX'_A$)] % and [X'_A - ($X'_DX'_A$)] %, respectively. F_{DA} was calculated as

$$F_{DA} = \frac{F'_{DA} - (X'_D - X'_D X'_A)\left(\frac{F_D}{X_D}\right) - (X'_A - X'_D X'_A)\left(\frac{F_A}{X_A}\right)}{X'_D X'_A} \qquad \text{eq. 30}$$

The lifetime measurement does not require knowing the percentage of labeling; therefore, the measurement avoided any error from the calculation of labeling yield. The disadvantage of the lifetime measurement is that it has to rely on a concentration of probe with a large enough signal to detect.

7. RESULTS AND DISCUSSION

7.1 Studies of pseudoknot structure

In order to investigate the structure of pseudoknot via FRET techniques, we chose the 19-base oligoribonucleotide PK1 (5'-GGCUUACGGCGCCUAGCCG) (Puglisi et

al., 1988) since its structure was confirmed by enzymatic digestion. The proposed structure is shown in Figure 7.1.1. The CD spectra of this RNA is shown on Figure 7.1.2. which is very similar to the CD of PK5 (GCGAUUUCUGACCGCUUU-UUUGUCAG) (Johnson & Gray, 1992).

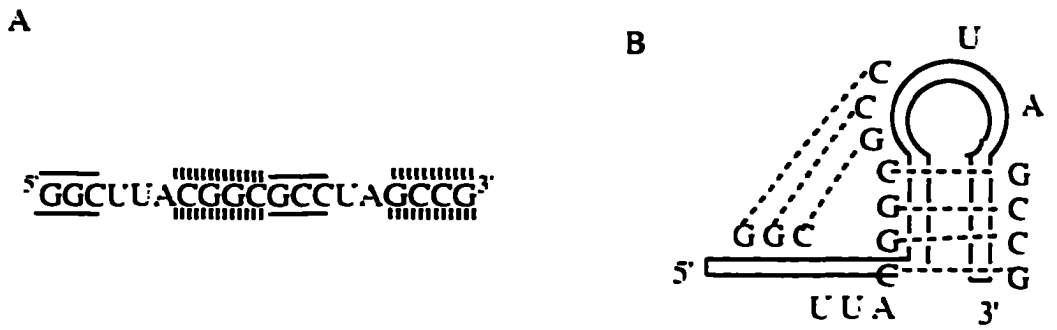

Figure 7.1.1 A schematic representation of pseudoknotted PK1. (A) The primary structure of PK1. The solid line and dotted line present their corresponding base-pairing. (B) secondary structure of PK1. The dotted line presents the formation of hydrogen bond between two bases.

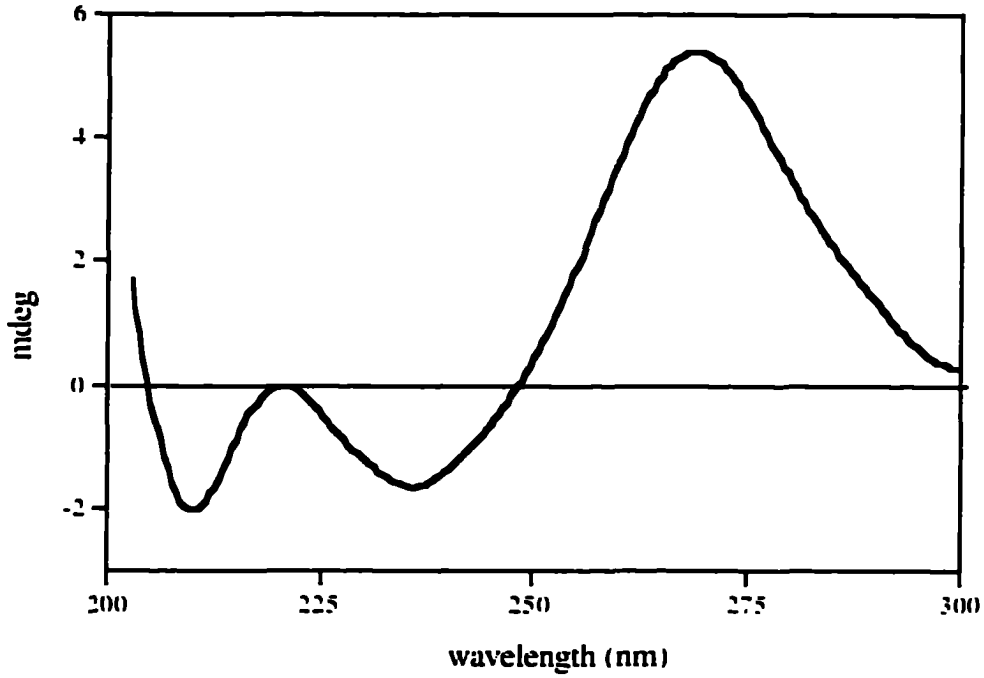

Figure 7.1.2 CD spectra of PK1 oligoribonucleotide. Sample was in 0.25 mM $MgCl_2$, 10 mM sodium phosphate, pH 7.0.

The pseudoknot structure of this synthetic RNA was confirmed by a UV melting curve that was compared to the literature (Puglisi et al., 1988). Labeling of both of 5' end and 3' end was carried out. The methods for 3' end labeling and 5' end labeling are presented in Figure 7.1.3 and Figure 7.1.4. The FC and CPM were chosen to label the 3' and 5' ends of RNA, respectively. The spectral overlap of this donor and acceptor (Figure 7.1.5) was given a Förster distance 56 Å. Figure 7.1.6 shows the energy transfer occurs in this kind of RNA. The distance between the 5' end and 3' end of PK1 was calculated to be 35 Å for steady-state and 32 Å for lifetime measurement.

The data is summarized in Table 5. From the FRET measurement, the distance between the 5' end and 3' end of PK1 was determined to be shorter than a random coil, which the distance between both ends is approximately more than 45 Å (modeling results using a HyperChem software), indicating this RNA should form a tertiary structure.

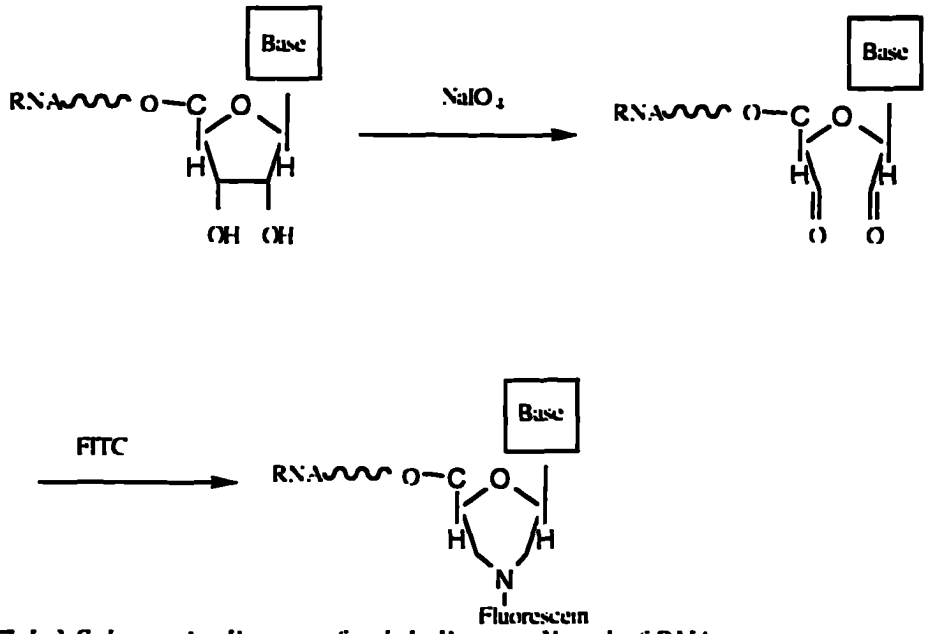

Figure 7.1.3 Schematic diagram for labeling on 3' end of RNA.

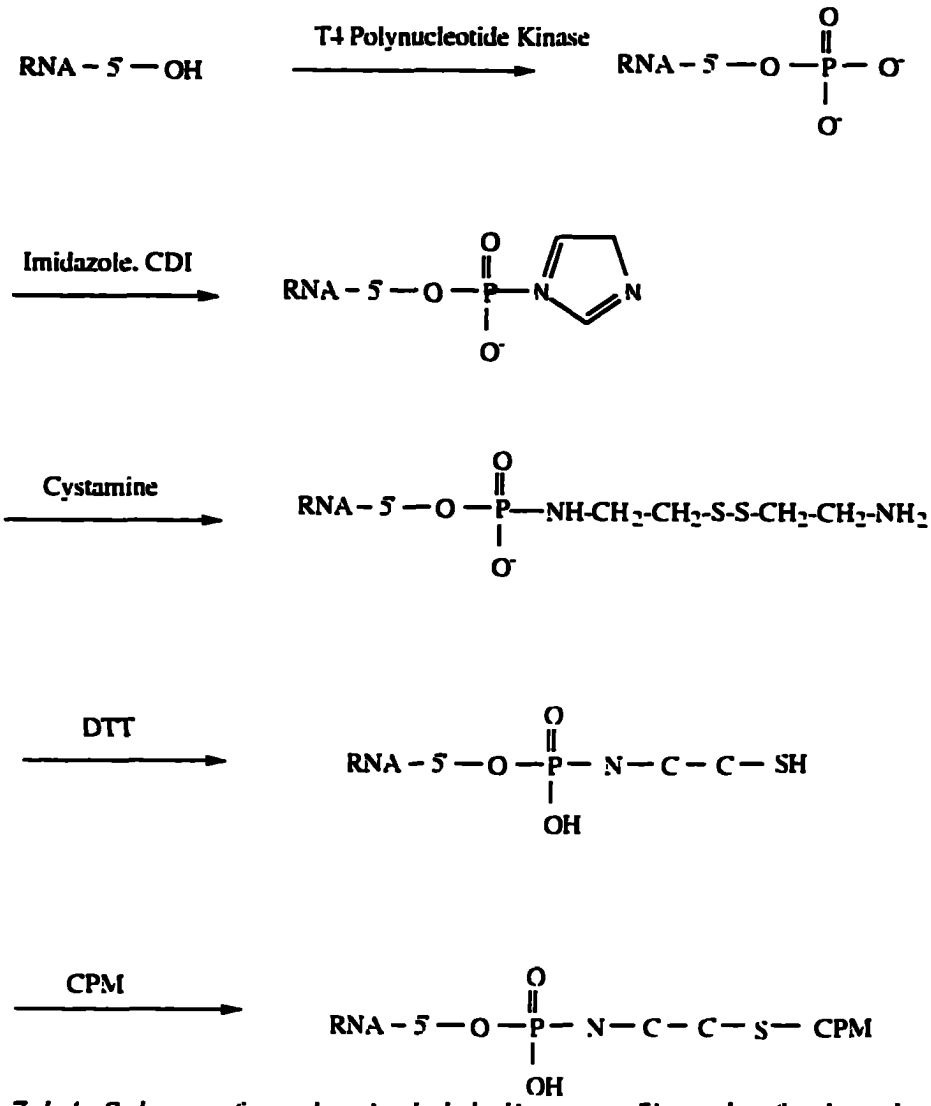

Figure 7.1.4 Scheme for chemical labeling on 5' end of phosphorylated oligoribonucleotide.

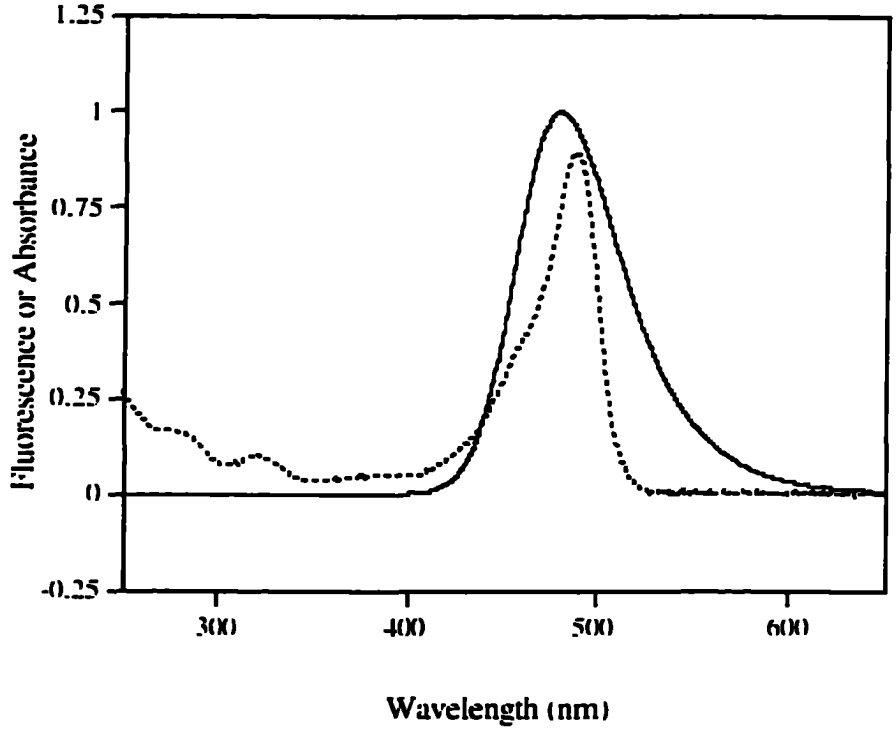

Figure 7.1.5 Spectra overlap of absorption of Fluorescein (broken line) and emission of CPM (solid line) in a neutral buffer. The fluorescence of CPM was excited at 380 nm.

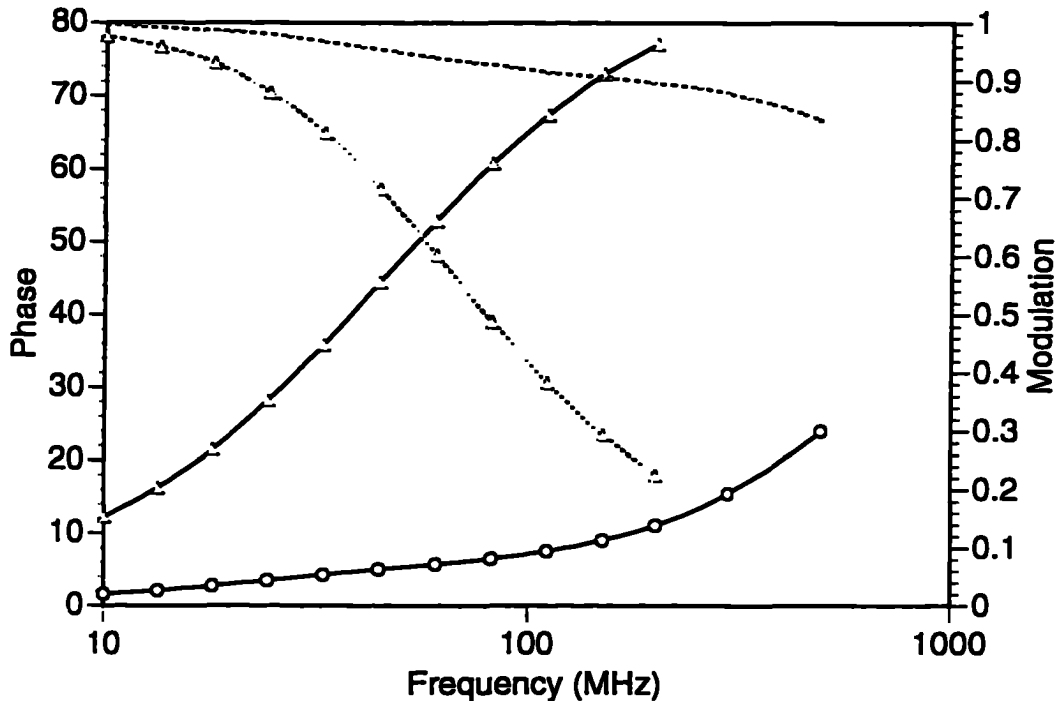

Figure 7.1.6 Fluorescence lifetime measurement of 5'-CPM-PK1 (triangles) and 5'-CPM-PK1-3'-FC (circles) in a neutral buffer. The excitation wavelength was 360 nm and the emission was monitored at 480 nm. The solid line represents data fitted as one and two exponential decay for 5'-CPM-PK1 and 5'-CPM-PK1-3'-FC, respectively. For 5'-CPM-PK1, the lifetime was fitted as 3.42 nsec and fraction amplitude as 1.00. For 5'-CPM-PK1-3'-FC, τ_1 = 3.46 ns and τ_2 = 0.138 ns having a fractional amplitude f_1 = 0.098 and f_2 = 0.902 was obtained. The energy transfer efficiency was calculated to be 96% using eq. 28.

Term	Value
ϕ_{CPM}	0.82
τ_{CPM} (nsec)	3.46
ϕ_{FC}	0.56
τ_{FC} (nsec)	4.02
n	1.33
κ^2	2/3
J (cm^3 dm^3/mole)	2.022×10^{-13}
R_0 (Å)	56
E %	94
E (by lifetime) %	96
R (Å)	39
R (by lifetime) (Å)	32

Table 5 FRET measurement for 5'-CPM-PK1-3'-FC. The orientation of these probes was assumed to be random, and the corresponding κ^2 is 2/3.

We therefore expanded our studies to map the pseudoknot. Synthetic RNAs with a special attached fluorescent probe are widely used in studies of DNA conformation

(Ozaki & McLaughlin, 1992). Fluorescent adenosine analog, ethanoadensine (εA), has been shown to be a good substitute for adenosine. Incorporation of this fluorescent probe into the synthetic RNA may provide another potential technique in these types of studies. T4 RNA ligase has been shown to catalyze intra- and intermolecular joining of the 5' phosphate and the 3' hydroxyl group of RNA (Silber et al., 1972). The ligation of two oligonucleotides requires that both acceptor RNA ends are hydroxyl groups to prevent self-polymerization and that the donor RNA has a 5' phosphoryl group as shown in Figure 7.1.7. In order to prevent the self-ligation of the donor RNA, the 3' end of donor RNA can be blocked via substitution with a phosphate group or kept at a concentration where the donor is less than that of the acceptor RNA. A strategy for making this RNA is presented in Figure 7.1.8.

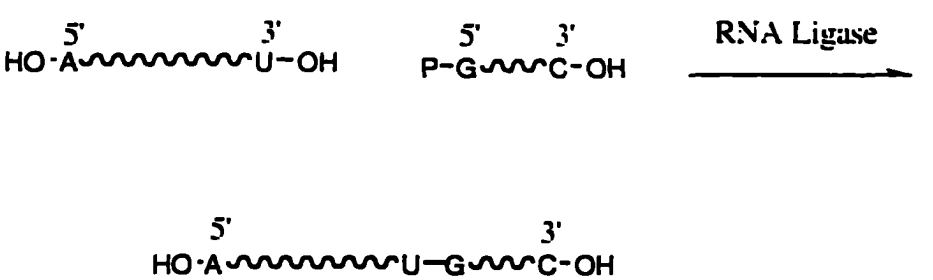

Figure 7.1.7 Schematic diagram for ligation of two single strand RNA.

Figure 7.1.8 Strategy to incorporate εA into the PK1 oligoribonucleotide. The sequence of RNA is from 5' -3'. The symbol p stands for phosphoryl group and, if not specified, the end bears the hydroxyl group. The asterisks were the sites available for fluorescence labeling.

The smallest donor can be a single nucleotide which is 3' and 5' phosphorylated. The ethanoadenosine group (p(εA)p) was prepared from its parent compound, 5'.3'-diphosphorous adenosine, by treatment with chloroacetaldehyde (Figure 7.1.9). The final product that was isolated was approximately 100% pure. The excitation and emission spectra were similar to that of poly(εA) (Figure 7.1.10). The quantum yield of p(εA)p was determined to be approximately 0.5. It also showed a very long lifetime, 20 nsec (Figure 7.1.11).

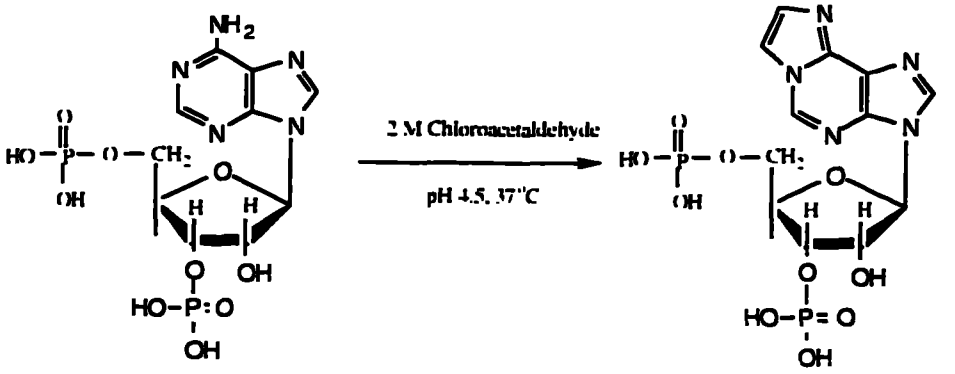

Figure 7.1.9 Synthesis scheme for 5', 3' phosphorous ethanoadenosine

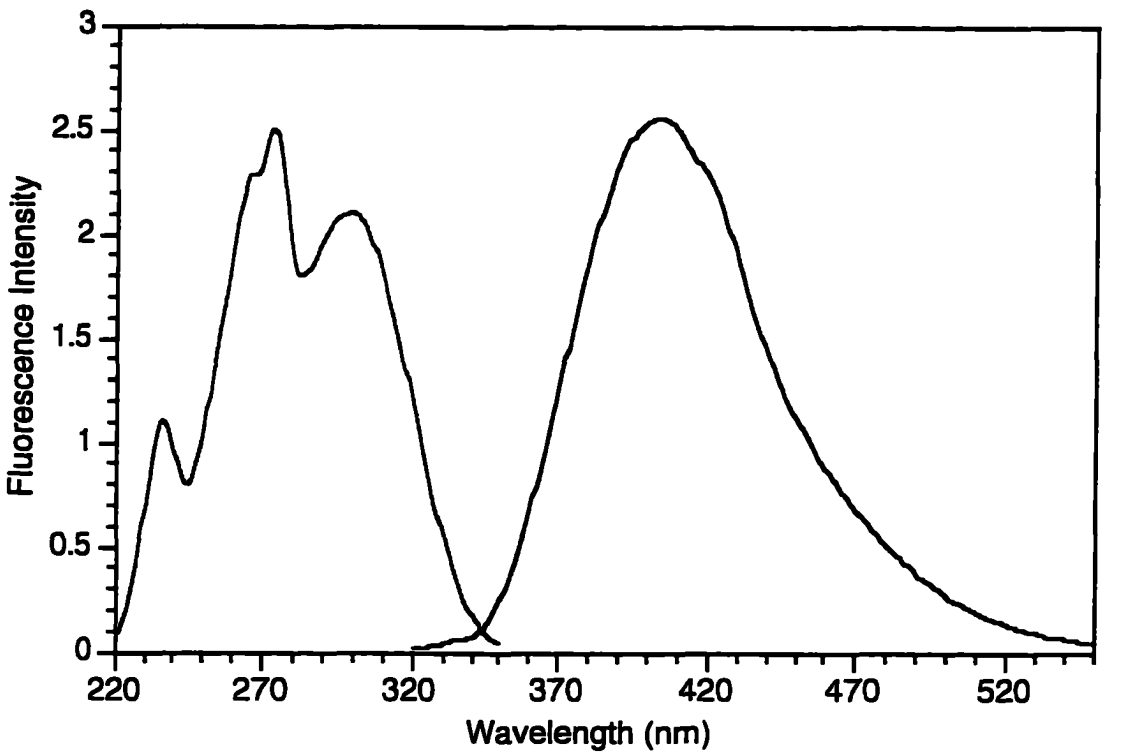

Figure 7.1.10 Excitation and emission spectra of p(EA)p in a neutral buffer. The excitation spectrum was monitored at 410 nm and emission spectrum was excited at 309 nm.

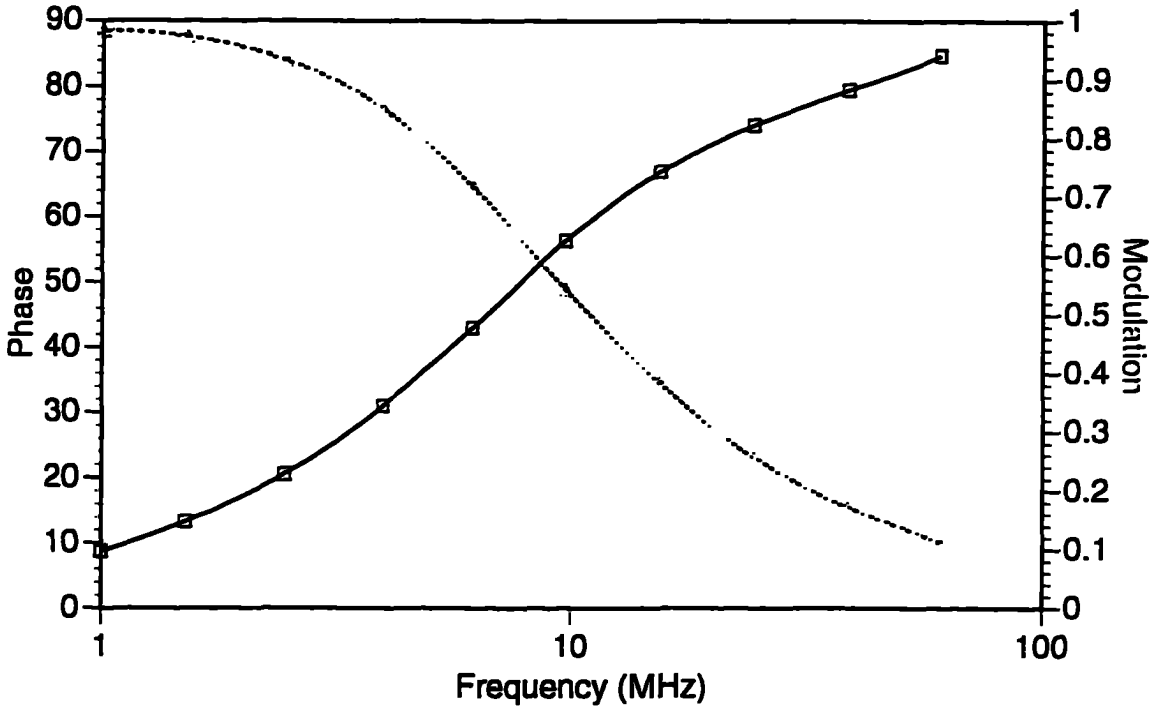

Figure 7.1.11 Lifetime measurement of p(εA)p in a neutral buffer. The excitation wavelength was 309 nm and emission was monitored using a 350 nm cut-off filter. The temperature was 20 °C and the lifetime was fitted as 20.5 nsec.

For 5'-CPM-6-(εA)-PK1 (the 5' end of PK1 was labeled with CPM, and the sixth adenosine residue from the 5' end of PK1 was substituted with εA), the strand PK1α (GGCUU, see Figure 7.1.8) was synthesized and purified as described in the

Experimental Procedure. This RNA was then conjugated with p(εA)p by T4 RNA ligase. The final purified product which contained 60 % modification was then conjugated with another strand PK1β (CGGCGCCUAGCCG). The subsequent 6-(εA)-PK1 was modified on the 5' end and was covalently bound with CPM. The spectra overlap of absorption of 5'-CPM-PK1 and emission of 6-(εA)-PK1 is shown in Figure 7.1.12.

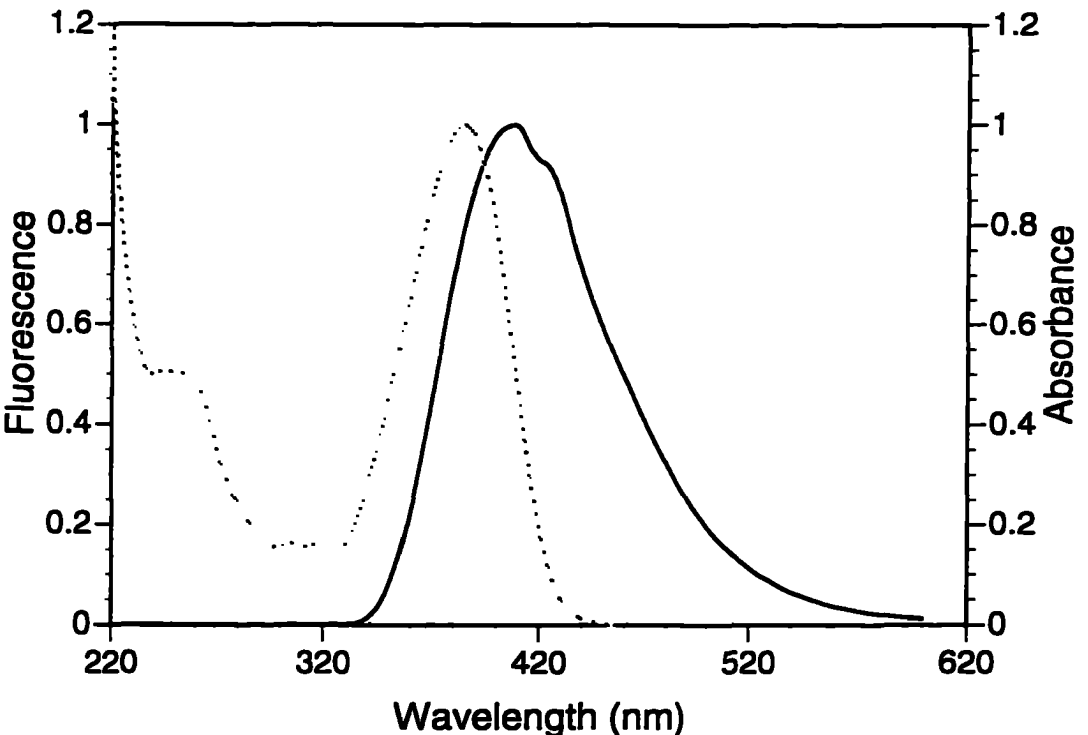

Figure 7.1.12 Spectra overlap of absorbance of CPM (broken line) and emission of εA (solid line) in a neutral buffer. The emission of εA was excited at 309 nm. For presentation, absorbance and fluorescence were normalized to have the same maximum values.

3'-FC-6-(εA)-PK1 could be obtained in with a similar strategy. Strand PK1β was first oxidized and labeled with FC. After phosphorylation at the 5' end, this labeled strand was conjugated with GGGCUUACGGCGCCU(εA) by RNA ligase. Although the fluorescent probe could be labeled after the ligation (labeled the 6-(εA)–PK1), we found that the labeling of a short strand of Pk1β had the advantage that the 3'-FC served as a blocking group. This eliminated the self-ligation during the conjugation with acceptor. The ligation yield was around 60%. The FRET measurements are summarized in Tables 5 and 6. The quantum yield of εA in strand 6-(εA)–PK1 was decreased which may due to the effect of stacking of εA and its neighbors. The Förster distance, R_0, for the εA-CPM pair were calculated to be 30 Å, respectively.

Term	Value
$\phi_{\varepsilon A}$	0.22
$\tau_{\varepsilon A}$ (nsec)	9.55
ϕ_{CPM}	0.82
τ_{CPM} (nsec)	3.46
n	1.33
κ^2	2/3
J (cm^3 dm^3/mole)	5.51×10^{-14}
R_0 (Å)	30
E %	81
E (by lifetime) %	85
R (Å)	24
R (by lifetime) (Å)	22

Table 6 FRET measurement for 5'-CPM-6-(εA)-PK1. The orientation of these probes was assumed to be random, and the corresponding κ^2 is 2/3.

Inserting a fluorescent probe, such as ethanoadensine, also provides the advantage that the adenosine analog, εA, did not interrupt the tertiary structure of any pseudoknot structures based on the melting curve (Figure 7.1.13). No significant melting temperature changes were observed for fluorescent labeled PK1 compared with unmodified PK1. By extending this method using a series of donor-acceptor pairs in different positions, we may construct the model shown in Fig 7.1.14. The different

positions of donor-acceptor probes were inserted, and their corresponding distances could be measured. The 3D structure may be constructed with a computer simulation.

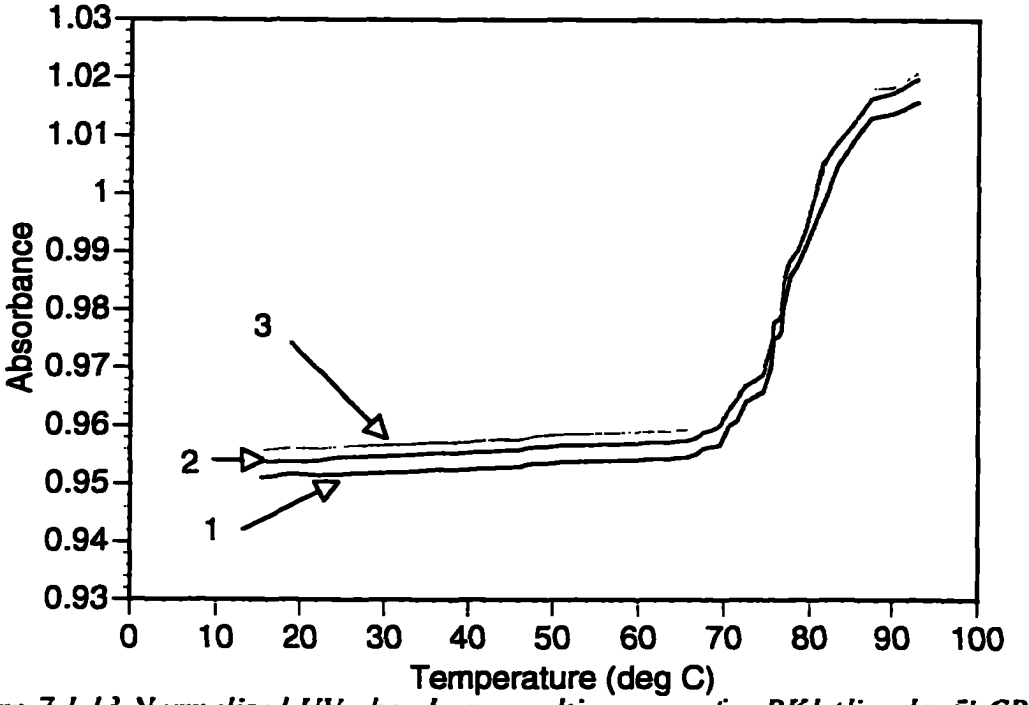

Figure 7.1.13 Normalized UV-absorbance melting curve for PK1 (line 1), 5'-CPM-PK1-3'-FC (line 3), and 5'-CPM-6-(εA)-PK1 (line 2) in 0.25 mM $MgCl_2$, 10 mM sodium phosphate, pH 7.0. Data were collected at 260 nm. All RNA concentrations were 2 μM.

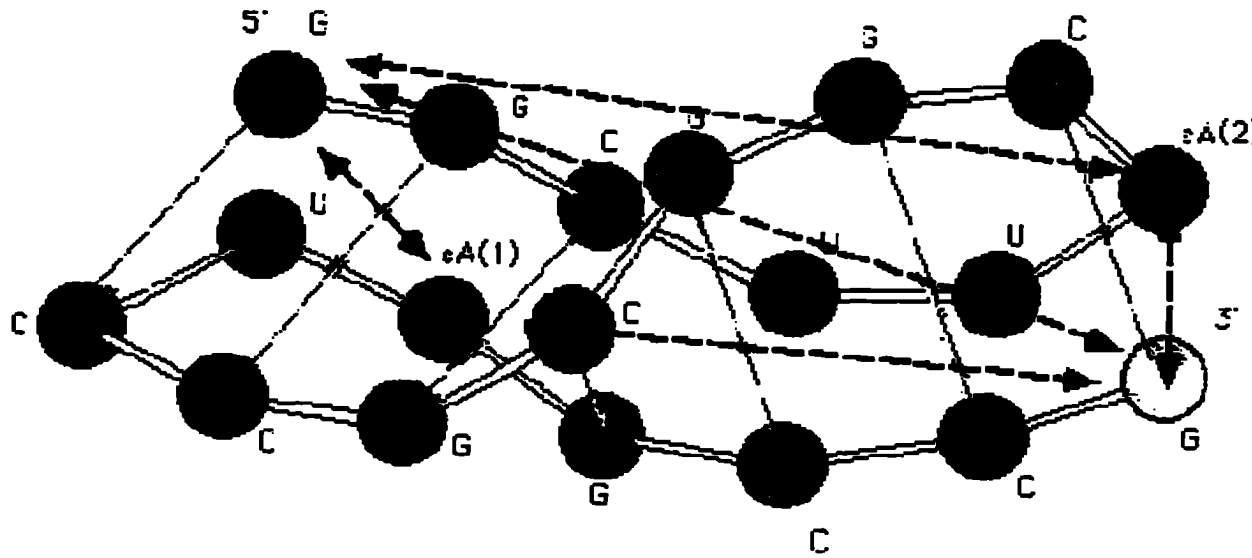

Figure 7.1.14 Proposed model for studies of PK1 pseudoknot structure. The dark spheres represents the nucleotides which could be labeled with fluorescence probes or substituted with fluorescence εA. The thin line connected two spheres represents the hydrogen bond. The arrows between the dark sphere are the distance that could be measured by FRET.

7.2 Studies of helicase activity of initiation factors

For the model to mimic the hairpin structure, two strands of homopolymer were chosen to examine helicase activities. Fluorescent poly(εA) which has been described in Part I may be useful in these studies. To make a double strand of RNA, 1.0 μM poly(εA)$_{20}$ and 1.0 μM poly(U)$_{20}$ were mixed together. Figure 7.2.1 showed the fluorescence quenching of poly(εA)$_{20}$ upon addition of poly(U)$_{20}$. The excitation wavelength was 309 nm, and therefore, no inner-filter effect needed to be considered since no absorption of poly(U) was detected in this region. The fluorescence intensity

did not show any significant change when eIF-4B, eIF-4F, eIF-4A, and ATP were introduced into this mixture, indicating that no helicase activity was observed (Figure 7.2.1).

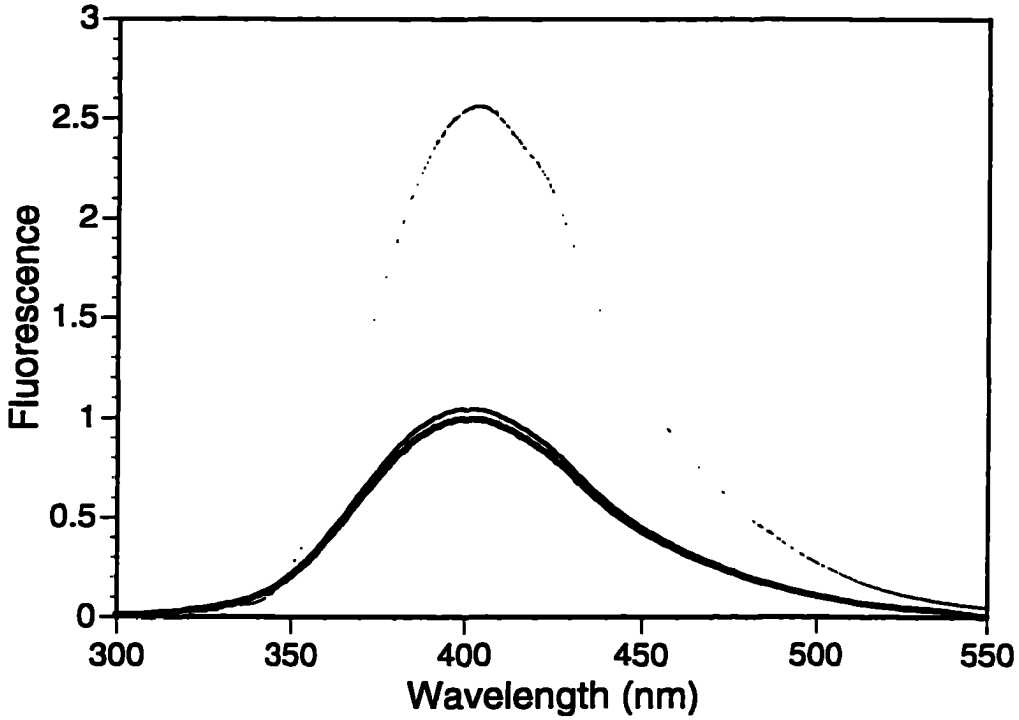

Figure 7.2.1 Helicase study of poly(εA)$_{20}$/poly(U)$_{20}$. The dotted line was the fluorescence intensity of 1.0 μM poly(εA)$_{20}$ alone. The thick line was the fluorescence intensity of 1.0 μM poly(εA)$_{20}$/poly(U)$_{20}$ complex and the thin line was the fluorescence intensity from the solution containing 1.0 μM poly(εA)$_{20}$/poly(U)$_{20}$, 2.0 μM eIF-4B, 2.0 μM eIF-4A, 2.0 μM eIF-4F, and 1 mM ATP.

These results agreed with the studies of DNA helicase activity (Amaratunga & Lohman, 1993) which showed that only Rep helicase requires only a 3'-ss-DNA tail to initiate unwinding *in vitro*. Therefore, a mixture containing poly(εA)$_{20}$ and poly(U)$_{40}$

was prepared. No helicase activity was observed. The reason may be due to the preparation of double stranded RNA. Triple strand poly(A)(A)(U) was formed instead poly(A)(U). Therefore, we prepared the poly(A)(A)(U) and measured its melting curves by UV. The melting curve observed at 280 nm and 260 nm for poly(A)(A)(U) is shown in Figure 7.2.2 and Figure 7.2.3. The absorbance at 260 nm showed only a single melting curve. On the other hand, the absorbance at 280 nm showed two melting curves. The poly(A)(U) was melted at approximately 80 °C and then was transformed to poly(A)(A)(U) at around 40 °C (Broitman et al., 1987). This confirms that in this condition the triplet stand RNA was dominant, and the initiation factor complex does not have the ability to melt the triple strand RNA.

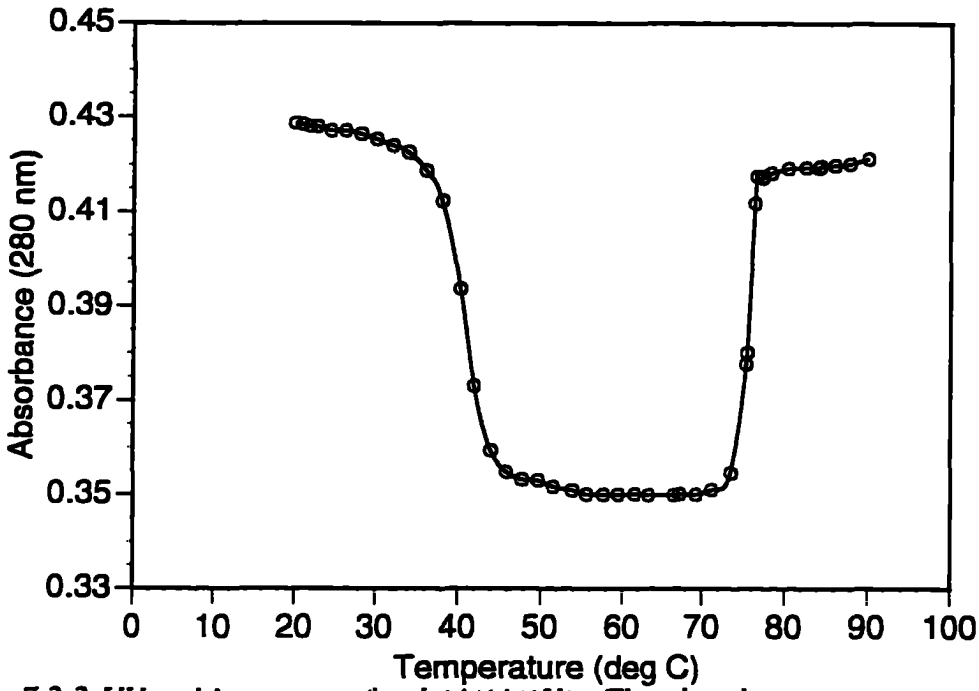

Figure 7.2.2 UV melting curve of poly(A)(A)(U). The absorbance was measured at 280 nm.

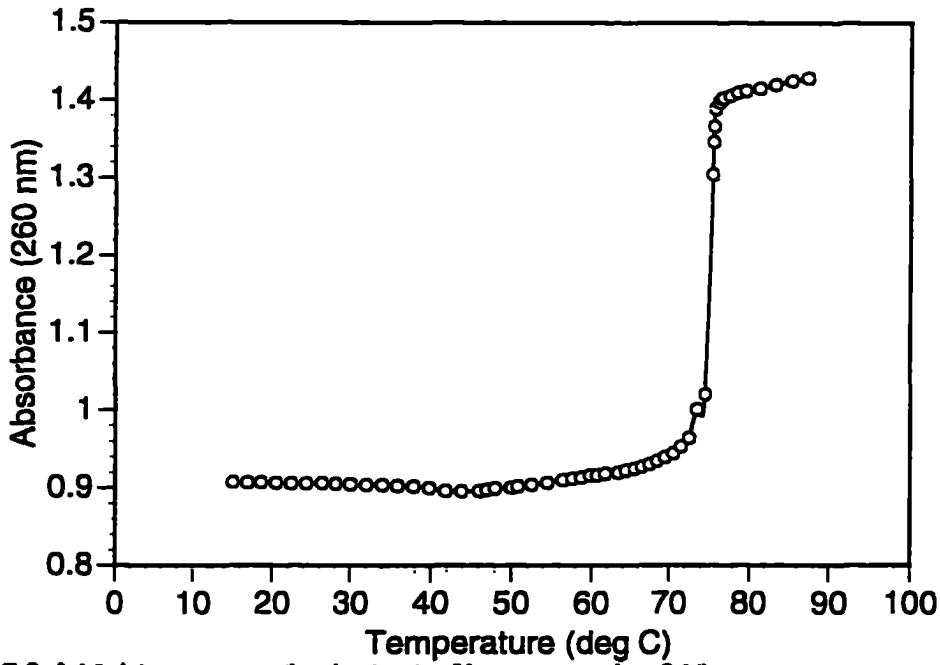

Figure 7.2.3 Melting curve of poly(A)(A)(U) measured at 260 nm.

In order to prevent the formation of tripled stranded RNA, a mixture containing 1.0 μM poly(εA)$_{15}$ and 1.0 μM poly(U)$_{30}$ was heated to 90 °C and cooled to room temperature very slowly. The length of homopolymer was chosen based on the result from Broitman et al. (1987). These authors demonstrated that the formation of poly(A)(A)(U) is limited by the size of the poly(A) strand but is unaffected by the size of the poly(U). Figure 7.2.4 shows the helicase activity. The double stranded RNA was incubated 30 min at room temperature. The fluorescence signal of this double strand was quenched compared with its corresponding single strand (similar to Figure 7.2.1). The phenomena is due to the stacking of bases in the double strand. As was expected, 4A, 4B, or 4F alone did not affect the fluorescence signal (lane 2 to 7 in Figure 7.2.4). eIF-4B is known as a RNA-binding protein which only binds to the single stranded poly(U) part, and does not interrupt the poly(εA) part, since all of poly(εA) was in a double stranded form. eIF-4F and eIF-4A, only in the presence of ATP, enhance the signal around 160% (lane 8 and 9). Addition of eIF-4B increased the fluorescence signal to 187% (lane 10). If the sample was heated 10 min at 37 °C and then subsequently cooled to 20 °C, the fluorescence signal was increased approximately 200% compared with that of double stranded RNA (lane 11). The fluorescence enhancement is due to formation of protein/RNA complexes which unstack the double stranded RNA. Our results conclude that eIF-4A, eIF-4F, and ATP have a partial helicase activity. In addition, eIF-4A, eIF-4B, eIF-4F, and ATP showed stronger activity. But in the absence of ATP, no helicase activity was observed. With

higher incubation temperature. the secondary structure of dsRNA was easily melted. These conclusions were consistent with the results from the gel filtration studies of double stranded RNA (Jaramillo et al., 1991).

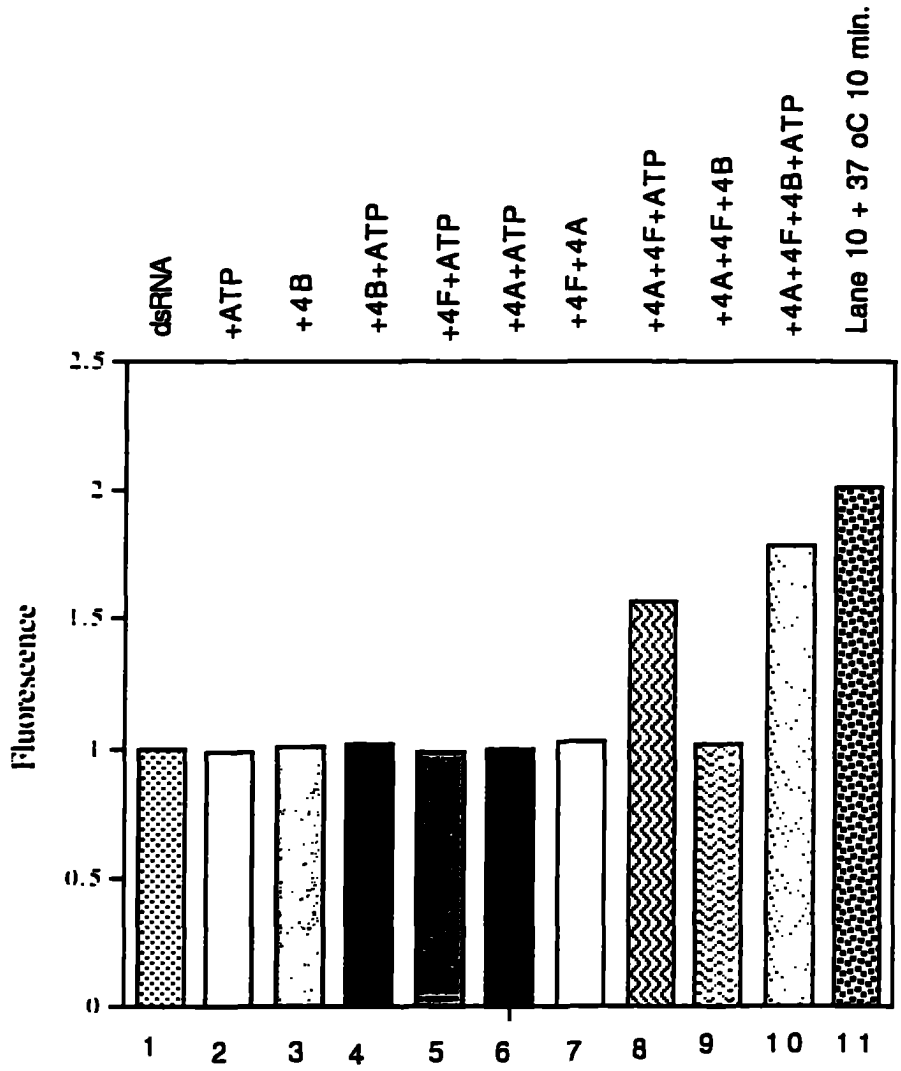

Figure 7.2.4 Helicase studies of initiation factors on poly(εA*)*$_{15}$*(U)*$_{30}$*. Solution were incubated 30 min. at 25 °C. The concentration of nucleic acid, proteins , and ATP was 1.0 μM, 2.0 μM, and 1.0 mM, respectively.*

For the FRET measurements, the poly(A)$_{15}$ was labeled with FC on its 3' end and poly(U)$_{30}$ was labeled on it 5' end to establish the minimum distance between these

probes. Similarly these dsRNA were used to examine the activity of translation initiation factors. Figure 7.2.5 showed the double labeled dsRNA which were excited at 380 nm. Upon addition of the initiation factors and ATP, the donor fluorescence was quenched and the acceptor fluorescence was enhanced compared with dsRNA only, indicating the double stranded RNA was unwound and formed a single stranded RNA/protein complex. The separation of 3'-FC-poly(A)$_{15}$ and 5'-CPM-poly(U)$_{30}$ results in the loss of fluorescence energy transfer.

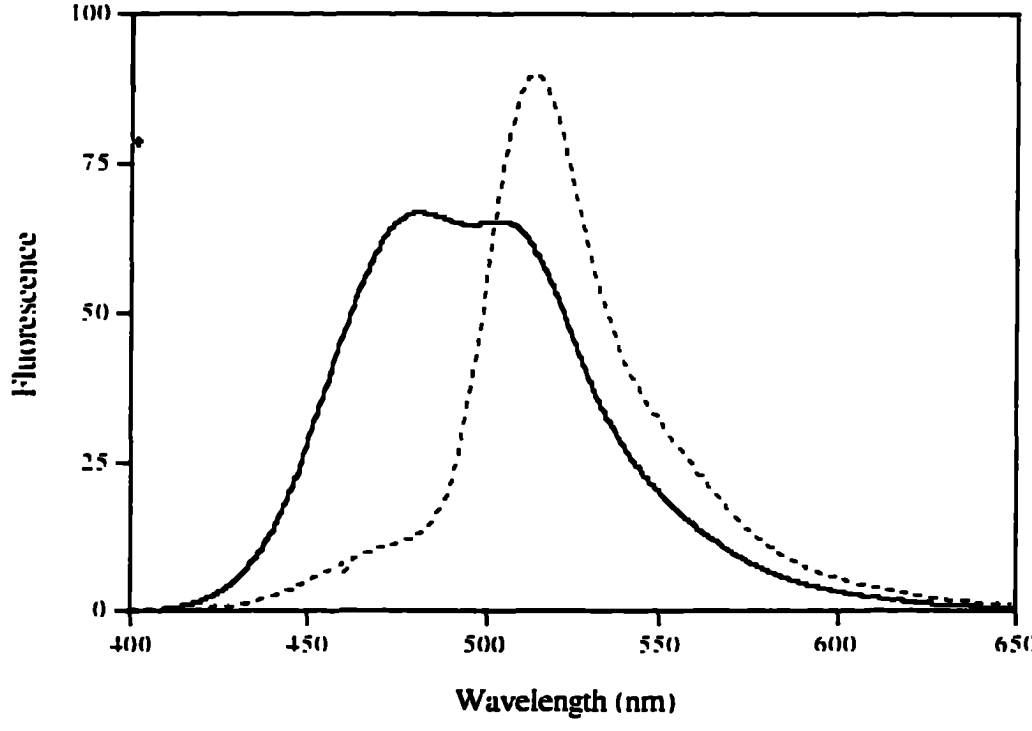

Figure 7.2.5 Helicase study using FRET. The broken line is the fluorescence intensity of double stranded RNA (3'-FC-poly(A)15/5'-CPM-poly(U)$_{30}$). The solid line the fluorescence intensity of this RNA after incubation with eIF-4F, eIF-4B, eIF-4A, and ATP. The enhancement of fluorescence intensity of donor and decreasing of fluorescence intensity of acceptor represent that the double strand RNA was unwound and formed a single stranded RNA/protein complex.

8. SUMMARY

In this report, we constructed several systems, with labeled specific fluorescent donor-acceptor pairs, and utilized FRET methods to give potential models in the structure analysis. The FRET occurs when these donor and acceptor are close to each other, providing the information about the distance between these probes.

The 19-mer oligoribonucleotide (PK1) was chosen as simple pseudoknot model and the FRET does show the distance between 5' end and 3' end is less than random single strand RNA. By selectively substituting the adenosine base with its fluorescent analog, εA, the distance calculation on position 6 (from 5' end) to 5' end also show a significant fluorescence energy transfer, suggesting this structure must be forming some kind of tertiary structure to have FRET. The UV melting measurements also demonstrated that these modifications do not lead to interruption of the RNA conformation.

In the helicase studies, steady-state fluorescence intensity and FRET were used. Double stranded Poly(εA)(U) was utilized as a model to test the helicase activity. Upon addition of eIF-4B, eIF-4F, and eIF-4A in the presence of ATP the fluorescence intensity was increased due to unstacking of the base pairing in the double strand RNA. FRET measurement confirms this result, indicating that the FRET was lost while the RNA double strands with fluorescent donor-acceptor probes on each strand were separated by helicase proteins.

For both of these studies. extending the labeling to proteins will give us an alternative way to study the molecular structure of enzymatic mechanism. It may also provide more thermodynamic and kinetic information regarding how the proteins and nucleic acids interact in concert to complete the helicase activity and the roles of pseudoknot structures in the RNA.

BIBLIOGRAPHY

PART I

Adam, S. A., Nakagawa, T., Swanson, M. S., Woodruff, T. K., & Dreyfuss, G. (1986) *Mol. Cell. Biol.* **6**, 2932-2943.

Barrio, J. R., Secrist, J. A. 3rd, & Leonard, N. J. (1972) *Biochem. Biophs. Res. Commun.* **46**, 597-604.

Beelman, C. A., & Parker, R. (1995) *Cell* **81**, 179-183.

Bergmann, I. E., & Brawerman, G. (1977) *Biochemistry* **16**, 259-264.

Bernstein, P., Peltz, S. W., & Ross, J. (1989) *Mol. Cell. Biol.* **9**, 659-670.

Bertholet, C., Van Meir, E., ten Heggeler-Bordier, B., & Wittek, R. (1987) *Cell* **50**, 153-162.

Birmachu, W., & Reed, J. K. (1988) *Photochem. Photobiol.* **47**, 675-681.

Birney, E., Kumar, S., & Krainer, A. R. (1993) *Nucleic Acids Res.* **21**, 5803-5816.

Blobel, G. (1973) *Proc. Natl. Acad. Sci. USA* **70**, 924-928.

Brahms, J., Michelson, A. M., & Van Holde, K. E. (1966) *J. Mol. Biol.* **15**, 467-488.

Brawerman, G. (1981) *Crit. Rev. Biochem.* **10**, 1-39.

Brewer, G., & Ross, J. (1988) *Mol. Cell Biol.* **8**, 1697-1708.

Brissette, P., Ballou, D. P., & Massey, V. (1989) *Anal. Biochem.* **181**, 234-238.

Broido, M. S., & Kearns, D. R. (1982) *J. Amer. Chem. Soc.* **104**, 5207-5216.

Browning, K. S., Kax, S. R., & Ravel, J. M. (1987) *J. Biol. Chem.* **262**, 11222-11232.

Browning, K. S., Fletcher, L., Lax, S. R., & Ravel, J. M. (1989) *J. Biol. Chem.* **264**, 8491-8494.

Brewer, G., & Ross, J. (1988) *Mol. Cell. Biol.* **8**, 1697-1708.

Burd, C. G., & Dreyfuss, G. (1994) *Science* **265**, 615-621.

Calhoun, D. B., Vanderkooi, J. M., & Englander, S. W. (1983) *Biochemistry* **22**, 1533-1539.

Caponigro, G., & Parker, R. (1995) *Genes Dev.* **9**, 2421-2432.

Carberry, S. E., Rhoads, R. E., & Goss, D. J. (1989) *Biochemistry* **28**, 8078-8083.

Chu, B. C., Wahl, G. M., & Orgel, L. E. (1983) *Nucleic Acids Res.* **11**, 6513-6529.

Darzynkiewicz, E., Ekiel, I., Lassota, P., & Tahara, S. M. (1987) *Biochemistry* **26**, 4372-4380.

Darzynkiewicz, E., Stepinski, J., Ekiel, I., Jin, Y., Haber, D., Sijuwade, T., & Tahara, S. M. (1988) *Nucleic Acids Res.* **16**, 8953-8962.

Darzynkiewicz, E., Stepinski, J., Ekiel, I., Goyer, C., Sonenberg, N., Temeriusz, A., Jin, Y. Sijuwade, T. Haber, D., & Tahara, S. M. (1989) *Biochemistry* **28**, 4771-4778.

Eriksson, S., Norden, B., & Takahashi, M. (1993) *J. Biol. Chem.* **268**, 1805-1810.

Evans, F. E., & Sarma, R. H. (1976) *Nature* **263**, 567-572.

Firpo, M. A., Connelly, M. B., Goss, D. J., & Dahlberg, A. E. (1996) *J. Biol. Chem.* **271**, 4693-4698.

Furuichi, Y., Shimotohno, K., & Miura, K. (1977) *Tanpakushitsu Kakusan Koso* **22**, 931-950.

Gallie, D. R. (1991) *Genes Dev.* **5**, 2108-2116.

Gallie, D. R., & Tanguay, R. (1994) *J. Biol. Chem.* **269**, 17166-17173.

Görlach, M., Burd, C. G., & Dreyfuss, G. (1994) *Exp. Cell Res.* **211**, 400-407.

Goumans, H., Thomas, A., Verhoeven, A., Voorma, H. O., & Benne, R. (1980) *Biochim. Biophys. Acta* **608**, 39-46.

Goss, D. J., Woodley, C. L., & Wahba, A. J. (1987) *Biochemistry* **26**, 1551-1556.

Goss, D. J., Carberry, S. E., Dever, T. E., Merrick, W. C., & Rhoads, R. E. (1990) *Biochim. Biophys. Acta* **1050**, 163-166.

Grange, T., de Sa, C. M., Oddos, J., & Pictet, R. (1987) *Nucleic Acids Res.* **15**, 4771-4787.

Grifo, J. A., Tahara, S. M., Morgan, M. A., Shatkin, A., & Merrick, W. C. (1983) *J. Biol. Chem.* **258**, 5804-5810.

Grifo, J. A., Abramson, R. D., Satler, C. A., & Merrick, W. C. (1984) *J. Biol. Chem.* **259**, 8648-8654.

Hershey, N., Mathews, M. B., & Sonenberg, N. (1996) *Translational Control*. Cold Spring Harbor Laboratory Press. Cold Spring Harbor, NY.

Heyduk, T., & Lee, J. C. (1990) *Proc. Natl. Acad. Sci. USA* **87**, 1744-1748.

Hiratsuka, T. (1983) *Biochim. Biophy. Acta* **742**, 496-508.

Hodgman, T. C. (1988) *Nature* **333**, 22-23, and correction (1989) *Nature* **333**, 578.

Iizuka, N., Najita, L., Franzusoff, A., & Sarnow, P. (1994) *Mol. Cell Biol.* **14**, 7322-7330.

Inners, L. D., & Felsenfeld, G. (1970) *J. Mol. Biol.* **50**, 373-389.

Jackson, R. J., & Standart, N. (1990) *Cell* **62**, 15-24.

Johnson, W. C. Jr. (1990) *PROTEINS: Structure, Function and Genetics* **7**, 205-214.

Karpel, R. L., Henderson, L. E., & Oroszlan, S. (1987) *J. Biol. chem.* **262**, 4961–4967.

Kuge, H., & Richter, J. D. (1995) *EMBO J.* **14**, 6301-6310.

Kühn, U., & Pieler, T. (1996) *J. Mol. Biol.* **256**, 20-30.

Laemmli, U. K. (1970) *Nature* **227**, 680-685.

Lakowicz, J. R. (1983) in *Principles in Fluoresence Spectroscopy* Plenum Press, New York

Lawson, T. G., Lee, K. A., Maimone, M. M., Abramson, R. D., Dever, T. E., Merrick, W. C., & Thach, R. E. (1989) *Biochemistry* **28**, 4729–4734.

Lax, S. R., Fritz, W., Browning, K., & Ravel, J. M. (1985) *Proc. Natl. Acad. Sci. USA* **82**, 330-333.

Lax, S. R., Lauer, S. J., Browning, K. S., & Ravel, J. M. (1986a) *Methods Enzymol.* **118**, 109-128.

Lax, S. R., Browning, K. S., Maia, D. M., & Ravel, J. M. (1986b) *J. Biol. Chem.* **261**, 15632-15636.

Le, H., Tanguay, R. L., Balasta, M. L., Wei, C. -C., Browning, K. S., Goss, D. J., & Gallie, D. R. (1997) *J. Biol. Chem.* **272**, 16247-16255.

Ledneva, R. K., Razjivin, A. P., Kost, A. A., & Bogdanov, A. A. (1978) *Nucleic Acids Res.* **5**, 4225–4243.

Lefrere, V., & Duncan, R. F. (1994) *Nucleic Acids Res.* **22**, 1640-1642.

Linder, P., Lasko, P. F., Ashburner, M., Leroy, P., Nielsen, P. J., Nishi, K., Schnier, J., & Slonimski, P. P. (1989) *Nature* **337**, 121-122.

Lockard, R. E., Currey, K., Browner, M., Lawrence, C., & Maizel, J. (1986) *Nucleic Acids Res.* **14**, 5827-5841.

Locke, B. C., MacInnis, J. M., Qian, S. -J., Gordon, J. I., Li, E., Fleming, G. R., & Yang, N. -C. (1992) *Biochemistry* **31**, 2376-2383.

Marcotrigiano, J., Gingras, A. -C., Sonenberg, N., & Burley, S. K. (1997) *Cell* **89**, 951-961.

Mendoza, J. A., Butler, M. C., & Horowitz, P. M. (1992) *J Biol. Chem.* **267**, 24648-24654.

Merrick, W. C. (1992) *Microbiol. Rev.* **56**, 291-315.

Merril, C. R., Goldman, D., Sedman, S. A., & Ebert, M. H. (1981) *Science* **211**, 1437-1438.

Methot, N., Pickett, G., Keene, J. D., Sonenberg, N. (1996) *RNA* **2**, 38-50.

Metz A. M., & Browning, K. S. (1993) *Gene* **131**, 299-300.

Munroe, D., & Jacobson A. (1990) *Mol. Cell Biol.* **10**, 3441-3455.

Muthukrishnan, S., Morgan, M., Banerjee, A. K., & Shatkin, A. J. (1976) *Biochemistry* **15**, 5761-5768.

Muthukrishnan, S., Moss B., Cooper J. A., & Maxwell E. S. (1978) *J. Biol. Chem.* **253**, 1710-1715.

Nudel U., Soreq, H., & Littauer, U. Z. (1976) *Eur. J. Biochem.* **64**, 115-121.

Odom, O. W. Jr., Robbins, D. J., Lynch, J., Dottavio-Martin, D., Kramer, G., & Hardesty, B. (1980) *Biochemistry* **19**, 5947-5954.

Prescott, B., Gamache, R., Livramento, J., & Thomas, G. J. Jr. (1974) *Biopolymers* **13**, 1821-1845.

Ptashne, M. (1986) *Nature* **322**, 697-701.

Ptashne, M. (1988) *Nature* **335**, 683-689.

Rabczenko, A., & Shugar, D. (1971) *Acta. Biochim. Pol.* **18**, 387–402.

Ray, B. K., Lawson, T. G., Kramer, J. C., Cladaras, M. H., Grifo, J. A., Abramson, R. D., Merrick, W. C., & Thach, R. E. (1985) *J. Biol. Chem.* **260**, 7651-7658

Ren, J., & Goss, D. J. (1996) *Nucleic Acids Res.* **24**, 3629-3634.

Rhoads, R. E. (1991) *Translation in Eukaryotes* (Trachsel, H., ed.) pp. 109-148; CRC press, Boca Raton, FL.

Rozen, F., Edery, I., Meerovitch, K., Dever, T. E., Merrick, W. C., & Sonenberg, N. (1990) *Mol. Cell Biol.* **10**, 1134-1144.

Rubin, H. N, & Halim, M. N. (1993) *Biochem. Mol. Biol. Int.* **31**, 267-278.

Sachs, A. B., & Kornberg, R. D. (1985) *Mol. Cell Biol.* **5**, 1993-1996.

Sachs, A. B., Bond, M. W., & Kornberg, R. D. (1986) *Cell* **45**, 827-835.

Sachs, A. B., Davis, R. W., & Kornberg, R. D. (1987) *Mol. Cell Biol.* **7**, 3268-3276.

Sarkar, P. K., & Yang, J. T. (1965) *Arch. Biochem. Biophys.* **112**, 512-518.

Seidel, B. L., & Somberg, E. W. (1978) *Arch. Biochem. Biophys.* **187**, 108-112.

Shatkin, A. J. (1985) *Cell* **40**, 223-224.

Sonenberg, N., & Shatkin, A. J. (1978) *J. Biol. Chem.* **253**, 6630-6632.

Sonenberg, N., Guertin, D., Cleveland, D., & Trachsel, H. (1981) *Cell* **27**, 563-572.

Sonenberg, N. (1994) *Curr. Opin. Genet. Dev.* **4**, 310-315.

Tahara, S. M., Morgan, M. A., & Shatkin, A. J. (1981) *J. Biol. Chem.* **256**, 7691-7694.

Tarun, S. Z. Jr., & Sachs, A. B. (1995) *Genes Dev.* **9**, 2997-3007.

Tarun, S. Z. Jr., & Sachs, A. B. (1996) *EMBO J.* **15**, 7168-7177.

Thiele, D., & Guschlbauer, W. (1973) *Biophysik* **9**, 261-277.

Weber, G., & Teale, F. W. J. (1957) *Trans. Faraday Soc.* **53**, 646-655.

Wang, Y., Sha, M., Ren, W. Y., van Heerden, A., Browning, K. S., & Goss, D. J. (1996) *Biochim. Biophys. Acta* **1297**, 207-213.

Yang, J., & Hunt, A. G. (1992) *Plant Physiol.* **98**, 1115-1120.

Young, P. R., & Kallenbach, N. R. (1978) *J. Mol. Biol.* **126**, 467-479.

Zelus, B. D., Giebelhaus, D. H., Eib, D. W., Kenner, K. A., & Moon, R. T. (1989) *Mol. Cell. Biol.* **9**, 2756-2760.

Part II

Amaratunga, M., & Lohman, T. M. (1993) *Biochemistry* **32**, 6815-6820.

Beardsley, K., & Cantor, C. R. (1970) *Proc. Natl. Acad. Sci. USA* **65**, 39-46.

Broitman, S. L., Im, D. D., & Fresco, J. R. (1987) *Proc. Natl. Acad. Sci. USA* **84**, 5120-5214.

Chamorro, M., Parkin, E., & Varmus, H. E. (1992) *Proc. Natl. Acad. Sci. USA* **89**, 713-717.

Chu, B. C., & Orgel, L. E. (1988) *Nucleic Acids Res.* **16**, 3671-3691.

Conroy, S. C., Dever, T. E., Owens, C. L., & Merrick, W. C. (1990) *Arch. Biochem. Biophys.* **282**, 363-371.

Czworkowski, J., Odom, O. W., & Hardesty, B. (1991) *Biochemistry* **30**, 4821-4830.

Darr, S. C., Zito, K., Smith, D., & Pace, N. R. (1992) *Biochemistry* **31**, 328-333.

Ehresmann, C., Philippe, C., Westhof, E., Benard, L., Portier, C., & Ehresmann, B. (1995) *Biochem. Cell Biol.* **73**, 1131-1140.

Förster, T. (1948) *Ann. Phys. (Leipzig)* **2**, 55-75.

Grifo, J. A., Tahara, S. M., Morgan, M. A., Shatkin, A., & Merrick, W. C. (1983) *J. Biol. Chem.* **258**, 5804-5810.

Grifo, J. A., Abramson, R. D., Salter, C. A., & Merrick, W. C. (1984) *J. Biol. Chem.* **259**, 8648-8654.

Jagus, R., Anderson, W. F., & Safer, B. (1981) *Prog. Nucleic Acid Res. Mol. Biol.* **25**, 127-185.

Jaramillo, M., Dever, T. E., Merrick, W. C., & Sonenberg, N. (1991) *Mol Cell Biol* **11**, 5992-5997.

Jeng, K. S., Daniel, A., & Lai M. M. (1996) *J. Virol.* **70**, 2403-2410.

Johnson, K. H., & Gray, D. M. (1992) *J. Biomol. Struct. Dyn.* **9**, 733-745.

Merrick, W. C. (1992) *Microbiol. Rev.* **56**, 291-315.

Moazed, D., & Noller, H. F. (1987) *Nature* **327**, 389-394.

Murchie, A. I., Clegg, R. M., von Kitzing, E., Duckett, D. R., Diekmann, S., & Lilley, D. M. (1989)*Nature* **341**, 763-766.

Odom, O. W. Jr., Robbins, D. J., Lynch, J., Dottavio-Martin, D., Kramer, G., & Hardesty, B. (1980) *Biochemistry* **19**, 5947-5954.

Ohtsuka, E., Nishikawa, S., Markham, A. F., Tanaka, S., Miyake, T., Wakabayashi, T., Ikehara, M., & Sugiura, M. (1978) *Biochemistry* **17**, 4894-4899.

Ozaki, H., & McLaughlin, L. W. (1992) *Nucleic Acids Res.* **20**, 5205-5214.

Pleij, C. W., Rietveld, K., & Bosch, L. (1985) *Nucleic Acids Res.* **13**, 1717-1731.

Puglisi, J. D., Wyatt, J. R., & Tinoco, I. Jr. (1988) *Nature* **331**, 283-286.

Rietveld. K.. Van Peolgeest. R.. Pleij. C. W.. Van Boom. J. H.. & Bosch. L. (1982) *Nucleic Acid Res.* **10.** 1929-1946.

Rhoads. R. E. (1991) *Translation in Eukaryotes* (Trachsel. H.. ed.) pp. 109-148: CRC press. Boca Raton. FL.

Silber. R.. Malathi. V. G.. & Hurwitz. J. (1972) *Proc. Natl. Acad. Sci. USA* **69.** 3009-3013.

Sonenberg. N. (1988) *Prog. Nucleic Acid Res. Mol. Biol.* **35.** 173-207.

Spedding. G.. Gluick. T. C.. & Draper. D. E. (1993) *J. Mol. Biol.* **229.** 609-622.

Stryer. L.. & Haugland. R. P. (1967) *Proc. Natl. Acad. Sci.* **58.** 719-726.

Taramillo. M.. Browning. K.. Dever. T. E.. Blum. S.. Trachsel. H.. Merrick. W. C.. Ravel. J. M.. & Sonenberg. N. (1990) *Biochim. Biophys.Acta* **1050.** 134-139.

Teare. J.. & Wollenzien. P. (1989) *Nucleic Acids Res.* **17.** 3359-3372.

Trachsel. H.. Erni. B.. Schreier. M. H.. Staehelin. T. (1977) *J. Mol. Biol.* **116.** 755-767.

Tuschl. T.. Gohlke. C.. Jovin. T. M.. Westhof. E.. & Eckstein. F. (1994) *Science* **266.** 785-789.

Van Belkum A.. Abrahams. J. P.. Pleij. C. W.. & Bosch. L. (1985) *Nucleic Acids Res.* **13.** 7673-7686.

IMAGE EVALUATION TEST TARGET (QA-3)

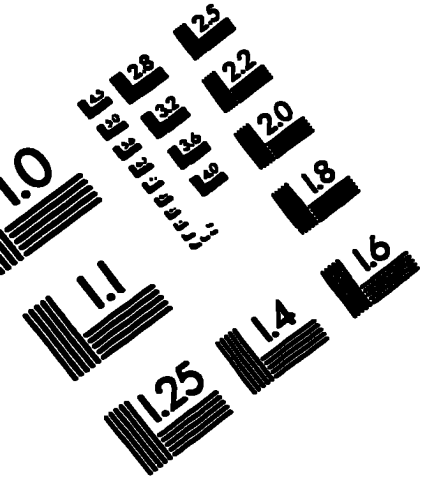

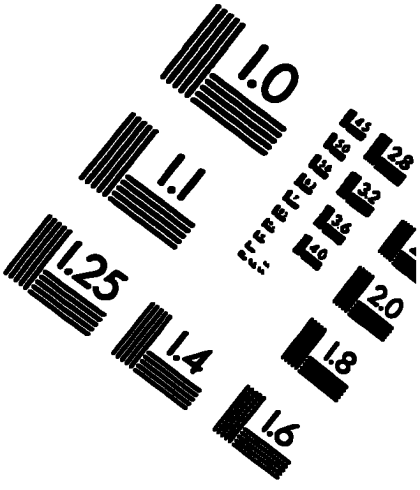

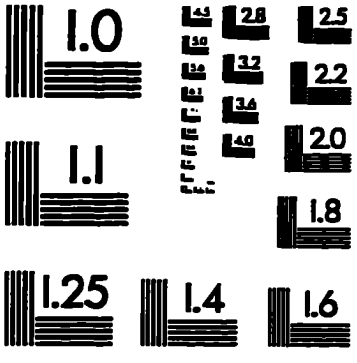

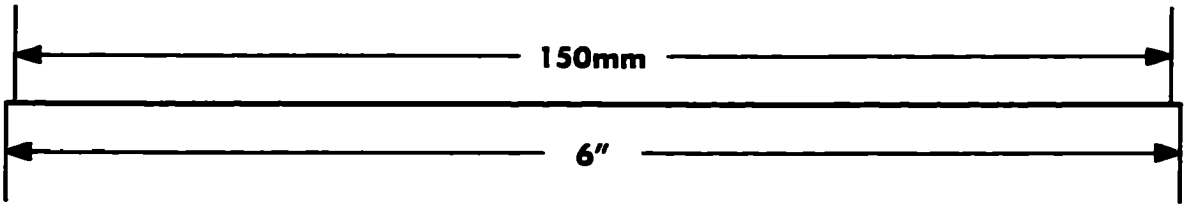

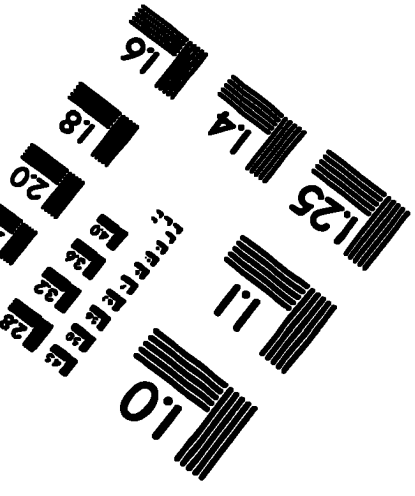

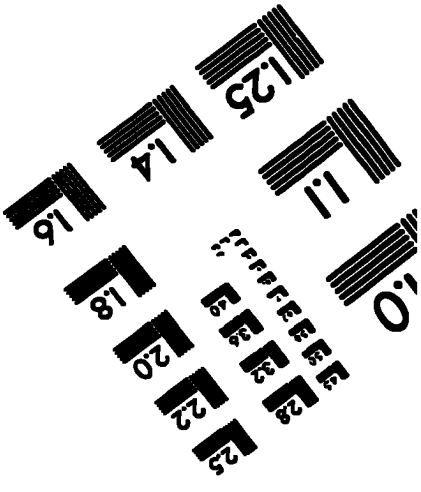

APPLIED IMAGE. Inc
1653 East Main Street
Rochester, NY 14609 USA
Phone: 716/482-0300
Fax: 716/288-5989